PERFORMANCE EVALUATION OF CEMENT-FREE GEOPOLYMER CONCRETE MADE WITH RECYCLED CONCRETE AGGREGATES AND STEEL FIBERS

Jamal Ahmad Samer Medljy

United Arab Emirates University

College of College of Engineering

Department of Civil and Environmental Engineering

PERFORMANCE EVALUATION OF CEMENT-FREE GEOPOLYMER CONCRETE MADE WITH RECYCLED CONCRETE AGGREGATES AND STEEL FIBERS

Jamal Ahmad Samer Medljy

This thesis is submitted in partial fulfilment of the requirements for the degree of Master of Science in Civil Engineering
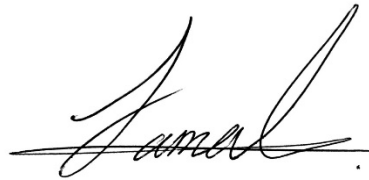
Under the Supervision of Dr. Hilal El-Hassan

April 2021

Declaration of Original Work

I, Jamal Ahmad Samer Medljy, the undersigned, a graduate student at the United Arab Emirates University (UAEU), and the author of this thesis entitled "*Performance Evaluation of Cement-free Geopolymer Concrete Made with Recycled Concrete Aggregates and Steel Fibers*", hereby, solemnly declare that this thesis is my own original research work that has been done and prepared by me under the supervision of Dr. Hilal El-Hassan, in the College of Engineering at UAEU. This work has not previously formed the basis for the award of any academic degree, diploma or a similar title at this or any other university. Any materials borrowed from other sources (whether published or unpublished) and relied upon or included in my thesis have been properly cited and acknowledged in accordance with appropriate academic conventions. I further declare that there is no potential conflict of interest with respect to the research, data collection, authorship, presentation and/or publication of this thesis.

Student's Signature: _____   Date: 28-11-2021

Advisory Committee

1) Advisor: Dr. Hilal El-Hassan

Title: Associate Professor

Department of Civil & Environmental Engineering

College of Engineering

2) Co-advisor: Prof. Tamer El-Maaddawy

Title: Professor

Department of Civil & Environmental Engineering

College of Engineering

Approval of the Master Thesis

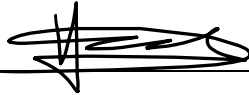This Master Thesis is approved by the following Examining Committee Members:

1) Advisor (Committee Chair): Hilal El-Hassan

   Title: Associate Professor

   Department of Civil and Environmental Engineering

   College of Engineering

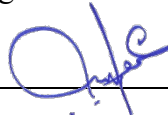   Signature _____   Date ___16/12/2021___

2) Member: Amr El-Dieb

   Title: Professor

   Department of Civil and Environmental Engineering

   College of Engineering

   Signature _____   Date ___16 Dec. 2021___

3) Member (External Examiner): Andrew Boyd

   Title: Associate Professor

   Department of Civil Engineering and Applied Mechanics

   Institution: McGill University, Canada

   On behalf of external examiner

   Signature _____   Date ___December 16, 2021___

This Master Thesis is accepted by:

Dean of the College of Engineering: Professor James Klausner

Signature _James F. Klausner_   Date _11/1/2022_

Dean of the College of Graduate Studies: Professor Ali Al-Marzouqi

Signature _Ali Hassan_   Date _11/1/2022_

Copy ____ of ____

Abstract

Sustainable and innovative alternatives have been investigated to replace concrete's main components, natural aggregates, and cement. Previous studies have been carried out to replace NA and cement with recycled concrete aggregates (RCA) and inorganic alkali-activated geopolymeric binders, respectively. Yet, such sustainable concrete has only been proposed for non-structural purposes, owing to the inferior properties of RCA. This research work aims to assess the feasibility of reutilizing RCA from construction and demolition waste and locally available industrial solid by-products in the production of sustainable geopolymer concrete for structural applications. The binding materials were either in the form of a single precursor, ground granulated blast furnace slag (simply slag), or a blend of slag and class F fly ash. Steel fiber reinforcement was added at different volume fractions to promote the use of structural geopolymer concrete made with 100% RCA. The mechanical behavior of such steel fiber-reinforced RCA geopolymer concrete was studied through extensive testing of compressive strength, splitting tensile strength, and modulus of elasticity. The flexural strength, toughness, deflection, and residual strength were used to describe the flexural performance. In turn, the durability properties were assessed by measuring the bulk electric resistivity, water absorption, sorptivity, and abrasion resistance. Experimental findings revealed the ability to produce 100% RCA slag-based and slag-fly ash blended geopolymer concrete incorporating a 2% steel fiber volume fraction having superior mechanical performance and comparable durability properties relative to those of the plain NA-based control mix. The steel fiber-reinforced RCA geopolymer concrete developed in the current study is considered a feasible and sustainable alternative to conventional concrete that promises to recycle industrial wastes, alleviate carbon dioxide emissions, and conserve natural resources without compromising performance.

Keywords: Geopolymer, recycled concrete aggregate, steel fibers, performance evaluation.

Title and Abstract (in Arabic)

تقييم الأداء للخرسانة الجيوبوليمرية الخالية من الإسمنت و المصنوعة من الركام الخرساني المعاد تدويره وألياف الفولاذ

الملخص

تم فحص البدائل المستدامة والمبتكرة لتحل محل المكونين غير الصديقين للبيئة وهم الركام والأسمنت. تم إجراء العديد من الدراسات لاستبدال الركام الطبيعي (NA) والأسمنت بركام الخرسانة المعاد تدويره (RCA) والمواد الرابطة الجيوبوليميرية غير العضوية المنشطة القلوية، على التوالي. ومع ذلك، تم اقتراح هذه الخرسانة المستدامة فقط للأغراض غير الهيكلية، بسبب الخصائص السفلية لـ RCA يهدف هذا العمل البحثي إلى سد هذه الفجوة من خلال تقييم جدوى إعادة استخدام RCA من نفايات البناء والهدم والمنتجات الثانوية الصلبة الصناعية المتاحة محليًا في إنتاج الخرسانة الجيوبوليمرية للتطبيقات الهيكلية. كانت مواد الربط إما في شكل سلائف مفردة، خبث فرن صهر حبيبي مطحون (خبث بسيط)، أو مزيج من الخبث والرماد المتطاير. تمت إضافة تقوية الألياف الفولاذية بأجزاء مختلفة الحجم لتعزيز استخدام الخرسانة الجيوبوليمرية الإنشائية المصنوعة من 100 ٪. RCA تمت دراسة السلوك الميكانيكي لهذه الخرسانة الجيوبوليمرية المقواة بألياف الصلب RCA من خلال اختبار مكثف لقوة الانضغاط وقوة الشد الانشقاقي ومعامل المرونة. تم استخدام قوة الانحناء والصلابة والانحراف والقوة المتبقية لوصف أداء الانحناء. في المقابل، تم تقييم خصائص المتانة عن طريق قياس المقاومة الكهربائية، وامتصاص الماء، والامتصاصية، ومقاومة التآكل. كشفت النتائج التجريبية عن القدرة على إنتاج خرسانة جيوبوليمر مخلوطة تعتمد على خبث RCA بنسبة 100٪ وتشتمل على نسبة 2٪ من ألياف الصلب. في الواقع، أظهرت هذه الخرسانة أداءً ميكانيكيًا فائقًا وخصائص متانة مماثلة لمزيج التحكم العادي القائم على NA. على هذا النحو، تقدم هذه الخرسانة لتكون بديلاً مجديًا ومستدامًا للخرسانة التقليدية التي تعد بإعادة تدوير النفايات الصناعية، وتخفيف انبعاثات ثاني أكسيد الكربون، والحفاظ على الموارد الطبيعية دون المساس بالأداء.

مفاهيم البحث الرئيسية: الجيوبوليم، الركام الخرساني المعاد تدويره، الألياف الفولاذية، تقييم الأداء.

Acknowledgements

This thesis has become a reality with the kind help and support of many individuals. I would like to extend my sincere thanks to all of them.

First and foremost, praises and thanks to God the Almighty, for the wisdom that has been bestowed upon me, the strength, and for blessing me throughout my research work to complete this research and thesis successfully.

I would like to express my sincere gratitude towards my advisor and research supervisor, Dr. Hilal El-Hassan, for giving me the opportunity to work on this research and for the support he provided me, and for the invaluable guidance throughout this research. His dynamism, vision, sincerity, dedication, and motivation have deeply inspired and encouraged me. He has taught me to carry out the research and to present the research works as clearly as possible. It was a great privilege and honor to work and study under his guidance. I am extremely grateful to my parents, Eng. Ahmad Samer Medljy and Mrs. Maha Fatayerji for their unconditional love, endless support, and huge sacrifices. I would like to express my sincere thanks and gratitude to them for believing in me and encouraging me throughout this research. My sincere thanks also go to my brother Majd Medljy, for the stimulating discussions, the support, and for being a true friend.

I also would like to thank Dr. Tamer El Maaddawy, for the valuable knowledge and support he provided me throughout the research time. Special thanks to Eng. Abdelrahman Alsallamin, Eng. Tarek Salah and Mr. Faisal Abdulwahab, for their great help in the lab, and my colleagues, Eng. Omar Najm, Eng. Mohammad H.H Alzard, and Eng. Abdalla Moallim Hussein, for all the support they provided.

Dedication

To my beloved parents and family, this humble work is a sign of my love for you.

"I think, therefore I am." - René Descartes.

Table of Contents

List of Tables

List of Figures

List of Abbreviations

I	Absorption
AAS	Alkaline Activator Solution
CA	Coarse Aggregate
f_{cu}	Cube Compressive Strength of Concrete
f'_c	Cylinder Compressive Strength of Concrete
d	Depth of Specimen
D	Diameter of the Cylinder Specimen
DS	Dune Sand
$R_{T,150}^{100}$	Equivalent Flexural Strength Ratio
f_r	Flexural Strength
T_{150}^{100}	Flexural Toughness
GC	Geopolymer Concrete
GGBS	Ground Granulated Blast Slag
L	Length of Specimen
LVDT	Linear Variable Displacement Transducer
P	Load at Peak
LA	Los Angeles Abrasion Test
E_c	Modulus of Elasticity of Concrete
NA	Natural Aggregate
NMS	Nominal Maximum Size
NC	Normal Concrete
OPC	Ordinary Portland Cement
δ_p	Peak Deflection
RCA	Recycled Concrete Aggregate

f_{150}^{100}	Residual Flexural Strength at L/150
f_{600}^{100}	Residual Flexural Strength at L/600
SSD	Saturated Surface Dry
SEM	Scanning Electron Microscope
SH	Sodium Hydroxide
SS	Sodium Silicate
f_{sp}	Splitting Tensile Strength
SF	Steel Fiber
SP	Superplasticizer
SCM	Supplementary Cementitious Material
t	Time
UPV	Ultrasonic Pulse Velocity
b	Width of Specimen
B	Width of the Prism Specimen
XRD	X-ray Diffraction
XRF	X-ray Fluorescence

Chapter 1: Introduction

1.1 Overview

The continuous renovation, rehabilitation, and replacement of aging superstructure and infrastructure have led to an increase in demand for new construction materials. Of these materials, concrete is one of the most produced and consumed. As a result, there is a pressing need for its main components, aggregates, and cement. The production of these constituents consumes non-renewable natural resources and emits carbon dioxide gas, making concrete a non-environment-friendly material. To reduce the environmental footprint and enhance the sustainability of the construction industry, researchers have proposed the replacement of natural aggregates (NA) with recycled concrete aggregates (RCA) from construction and demolition waste. Yet, their use in concrete has been restricted to non-structural, low-grade applications, owing to their inferior physical, mechanical, and durability performance in comparison to natural aggregates [1, 2]. Nonetheless, efforts have been made to improve the properties of concrete incorporating RCA through special treatment methods or modifications to the concrete mixture proportions. However, these techniques are associated with excessive energy or cement consumption, leading to solutions that are not economic, feasible, or environment friendly.

Numerous other studies have addressed the matter of cement replacement. Complete replacement of cement with industrial solid wastes has been successful. The produced inorganic geopolymeric binder promised to reduce carbon emissions, replenish natural resources, and recycle waste materials [3]. As aggregates and cement are the two main components in concrete, it was interesting to realize the effect of replacing them with

more sustainable alternatives. Limited studies investigated the use of RCA in geopolymer concrete. The mechanical and durability properties of such concrete were found to be inferior to those of conventional cement-based concrete made with NA [4-7]. Despite being a promising sustainable material, its adoption by the construction industry is hindered unless it presents comparable performance to its conventional counterpart. In cement-based concrete, this challenge was addressed through the addition of steel fiber reinforcement [8-20]. However, the effect of such a technique on the mechanical and durability properties of RCA geopolymer concrete has not been investigated yet.

1.2 Scope and Objectives

This study aims to investigate the performance of slag-based and slag-fly ash blended geopolymer concrete made with different replacement percentages of RCA and volume fractions of steel fibers. The mechanical and durability properties will be evaluated through standardized tests. The specific objectives of this work are as follows:

- Study the impact of RCA replacement and steel fiber addition on the mechanical properties of slag-based and slag-fly ash blended geopolymer concrete.

- Evaluate the durability properties of slag-based and slag-fly ash blended geopolymer concrete incorporating different quantities of RCA (0, 30, 70, and 100%, by mass) and steel fibers (0, 1, and 2%, by volume).

- Develop correlation equations among the properties of geopolymer concrete made with RCA and steel fibers and compare them to codified equations.

- Conduct a comparative analysis for the performance of steel fiber-reinforced RCA slag-based and slag-fly ash blended geopolymer concrete.

1.3 Outline and Organization of the Thesis

The research work carried out in this thesis is divided into six chapters. They are organized as follows:

- Chapter 1 offers a brief introduction and the research objectives to be addressed in this thesis. Further, it comprises the outline, organization, and research significance of this research work.

- Chapter 2 provides a comprehensive literature review on the available studies related to geopolymer concrete. Topics include fundamental background on concrete and geopolymers, replacement of NA by RCA in geopolymer concrete, and incorporation of steel fibers in geopolymer concrete.

- Chapter 3 highlights the properties and characteristics of the as-received materials, geopolymer mixture proportioning, and geopolymer concrete sample preparation. It also includes the experimental testing methodologies used to assess the mechanical and durability properties of geopolymer concrete.

- Chapter 4 presents the experimental test results, including compressive and splitting tensile strengths, compressive stress-strain curves, modulus of elasticity, water absorption, sorptivity, and abrasion resistance of 100% slag and slag-fly ash blended geopolymer concrete mixes incorporating RCA and steel fibers. The flexural performance, comprising load-deflection curves, strength, deflection, toughness, and residual strength are also illustrated and discussed. Correlations among these different properties are finally developed.

- Chapter 5 provides a detailed comparative analysis for the performance of slag-based and slag-fly ash blended geopolymer concrete with a focus on the effect of RCA replacement and steel fiber addition.

- Chapter 6 summarizes the research findings and provides the general conclusions and limitations of the completed thesis work. It also offers recommendations for future work on RCA geopolymer concrete incorporating steel fibers.

1.4 Research Questions

The replacement of natural aggregates by RCA has negatively impacted the performance of geopolymer concrete. The addition of steel fibers is a promising solution that may reverse this effect. However, there is a lack of knowledge about the mechanical and durability performance of steel fiber-reinforced RCA slag-based and slag-fly ash blended geopolymer concrete. Accordingly, this work aims to provide answers to the following research questions:

- What is the influence of replacing NA by RCA on the mechanical and durability performance of slag-based and slag-fly ash blended geopolymer concrete?

- What is the effect of adding steel fibers on the mechanical and durability performance of slag-based and slag-fly ash blended geopolymer concrete incorporating RCA?

- Can codified equations be applied to steel fiber-reinforced RCA geopolymer concrete or will newly developed equations be more valid?

- What is the difference in performance between slag-based and slag-fly ash geopolymer concrete made with RCA and steel fibers?

Chapter 2: Literature Review

2.1 Introduction

This chapter summarizes and discusses the findings of available research work on geopolymer concrete. The backgrounds of the production of concrete and the geopolymerization process are first described. Further, the use of recycled concrete aggregates and steel fibers in geopolymer concrete is highlighted. At the end of this chapter, the research significance is presented.

2.2 Concrete and the Environment

Concrete is one of the most consumed industrial materials with a total global consumption of approximately 15 billion tons per year. Its annual production has surpassed the mark of one cubic meter per capita [21]. These numbers are associated with an upsurge in demand for its main constituents, cement, and aggregates. In fact, nearly 4.8 billion tons of Portland cement have been produced per year around the world [22], inducing a pressing need for limestone, one of the main natural resources used in making cement, and a possible acute shortage within 50 years [23, 24].

To manufacture cement, limestone and clay are ground and mixed at elevated temperatures. A total of 1.6 kg of raw materials is consumed in the process of making 1 kg of cement, generating 3.7 MJ of energy and 1 kg of carbon dioxide gas [25, 26]. With 5-7% of the annual global man-made carbon emissions being associated with the cement industry [27, 28], it is clear that the production of cement poses serious ecological, social, and environmental challenges.

Scientists and environmentalists suggested the replacement of cement in concrete with supplementary cementitious material (SCMs). Such SCMs are typically industrial by-products with low and high pozzolanic activity. Their incorporation in the production of concrete promises to reduce cement usage with the added benefit of disposing of industrial solid wastes. These materials include but are not limited to fly ash, slag, metakaolin, microsilica, and rice husk ash, among others. However, the abundance of the former two wastes in the region and the enhancement in overall concrete performance has contributed to their extensive use by the construction industry [29]. Nevertheless, the true potential of utilizing such wastes cannot be fully achieved unless they completely replace cement to produce sustainable concrete mixes.

The other major component in concrete manufacture is aggregates. It typically comprises up to 80% of the concrete, by mass. Based on the current global production of concrete, it is estimated that 12 billion tons of aggregates are consumed annually. These aggregates are typically acquired from natural resources, thus imposing significant stress on their availability in the future. Unless a sustainable replacement is proposed, the irreversible environmental pollution attributed to the construction industry will be overwhelming to the point of no return. One such replacement is a recycled concrete aggregate (RCA) that is processed from construction and demolition wastes (CDW). It consists of 65-70% and 30-35% original aggregate and cement paste, by volume, respectively [30]. Not only does its use in concrete mixes serve to alleviate the demand on natural aggregates, i.e. natural resources, but also recycles such waste rather disposing of them in landfills or stockpiles [31, 32]. Indeed, the management of CDW is a global pressing issue that has resulted in economic leakages and an excessive need for landfills

[33]. Nevertheless, and despite this appealing, cost-effective, and sustainable solution, the use of RCA in structural concrete has not been well-received due to a reduction in the mechanical and durability performance of the RCA concrete product compared to the counterpart made with natural aggregates (NA) [1, 2, 34, 35].

2.3 Background on Geopolymers

Geopolymers are inorganic polymeric materials part of the family of alkali-activated materials [36]. To form a geopolymer, a precursor binding agent that is rich in alumina, silica, and possibly calcium oxide is activated using an alkaline solution. In fact, the chemical composition of this precursor is the determining factor to categorize a geopolymer as a calcium-silicon (Ca-Si) or aluminum-silicon (Al-Si) system [37]. Each of these systems is characterized by certain reaction products and associated with specific concrete performance.

The first system corresponds to the activation of calcium-dominant precursors, such as slag, using an alkaline solution to produce calcium aluminosilicate hydrate (C-A-S-H) gel with a low Ca/Si ratio and high Al content. Such reaction product is coupled with impressive mechanical performance but limited workability and excessive drying shrinkage [38-43]. To promote the use of such a sustainable cement-free product by the cement industry, there is a need to enhance its fresh and durability properties.

The second system relates to the activation of aluminosilicate-rich precursors, such as fly ash, silica fume, metakaolin, or kaolinite clay, among others. The reaction involves dissolution, coagulation, condensation, and crystallization of the reactants to produce sodium aluminosilicate hydrate (N-A-S-H) gel within three-dimensional networks [37].

For fly ash, a study by Fernández-Jiménez and Puertas [44] noted that class F fly ash was most suitable for optimum geopolymerization reaction. Nevertheless, the activation of this Al-Si system typically required heat curing at temperatures up to 80°C. Accordingly, the adoption of such geopolymer by the construction industry for cast-in-place concrete applications is hindered. Thus, to promote its utilization, the curing should take place at ambient conditions.

It is apparent that each of these systems, individually, has several issues. Thus, it was suggested to combine them into a blended system that balances between maximizing the fresh and hardened properties while curing at ambient conditions [45-60]. The performance was indeed superior to counterparts made with a single precursor binder, owing to the coexistence of C-A-S-H and N-A-S-H gels at a higher cross-linking degree [61]. The proposed blended system has been accepted by the construction industry and has been applied in practice in high-rise buildings, precast structural concrete members, slabs, and wall panels, among others [62, 63].

As for the alkaline activator solutions, the typical practice involved the combination of sodium or potassium hydroxide with corresponding sodium or potassium silicate. Nevertheless, some researchers investigated the use of a single activator [44, 64]. The addition of water, in most cases, was to provide a transport medium and enhance the workability, as it was not directly involved in the geopolymeric activation reaction [65].

2.4 Slag-based Geopolymer Composites

To be adopted by the construction industry for cast-in-situ applications, geopolymer products should not rely on heat curing. Such geopolymers are typically

dominated by the Ca-Si system. Slag-based geopolymer concrete cured in ambient conditions has been extensively investigated in the past. While some researchers denoted mixes as alkali-activated slag, the designation in this thesis will be consistent as slag-based geopolymer.

Puertas et al. [66] examined the effect of mixing time on the fresh and hardened properties of slag-based geopolymer activated with sodium silicate or sodium hydroxide. Results showed that extended mixing of geopolymer activated with sodium silicate had better rheological and mechanical properties. Conversely, mixes activated with sodium hydroxide experienced a decrease in rheology and an increase in mechanical performance upon further mixing.

Ray et al. [67] investigated the influence of elevated curing temperatures up to 500°C on the mechanical properties of geopolymer concrete made with slag. Results showed that curing up to 100 and 200°C increased the 28- and 56-day strengths after which they both decreased, owing to the expansion of aggregates and elevated thermal effect. A less porous structure and enhanced binding capacity were also noted with temperature.

Bernal et al. [68] evaluated the mechanical and durability performance of geopolymer concrete made with 300-500 kg/m^3 of slag. Results showed that an increase in binder content led to higher compressive strength, water sorptivity, permeability, and carbonation resistance.

Collins and Sanjayan [69] studied the performance of slag-based geopolymer exposed to different curing regimes. The authors found that higher strength was obtained when samples were cured in a water bath or sealed compared to being exposed to open air

in the laboratory. This was primarily owed to the development of microcracks on the surface within the first three days of age with crack widths expanding over time.

Collins and Sanjayan [70] also investigated the workability and mechanical properties of slag-based geopolymer concrete using two types of activator solutions. The use of powdered sodium silicate did not have a significant impact on the slump of concrete compared to samples made with liquid sodium silicate. The compressive strength at 1 day was similar to that of cement-based concrete but higher at 28 days. Nevertheless, the geopolymer concrete experienced drying shrinkage and cracking at a later age.

The workability of slag geopolymer concrete incorporating different admixtures was assessed [71]. Lignosulphonate admixture enhanced the workability and shrinkage resistance but reduced the setting time and strength development. Conversely, naphthalene formaldehyde superplasticizer led to an increase in shrinkage and decrease in strength.

Bondar et al. [72] developed and validated a mix design procedure for slag-based geopolymer concrete. Results highlighted the ability to enhance the workability of such concrete by increasing the binder content beyond 400 kg/m^3. Yet, an increase in porosity may be expected. The strength of these concrete mixes was C16/20 to C32/40.

A new type of high-performance self-compacting geopolymer concrete was developed using slag as the sole binder. Compressive strength values exceeded 70 MPa while maintaining excellent workability for a self-compacting nature. Upon exposing this concrete to an aggressive magnesium sulfate environment, a loss in strength was experienced. Similar findings were noted when subjecting the concrete to elevated temperatures.

Recently, slag-based geopolymer concrete was produced using seawater and sea sand [73]. Samples experienced higher drying shrinkage and lower chloride ion penetration compared to counterparts made with fresh water and river sand. Nevertheless, the hydration product was mainly C-A-S-H gel.

In other work utilizing alternative sand, the performance of slag-based geopolymer concrete made with waste foundry sand was evaluated [74]. The replacement of natural sand with up to 40% waste foundry sand reduced the workability of geopolymer concrete but enhanced the strength and sorptivity.

The effect of different mixture proportions and curing temperatures on the mechanical properties of slag-based geopolymer concrete was studied [75-77]. The authors concluded that an increase in sodium hydroxide molarity and sodium hydroxide-to-sodium silicate ratio increased the mechanical properties. The curing temperature and solution-to-slag ratio had an adverse effect.

2.5 Blended Geopolymer Composites

Based on past literature, a blended system combining Ca-Si and Al-Si provided more optimal performance. As such, this section focuses on the performance of geopolymer composites incorporating calcium- and aluminosilicate-rich precursors, such as slag and fly ash. In fact, Shang et al. [78] noted that adding slag to fly ash-based geopolymer improved the early-age properties. Also, it was reported that blending the two precursors was essential to optimize setting time, workability, volume stability, mechanical performance, and durability properties.

The mechanical properties of fly ash-slag blended geopolymer pastes were evaluated by Puertas et al. [79]. The main contributors to the development of strength were found to be the fly ash-to-slag ratio and alkaline activator content and concentration. Upon the incorporation of slag, the impact of curing at elevated temperatures was less prominent. Further, a compressive strength of around 50 MPa was attained in an optimum mix made with a 1:1 slag:fly ash ratio, a sodium hydroxide solution with a molar concentration of 10, and cured at ambient 25°C.

In similar work, Garanayak [50] examined the performance of alkali-activated fly ash-slag blended paste under ambient curing conditions. The slag-to-fly ash ratio and molarity of the sodium hydroxide solution were varied to maximize mechanical strength. Results showed that strength of 89 MPa could be attained with slag:fly ash ratio of 7:3 and solution molarity of 12.

Rafeet et al. [80] also noted an increase in compressive strength when slag was added to fly ash-based geopolymer pastes. In their work, the authors refrained from curing in the oven to promote the use of geopolymer in construction applications. The developed blended paste mixes were found to be more environment-friendly and less costly as less activator was in the mixture proportioning.

In other work, Nath and Sarker [81] added slag to fly ash-based geopolymer concrete to promote curing at room temperature. The blended binder was activated in an alkaline solution combining sodium hydroxide and sodium silicate. The authors reported that it was possible to proportion the geopolymer concrete mixture proportions for

optimum workability and setting time while being able to attain high compressive strength. In fact, a strength of 55 MPa was noted when slag replaced 30% fly ash.

The mechanical properties of slag-fly ash blended geopolymer concrete were also investigated by Sofi et al. [82]. The development of splitting tensile and flexural strength of geopolymer concrete mixes was found to be similar despite having a difference of around 2 MPa. A comparison to the values predicted from equations developed by AS3600 [83] for conventional cement-based concrete highlighted the possibility to use these equations for slag-fly ash blended geopolymer concrete.

Moreover, Deb et al. [48] studied the effect of replacement of fly ash by slag to create a blended geopolymer concrete. Results showed an increase in compressive and tensile strength when fly ash was replaced by 10-20% slag with values of the former reaching 51 MPa. Simultaneously, a decrease in workability was reported. It is also worth noting that geopolymer concrete samples incorporating slag were cured at 20°C. When compared to equations of ACI 318 [84] and AS3600 [83], tensile strength results of ambient-cured geopolymer concrete could be accurately predicted while less accurate predictions were obtained for counterparts cured at elevated temperatures.

Prusty and Pradhan [85] examined the influence of adding slag on the fresh and hardened properties of fly ash-based geopolymer concrete. A decrease in a slump was reported upon the addition of slag, owing to their higher water demand. The 7-day compressive strength was found to be nearly 80% higher when fly ash was partially replaced by slag. Also, lower potential values, corresponding to better corrosion

resistance, were obtained upon incorporating slag into fly ash-based geopolymer concrete mixes.

The mixture proportions of fly ash-based geopolymer concrete with slag replacement of up to 20% were optimized by Mehta et al. [57]. Experimental findings highlighted that the optimum mix included a solution-to-fly ash ratio of 0.55, a sodium silicate-to-sodium hydroxide ratio of 2.5, and molarity of sodium hydroxide solution of 10. Also, results showed that 20% slag replacement increased the 3-day compressive strength to 65 MPa, achieving up to 99% of that at the age of 28 days.

The effect of slag incorporation on the compressive strength and modulus of elasticity of fly ash-based geopolymer concrete was evaluated by Bellum et al. [46]. A 70% replacement of fly ash by slag resulted in the highest compressive strength and modulus of elasticity with values reaching 38 MPa and 20 GPa, respectively.

Additionally, Prusty and Pradhan [86] examined the influence of mixture proportioning on the mechanical behavior of fly ash geopolymer concrete. Results showed that the 45% replacement of fly ash with slag, a sodium hydroxide solution molarity of 14, and a sodium silicate-to-sodium hydroxide ratio of 1.5 were optimum for maximum compressive, splitting tensile, and flexural strengths.

The mechanical and durability performance of slag-fly ash blended concrete was investigated by Yazdi et al. [87]. As more slag was incorporated into the mix, the compressive and flexural strengths attained up to 100 and 10 MPa, respectively, while the porosity decreased. Yet, it is worth noting that slag replacement more than 50% did not affect the performance as significantly.

Unlike conventional concrete, where a systematic mix design methodology has been developed and adopted, geopolymer concrete depends on the trial and error method. Yet, Reddy et al. [88] proposed and validated a procedure to proportion the mixture components for slag-fly ash blended geopolymer concrete. The ratios of fly ash-to-slag and solution-to-binder were set to 7:3 and 0.4-0.8. As the solution content increased, the workability, i.e., slump, increased, while the compressive strength decreased. However, compared to the impact of the water-to-cement ratio on the strength of conventional cement-based concrete, that of solution-to-binder ratio was less severe.

In other work, Lau et al. [89] designed an amorphous mix design framework for slag-fly ash blended geopolymer concrete. Results showed that the optimum Si/Al and (Na+2Ca)/Al ratios were 2.3 and 3.2, correspondingly, with compressive strength reaching up to 69 MPa.

Lee et al. [55] investigated the resistance of slag-fly ash blended geopolymer concrete to weathering and chloride penetration. Concrete mixes were cured for 180 days in outdoor and indoor conditions. The compressive strength increases with time to reach 53 and 67 MPa for each respective curing technique.

Samantasinghar and Singh [90] studied the effect of curing on slag-fly ash blended geopolymer concrete. It was found that curing at elevated temperatures was critical for fly ash-based mixes. In contrast, those incorporating slag experienced microcracks upon utilizing heat curing. Moreover, the highest strength development among the different curing techniques was noted for samples that were exposed to autoclaving and microwave radiation.

In most of the above work, the amount of fly ash was more than slag. In other words, the geopolymer was denoted as fly ash-based. However, the effect of adding fly ash to slag-based geopolymer mortar and concrete was also studied [39, 91-94]. Results showed that the addition of fly ash up to around 25-50% led to an increase in compressive strength and modulus of elasticity while becoming less dependent on heat curing. For such concrete, the influence of different curing regimes was examined [40, 49]. It was reported that a combination of open-air and water curing was optimum for slag-based geopolymer concrete mixes incorporating up to 25% fly ash. Yet, as more fly ash was added to the mix, the effect of curing was less apparent with compressive strength still achieving 40 MPa. Thus, to promote the adoption of geopolymer concrete by the construction industry, the binding agent can be a slag-fly ash blend with not more than 25% FA.

2.6 Recycled Aggregate Geopolymer Concrete

To improve the sustainability aspect of geopolymer concrete, several researchers investigated the feasibility to replace natural aggregates (NA) with recycled concrete aggregate (RCA). The focus of most of these studies was on the effect of RCA replacement on the mechanical performance of geopolymer concrete. Generally, the results showed that the RCA geopolymer concrete experienced inferior performance compared to NA-based counterparts, owing to the porous nature of RCA and the weak bond between the mortar and RCA [95]. This section provides a more in-depth review of these studies.

Peem Nuaklong [96] examined the influence of RCA on the properties of fly ash-based geopolymer concrete. Results showed that RCA can be used with fly ash

geopolymer concrete while slightly compromising the performance and loss of less than 10% in terms of the compressive strength.

The mechanical performance of fly ash-based geopolymer concrete made with up to 100% RCA as a replacement of NA was studied by Shi et al. [97]. The fly ash-based RCA geopolymer concrete exhibited higher compressive strength and elastic modulus compared to the cement-based RCA concrete, owing to a better interfacial transition zone. Nevertheless, the mechanical properties decreased with an increase in RCA replacement.

Nuaklong et al. [98] evaluated the influence of RCA on the mechanical and durability performance of high calcium fly ash-based geopolymer concrete. Compared to counterparts made with crushed limestone aggregates, geopolymer RCA concrete mixes showed slightly lower compressive strength but could reach up to 38 MPa. Also, the durability of geopolymer concrete was enhanced upon using a sodium hydroxide with higher molarity.

In similar work, Shaikh [99] assessed the mechanical and durability properties of fly ash-based RCA geopolymer concrete. The RCA in this work was obtained from local demolition and waste and set to replace natural aggregates by 15, 30, and 50%, by weight. Decreases in compressive strength, splitting tensile strength, and modulus of elasticity were reported when 50% of NA was replaced by RCA in the mix. The durability performance, including sorptivity and chloride penetration, was adversely impacted by this replacement as well.

Furthermore, the effect of replacing NA by RCA on the properties of slag-based geopolymer concrete was studied by Kathirvel and Kaliyaperumal [5]. Samples were

cured in ambient conditions to simulate industrial practice. With up to 50% RCA replacement, the concrete was characterized by lower porosity or voids, leading to an increase in the compressive strength development. Yet, higher RCA replacement had an adverse impact on the performance, including strength, sorptivity, and chloride diffusion.

Mesgari et al. [100] examined the performance of geopolymer and cement-based concrete made with different RCA replacement percentages, including 0, 20, 50, and 100%. Reductions in the compressive strength, modulus of elasticity, and flexural strength were 14, 1, and 3%, respectively, with up to 20% RCA replacement. Nevertheless, higher RCA replacement of up to 100% resulted in respective decreases of 33, 26, and 21%.

Xie et al. [101] investigated the effect of RCA replacement on the fresh and hardened properties of geopolymer concrete incorporating slag and metakaolin. It was reported that, when RCA replacement was 100%, the compressive strength decreased by up to 35%, while the slump increased by 75%. The compressive toughness was also reduced upon replacing NA with RCA.

The effect of slag and RCA replacements on the properties of fly ash-based geopolymer concrete was studied by Hu et al. [6]. The workability decreased as more slag was added to the mix, while it increased upon RCA replacement. Compared to the best NA geopolymer mix, the compressive strength, modulus of elasticity, splitting tensile strength, and flexural strength reduced for mixes made with 30% slag and 100% RCA. Nevertheless, its values were superior to mixes made with fly ash as the sole binder.

Xie et al. [102] and Xie et al. [103] evaluated the fresh and hardened properties of slag-fly ash blended geopolymer concrete with 100% RCA replacement. The slump

increased upon replacing NA with RCA due to the additional water required for the higher absorption capacity of the latter aggregate. On the other hand, the compressive strength and modulus of elasticity reduced by 16 and 21%, respectively.

2.7 Geopolymer Concrete Reinforced with Steel Fiber

Geopolymer concrete has been suggested as a more sustainable substitute to conventional cement-based concrete. Notwithstanding its impressive performance, geopolymer concrete has little tensile and flexural properties alongside a brittle behavior. To counter the brittle characteristics in conventional concrete, fiber reinforcement has been suggested. Such fibers have also been utilized in geopolymer concrete. The following section summarizes the work that has used steel fibers in geopolymer concrete and mortar.

Guo and Pan [104] studied the effect of different volume fractions and types of fibers on the mechanical properties of slag-fly ash blended geopolymer concrete. Among the various fibers investigated, steel fibers seemed to have the most significant positive impact on the flexural and tensile strength of geopolymer concrete.

Bernal et al. [105] evaluated the impact of steel fibers on the mechanical properties of slag-based geopolymer concrete. Results showed that the steel fibers reduced the compressive strength, water absorption, and sorptivity but improved the splitting tensile and flexural strengths of geopolymer concrete compared to mixes without fibers.

The flexural behavior of steel fiber-reinforced geopolymer concrete beams was evaluated by Devika and Nath [106]. The incorporation of steel fibers transformed the brittle geopolymer matrix into a more ductile one. It also significantly improved the tensile properties, including stress, strain, and toughness.

Al-Majidi et al. [107] evaluated the hardened properties of steel fiber-reinforced geopolymer concrete cured in ambient conditions. Experimental results revealed that steel fiber incorporated led to a loss in the compressive strength of the geopolymer made with 10 and 20% slag. Yet, at higher slag additions, the strength was significantly superior to the plain respective mixes, i.e., without steel fibers.

Islam et al. [15] developed geopolymer concrete made with palm oil fuel ash and slag. The aggregates were in the form of oil palm shell, while hooked-end steel fibers were employed. The study focused on understanding the impact resistance of the concrete upon fiber incorporation. Compared to plain geopolymer concrete, the addition of 0.5% steel fibers, by volume, increased the splitting tensile strength by up to 38%, the flexural strength by up to 44%, and the first crack load by up to 3.5 times.

Steel fibers were added to slag-based geopolymer concrete incorporating up to 50% fly ash. The effect of adding fibers on the mechanical properties was investigated [38, 108]. Upon the addition of 2% steel fibers, by volume, increases of 30, 31, and 25% were reported for the compressive, splitting tensile, and flexural strengths, respectively.

The impact of steel fibers and silica fume on the performance of ultra-high performance geopolymer concrete was studied by Liu et al. [109]. The workability decreased when steel fibers were added to the geopolymer concrete whereas the mechanical properties, including modulus of elasticity, splitting tensile strength, compressive strength, flexural strength, fracture energy, and stress intensity factor, increased.

Guo and Xiong [110] evaluated the durability performance of steel fiber-reinforced slag-fly ash blended geopolymer concrete reinforced. Samples were exposed to sulfate corrosion and drying-wetting cycles and the durability was assessed using strength retention. The addition of 0.4% steel fiber, by volume, maintained a geopolymer concrete compressive strength at 68 MPa even after 15 durability cycles.

Gülşan et al. [111] studied the effect of steel fiber addition on the properties of self-compacting fly ash-based geopolymer concrete. Steel fibers were added up to 1%, by volume. Results highlighted a reduction in slump flow, V-funnel flow time, flow time, and L-box passing ability. As for the mechanical properties, the incorporation of steel fibers enhanced the bond resistance, flexural strength, fracture toughness, and stress intensity factor.

Their and Özakça [112] added nanosilica and steel fibers to fly ash-based geopolymer concrete. The combined addition of these two materials allowed the compressive strength to attain 57 MPa alongside better water penetration resistance. Nevertheless, 1% steel fiber volume fraction improved the overall performance, but higher volume fractions led to a decrease in sorptivity and water penetration due to balling and higher void content.

The performance of steel fiber-reinforced geopolymer concrete post-exposure to elevated temperatures was examined by Shaikh and Hosan [113]. Steel fibers maximized the residual compressive and splitting tensile strength after high-temperature exposure. Limited cracking and spalling were also noted in steel fiber-reinforced samples.

Khan et al. [114] evaluated the mechanical performance of high-strength geopolymer concrete reinforced two types of steel fibers, namely spiral and hooked-end. The addition of steel fibers led to a reduction in the workability but an increase in compressive strength, load carrying capacity, toughness, and residual strength in comparison to plain counterparts.

2.8 Research Significance

Infrastructure and superstructures require constant replacement, rehabilitation, and renovation. This results in significant upsurges in the demand for new construction materials. Hence, more concrete will be needed, as it is one of the most used materials by the construction industry. This will place tremendous stress on the production of cement and supply of non-renewable natural aggregates, thereby consuming and diminishing the global supply of natural resources. As such, there is a pressing need to provide new materials to be used in the production of concrete. For aggregates, RCA has been suggested as a viable and sustainable alternative to NA that not only relieves the stress build-up on NA but also promises to beneficially recycle wastes from construction and demolition activities. For cement, geopolymer binders have been advocated as a more sustainable substitute to cement, as it allows to reutilize industrial wastes in the making of construction materials while reducing the production of cement, i.e., diminishing the emissions of carbon dioxide and preserving the natural resources.

The combination of these two solutions is optimal. However, the inferior mechanical and durability performance of RCA geopolymer concrete has limited its use to non-structural applications and hindered its adoption by the construction industry.

Indeed, several research works aspired to replace 100% NA with RCA but compromised the performance. Another reason for the limited use of geopolymer concrete, in general, is its brittle behavior. Accordingly, some research studies have investigated the addition of steel fiber reinforcement to geopolymer concrete made with NA to transform it into a more ductile material. With promising results, it seems that steel fibers may have a positive impact on the performance of geopolymer RCA concrete. Yet, no such study has been conducted on slag-based or slag-fly ash blended geopolymer concrete.

This research aims to fill this gap by evaluating the feasibility of producing a geopolymer concrete made with 100% RCA and steel fibers. The mixes will either utilize slag as the sole binder or a blend of slag and fly ash. Such an alteration in the binder serves to provide an understanding of the combined effect of RCA, steel fibers, and fly ash through a comparative analysis. The mechanical and durability performance of this sustainable concrete will be assessed. The experimental investigation and in-depth analysis of results will provide much-needed evidence on the ability to utilize steel fiber-reinforced geopolymer RCA concrete as a construction material that promises to reduce the demand for NA and cement, thereby enhancing the sustainability of the construction industry.

Chapter 3: Experimental Program

3.1 Introduction

The experimental program conducted in this research consists of designing, preparing, casting, and testing different geopolymer concrete mixes. These geopolymer concrete mixes were designed using two blends of binding materials, namely 100% slag and 3:1 slag-to-fly ash ratio. Recycled concrete aggregates (RCA) replaced normal coarse aggregates (NA) in proportions ranging from 0 to 100%. Abundant desert dune sand was employed as a sustainable fine aggregate in all mixes. Steel fibers were incorporated into the geopolymer concrete mixes in volumetric fractions up to 2%. Different specimens were used in various experimental tests to evaluate the mechanical properties, short-term durability performance, and microstructure of the geopolymer concrete. The details of the as-received materials, concrete mixture proportioning, experimental program, and testing methods are provided in this chapter.

3.2 Test Program

At the early stages of the thesis work, several trial mixes were designed, cast, and tested to obtain a cylinder compressive strength of 30 MPa. Such strength is typical for most concrete structures in the United Arab Emirates (UAE). Unlike conventional cement-based concrete, the mix design of geopolymer concrete does not follow a standard procedure. For this reason, the trial-and-error approach was adopted. Results are presented in Appendix A.

Table 1: Experimental test matrix

Group	Subgroup	Mix Number	Mixture				Mix Designation
			Slag %	Fly ash %	RCA %	SF %	
1	1	1	100	0	0	0	S100R0F0
	2	2	100	0	30	0	S100R30F0
		3	100	0	30	1	S100R30F1
		4	100	0	30	2	S100R30F2
	3	5	100	0	70	0	S100R70F0
		6	100	0	70	1	S100R70F1
		7	100	0	70	2	S100R70F2
	4	8	100	0	100	0	S100R100F0
		9	100	0	100	1	S100R100F1
		10	100	0	100	2	S100R100F2
2	1	11	75	25	0	0	S75R0F0
	2	12	75	25	30	0	S75R30F0
		13	75	25	30	1	S75R30F1
		14	75	25	30	2	S75R30F2
	3	15	75	25	70	0	S75R70F0
		16	75	25	70	1	S75R70F1
		17	75	25	70	2	S75R70F2
	4	18	75	25	100	0	S75R100F0
		19	75	25	100	1	S75R100F1
		20	75	25	100	2	S75R100F2

A test matrix was developed to study the effect of different recycled aggregate replacement ratios, steel fibers volume fractions on the performance of two types of

geopolymer concrete, i.e., one made with 100% slag, and another made with a 3:1 slag-to-fly ash ratio. The matrix is shown in Table 1. It is mainly divided into two main categories, representing the two blends of binding materials, which are subsequently categorized into four subgroups that signify the change in recycled aggregate replacement percentage, including 0, 30, 70, and 100%. The steel fiber volume fraction altered among 0, 1, and 2% within each subgroup. As a result, a total of 20 mixes were designed in this work. They are designated as SxRyFz, where x, y, and z denote the percent of binder that is slag, the recycled aggregate replacement percentage, and the steel fiber volume fraction, respectively. For instance, S100R30F1 refers to the concrete mixture that contains 100% slag as the binder material, 30% recycled aggregate replacement, and 1% steel fibers, by volume.

3.3 Material Properties

The materials used in this study included the binding material, i.e., slag and fly ash, coarse aggregates, including natural aggregates and recycled concrete aggregates, fine aggregates in the form of desert dune sand, chemical activators, and steel fibers. The properties of each material are shown in the below sub-sections.

3.3.1 Binding Material

The binding materials used in this work include slag and fly ash. The slag was obtained from Emirates Cement with a Blaine fineness of 4250 cm^2/g and a specific gravity of 2.70. In comparison, the fly ash was sourced from Ashtech India, having a Blaine fineness and specific gravity of 3680 cm^2/g and 2.32, respectively. Particle size

distribution, scanning electron microscopy (SEM) micrographs, and X-ray diffraction (XRD) spectra of slag and fly ash are shown in Figures 1 and 2, respectively. Figures 1(a-c) highlight the fine, irregular slag amorphous structure with peaks of quartz (SiO_2), mullite ($3Al_2O_3 \cdot 2SiO_2$), and gehlenite ($Ca_2Al\,[AlSiO_7]$) being identified in XRD. In comparison, the spherical structure of fly ash and the XRD peaks of (SiO_2), mullite ($3Al_2O_3 \cdot 2SiO_2$), and hematite (Fe_2O_3) are shown in Figures 2(a-c). The chemical composition and physical properties of the as-received materials are presented in Table 2.

Table 2: Chemical composition of as-received materials

Oxides	Material (%)		
	Slag	Fly ash	Dune sand
CaO	42.0	3.3	14.1
SiO_2	34.7	48.0	64.9
Al_2O_3	14.4	23.1	3.0
MgO	6.9	1.5	1.3
Fe_2O_3	0.8	12.5	0.7
Loss on ignition	1.1	1.1	0.0
Others	0.2	10.5	16.0
Physical properties			
Blaine Fineness (cm^2/g)	4250	3680	-
Specific gravity	2.70	2.32	2.77
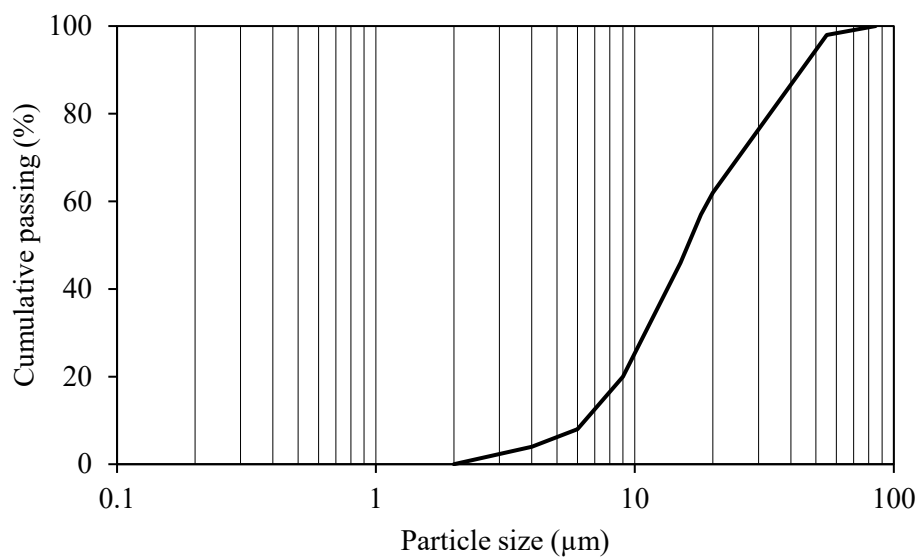
(a)
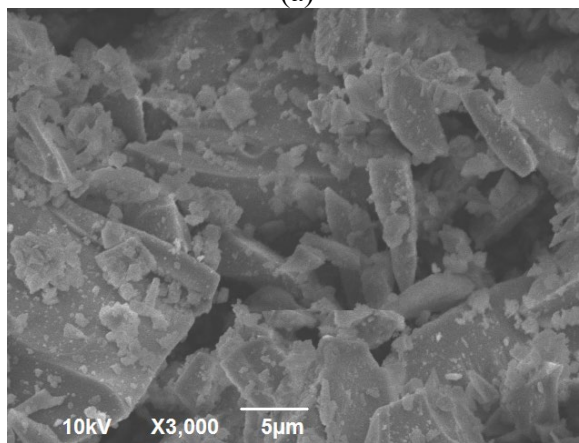
(b)
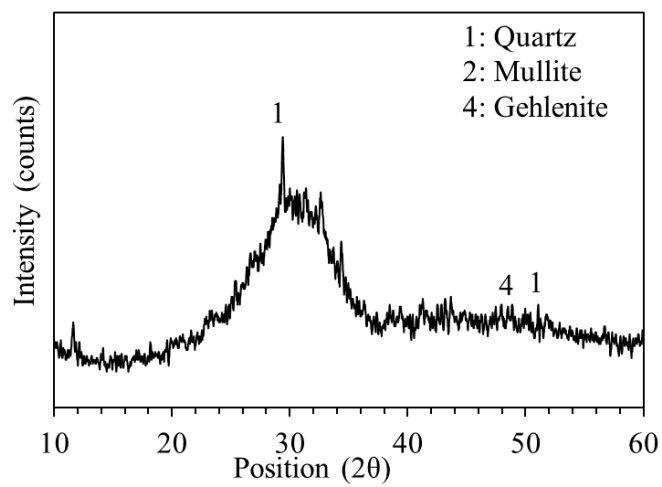
(c)

Figure 1: Binding material properties (Slag). (a) Particle size distribution; (b) SEM micrograph; and (c) XRD spectrum of slag
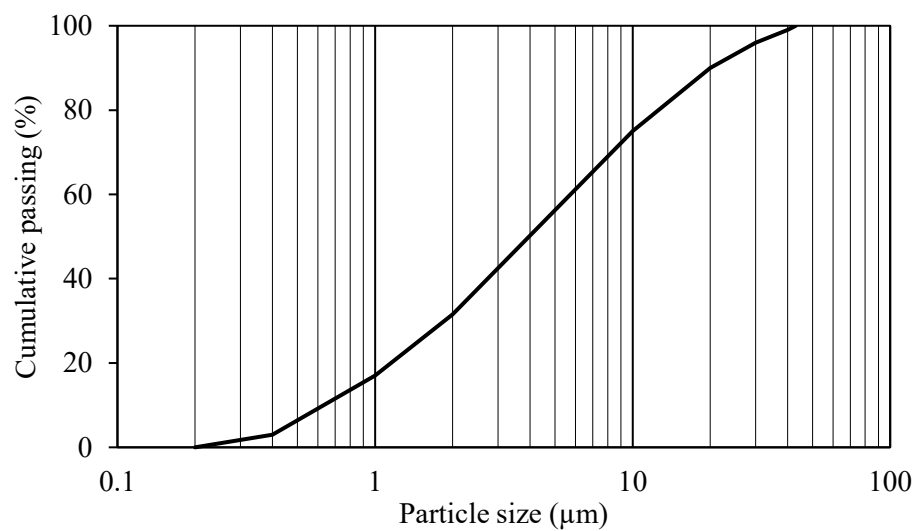
(a)
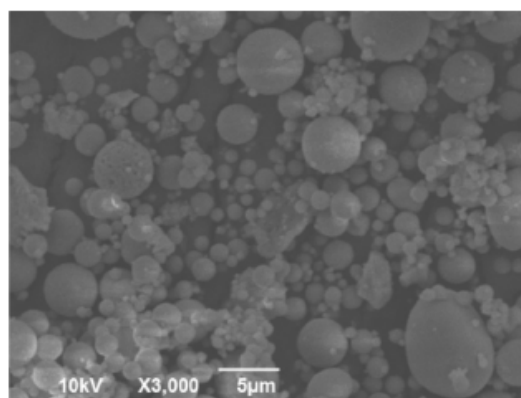
(b)
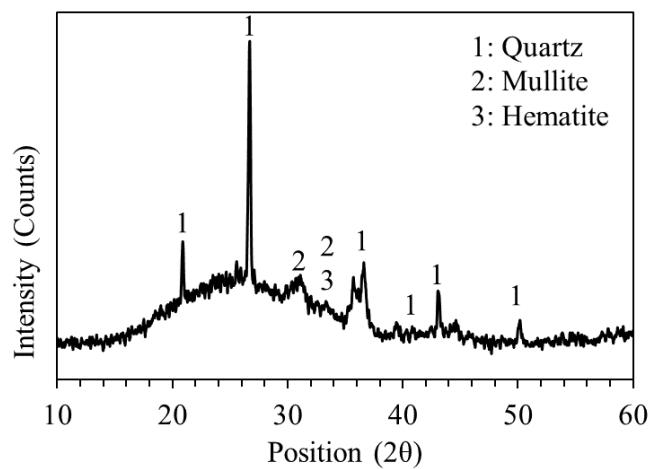
(c)

Figure 2: Binding material properties (Fly-ash). (a) Particle size distribution; (b) SEM micrograph; and (c) XRD spectrum of fly ash

3.3.2 Coarse Aggregates

The coarse aggregates used in this work were in the form of natural crushed dolomitic limestone coarse aggregates and recycled concrete aggregates. The natural aggregates were obtained from Ras Al Khaimah, UAE, with a nominal maximum size (NMS) of 20 mm, while the recycled counterparts were sourced from Al Dhafra Recycling Industries, Abu Dhabi, UAE, having an NMS of 25 mm, in their as-received conditions. The grading curves of both aggregates and their corresponding blends are illustrated in Figure 3. It is worth noting that all curves satisfy the limits set by ASTM C33 [115]. Further, the physical properties of the two types of coarse aggregates are shown in Table 3. The dry-rodded density and specific gravity of RCA were lower than those of NA, owing to the porous mortar attached to the surface of the RCA particles. In turn, the absorption, abrasion mass loss, soundness, and mass loss were higher in RCA than NA. This highlights the relatively weaker nature of the former compared to the latter. Nevertheless, it should be pointed out that the absorption of aggregates was accounted for by bringing them up to saturated surface dry (SSD) conditions prior to incorporation into the mixes.

Table 3: Physical properties of fine and coarse aggregates

Property	Unit	Standard Test	NA	RCA
Specific gravity	-	ASTM C127 [116]	2.82	2.63
Fineness modulus	-	ASTM C136 [117]	6.82	7.44
Soundness (MgSO$_4$)	%	ASTM C88 [118]	1.20	2.78
Absorption	%	ASTM C127 [116]	0.22	6.63
Los Angeles abrasion	%	ASTM C131 [119]	16.0	32.6
Dry-rodded density	kg/m^3	ASTM C29 [120]	1635	1563
Surface area	cm^2/g	ASTM C136 [117]	2.49	2.50
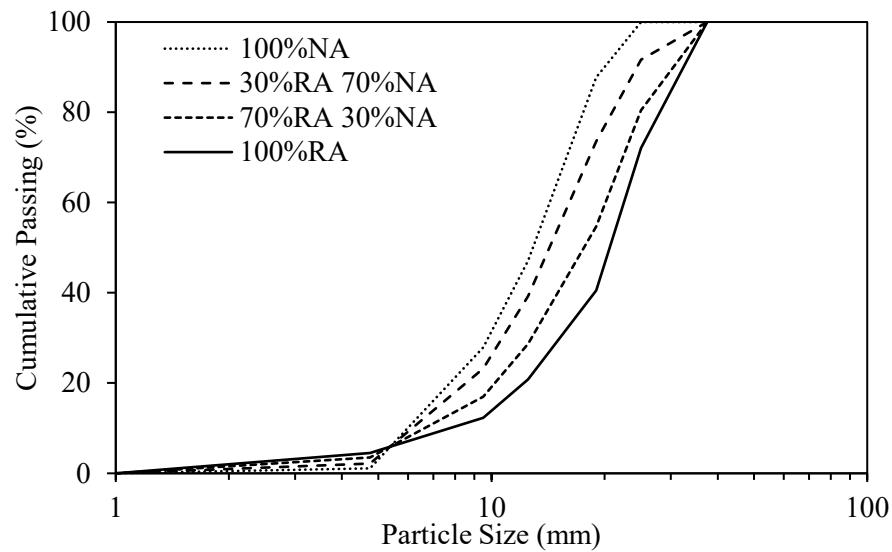
Figure 3: Particle size distribution of different mixes of NA and RCA

3.3.3 Fine Aggregates

Desert dune sand served as the fine aggregate in the geopolymer concrete mixtures. Their abundance in the UAE renders them the more sustainable alternative to the typical crushed stone used in the market. Its chemical composition mainly consists of silica, calcium oxide, and alumina, as shown in Table 2. The particle size distribution, SEM micrograph, and XRD spectrum are illustrated in Figure 4. Further, its dry-rodded density, specific gravity, surface area, and fineness modulus are 1663 kg/m^3, 2.77, 116.8 cm^2/g, and 1.45, respectively.
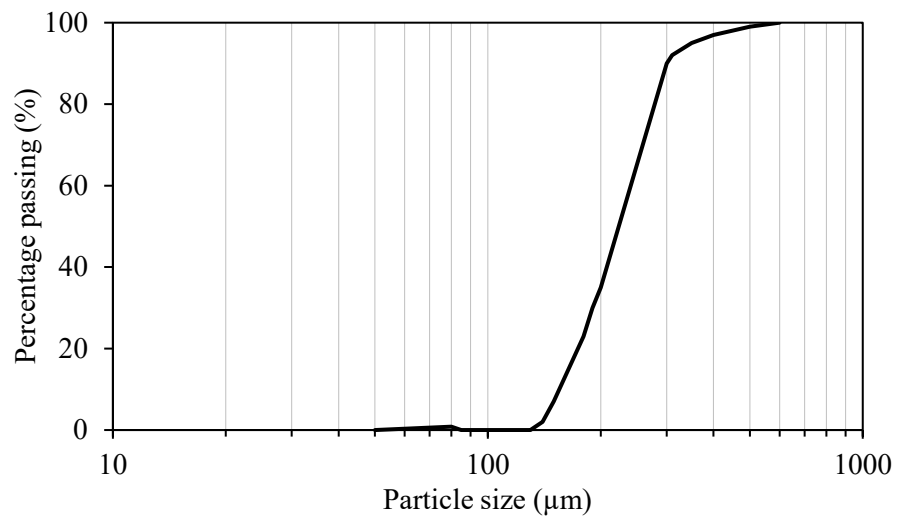
(a)
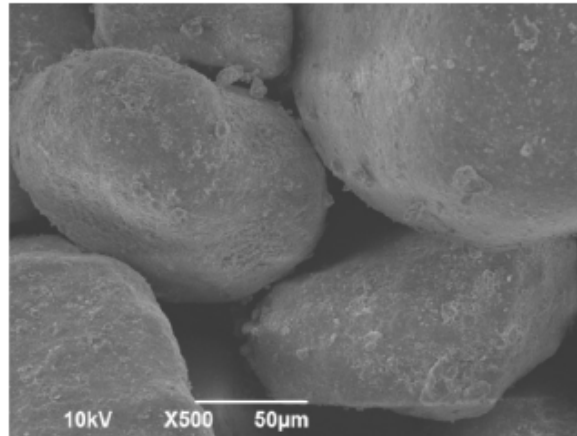
(b)
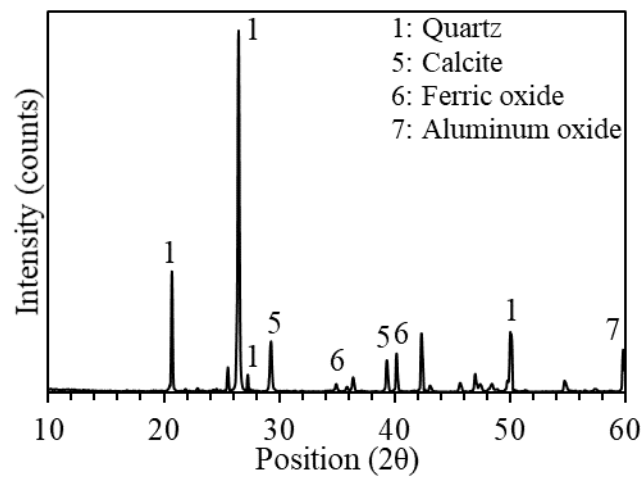
(c)

Figure 4: Fine aggregate properties. (a) Particle size distribution; (b) SEM micrograph; and (c) XRD spectrum of dune sand

3.3.4 Chemical Activators

The alkaline activator solution consisted of sodium hydroxide (SH) and sodium silicate (SS). The two chemicals were obtained from Al Rama Industries, UAE. The SH was in the form of 97-98% pure NaOH flakes. It was dissolved in tap water to get an SH solution with a molarity of 14M. This molarity was based on the optimization experiments conducted in previous research [121-123]. In comparison, the Grade N SS was sourced in liquid form. Its mass chemical composition is 26.3% SiO_2, 10.3% Na_2O, and 63.4% H_2O.

3.3.5 Steel Fibers

Double hooked-end steel fibers, manufactured by Bekaert, Belgium, were used in this work. They had a specific gravity of 7.9, aspect ratio of 65, and length of 35 mm [124]. The volume fraction was limited to 2% based on the inability to cast trial mixes made with 3% steel fibers, by volume.

3.3.6 Superplasticizer

A polycarboxylic superplasticizer (SP) was supplied by BASF Chemicals Company to maintain the workability of geopolymer concrete without affecting its mechanical performance [125, 126].

3.4 Concrete Mixture Proportions

A total of twenty mixtures were designed to evaluate the effect of replacing natural aggregates with recycled concrete aggregates and the incorporation of steel fibers on the performance of slag-based geopolymer concrete made with 0 and 25% fly ash. To achieve

this objective, the replacement of NA by RCA was altered among 0, 30, 70, and 100%, and the steel fiber volume fraction varied among 0, 1, and 2 %. The contents of binder (slag and fly ash), dune sand, coarse aggregates, SS, SH, and superplasticizer (SP) were optimized to attain a 30-MPa concrete mix. This was achieved by conducting numerous trial mixes that are shown in Appendix A. Accordingly, the aforementioned contents for 100% slag-based geopolymer concrete mixes were 300, 725, 1210, 99, 66, and 10.5 kg/m^3. They were slightly modified for the mix incorporating 25% fly ash. The steel fibers varied from 0 to 78 and 156 kg/m^3, representing a 0 to 1 and 2% addition, by volume. Table 4 summarizes the mixture proportions of geopolymer concrete.

Table 4: Mixture proportions by weight (kg/m^3)

Mix Number	Mix Designation	Slag	FA	DS	NA	RCA	SS	SH	SP	SF
1	S100R0F0	300	0	725	1210	0	99	66	7.5	0
2	S100R30F0	300	0	725	847	363	99	66	7.5	0
3	S100R30F1	300	0	725	847	363	99	66	7.5	78
4	S100R30F2	300	0	725	847	363	99	66	7.5	156
5	S100R70F0	300	0	725	363	847	99	66	7.5	0
6	S100R70F1	300	0	725	363	847	99	66	7.5	78
7	S100R70F2	300	0	725	363	847	99	66	7.5	156
8	S100R100F0	300	0	725	0	1210	99	66	7.5	0
9	S100R100F1	300	0	725	0	1210	99	66	7.5	78
10	S100R100F2	300	0	725	0	1210	99	66	7.5	156
11	S75R0F0	187.5	62.5	765	1220	0	99	66	6.25	0
12	S75R30F0	187.5	62.5	765	854	366	99	66	6.25	0
13	S75R30F1	187.5	62.5	765	854	366	99	66	6.25	78
14	S75R30F2	187.5	62.5	765	854	366	99	66	6.25	156
15	S75R70F0	187.5	62.5	765	366	854	99	66	6.25	0
16	S75R70F1	187.5	62.5	765	366	854	99	66	6.25	78
17	S75R70F2	187.5	62.5	765	366	854	99	66	6.25	156
18	S75R100F0	187.5	62.5	765	0	1220	99	66	6.25	0
19	S75R100F1	187.5	62.5	765	0	1220	99	66	6.25	78
20	S75R100F2	187.5	62.5	765	0	1220	99	66	6.25	156

3.5 Sample Preparation

Geopolymer concrete specimens were prepared and cast under ambient laboratory conditions of $23\pm2^{\circ}$C and relative humidity of $50\pm5\%$. The alkaline activator solution was prepared 24 hours prior to casting to allow for heat dissipation from the reactions of SH flakes with water and then the 14M-SH solution with the SS solution. The dry components, including the coarse and fine aggregates and binding materials, were mixed in a pan mixer for 3 minutes. In the event of using steel fibers, they were added to the dry components to ensure proper dispersion. A few seconds before incorporating the wet components into the mix, the superplasticizer was added and mixed swiftly. Further, the wet components, including SS, SH, and SP, were gradually added to the dry mix and mixed in the pan mixer for another 3 minutes to ensure homogeneity. The fresh geopolymer concrete was then placed in two to three layers into 100 mm diameter x 200 mm height cylinders, 150 mm diameter x 300 mm height cylinders, 100 mm cubes, and 100 mm height x 100 mm width x 500 mm length prisms, and vibrated on a vibrating table for 5-10 seconds per layer. The cast specimens were then covered and left at ambient conditions until testing age to simulate an on-site construction setting. Figure 5 presents a sample of the hardened geopolymer concrete specimens.

Figure 5: Hardened geopolymer concrete specimens

3.6 Concrete Testing Methodology

3.6.1 Compressive Strength

The compressive strength of concrete was determined using a Wykeham Farrance machine with a loading capacity of 2000 kN. An axial compression load was applied to cylindrical (100 mm diameter, 200 mm height) and cube (100 mm) geopolymer concrete

specimens at a rate of 7 kN/s until failure, as per ASTM C39 [127] and BS EN 12390-3 [128]. The maximum load was then divided by the cross-sectional area of each specimen. The resulting compressive strengths are denoted as f'_c and f_{cu}. Three cube and three cylinder samples were used to obtain an average f'_c and f_{cu} for each mix. While f'_c was measured at the age of 1 day, f_{cu} was determined at 1, 7, and 28 days. Figures 6 and 7 present the compressive strength testing of geopolymer concrete cube and cylinders, respectively.

Figure 6: Compressive strength testing of geopolymer concrete cube

Figure 7: Compressive strength testing of geopolymer concrete cylinder

3.6.2 Modulus of Elasticity

The modulus of elasticity (E_c) represents the concrete's resistance to deformation under an applied compression load. It was determined following the procedure of ASTM C469 [129], whereby a 500-kN load cell recorded the applied load and four 60-mm-long strain gauges attached to the sides of the 100 mm x 200 mm (diameter x height) cylinder at diametrically opposite locations recorded the strain. Then, the modulus of elasticity was calculated as per Equation (1).

$$E_c = \frac{S_2 - S_1}{\varepsilon_2 - 0.00005} \tag{1}$$

Where E_c is chord modulus of elasticity in (MPa), S_2 is stress corresponding to 40% of ultimate load, S_1 is stress corresponding to a longitudinal strain ε_1, of 50 millionths in (MPa), ε_2 is the longitudinal strain produced by stress S_2. Triplicate specimens were used to attain an average.

3.6.3 Tensile Splitting Strength

The tensile splitting strength (f_{sp}) of geopolymer concrete was determined according to the procedure of ASTM C496 [130]. A Wykeham Farrance machine with a loading capacity of 2000 kN applied the load at a rate of 1 kN/s to cylindrical specimens (100 mm diameter × 200 mm height). Three samples were tested to obtain an average. The tensile splitting strength (f_{sp}) was calculated using Equation (2).

$$f_{sp} = \frac{2P}{\pi DL} \tag{2}$$

Whereas P is the compressive load at failure (N), L is the length of the cylinder (mm),

and D is the diameter of the cylinder (mm).

3.6.4 Flexural Strength

The flexural strength (f_r) of concrete, also known as the modulus of rupture, was

assessed following the procedure of ASTM C1609 [131]. A Wykeham Farrance machine

with a loading capacity of 2000 kN was used to apply the load at a rate of 1 kN/s to

concrete prism specimens (100×100×500 mm). A load cell was placed beneath the loading

jack to measure the applied load and find the flexural strength (f_r) using Equation (3),

while a linear variable displacement transducer (LVDT) was used to measure the mid-

span deflection. Using these two instruments, the load-deflection curve was developed.

Then, it was used to determine the peak or flexural strength (f_r), the peak load deflection

(δ_p), and the residual strengths f_{150}^{100} and f_{600}^{100} corresponding to the loads at 0.75 and 3 mm

deflections. The curves were also utilized in finding the toughness T_{150}^{100}, which is the area

under the curve up to a deflection of L/150, i.e., 3 mm, and relates to concrete's capacity

to absorb energy. The toughness was subsequently employed in findings the equivalent

flexural ratio $R_{T,150}^{100}$, as per Equation (4).

$$f_r = \frac{PL}{bd^2} \tag{3}$$

$$R_{T,150}^{100} = \frac{150 \text{ x } T_{150}^{100}}{f_r bd^2} \text{ x } 100\% \tag{4}$$

Where P is the load at the peak (N), L is the span length of the prism specimen (mm), b is

the width of the prism specimen (mm), and d is the depth of the prism specimen (mm).

3.6.5 Water Absorption

The water absorption test was conducted on 100 mm x 50 mm (diameter x height) 28-day geopolymer concrete discs at the age of 28 days as per ASTM C642 [132]. Three specimens per mix were tested for an average. The test specimens were oven-dried for 24 hours at 105°C and weighed until a mass change of less than 0.5% was obtained. They were then placed in a water container for 24 hours, after which their saturated surface dry (SSD) mass was recorded. The water absorption was calculated using Equation (5):

$$\text{Water absorption (\%)} = \frac{\text{SSD mass (g) - Oven-dried mass (g)}}{\text{Oven-dried mass (g)}} \times 100\% \tag{5}$$

3.6.6 Sorptivity

Sorptivity is defined as the rate of absorption of water in concrete. It is determined by measuring the increase in the mass of a concrete sample over time with only one surface being exposed to water. The test was conducted following the procedure of ASTM C1585 [133]. Concrete disc specimens (100 mm × 50 mm, diameter x height) were used after 28 days of curing. The test specimen s were first vacuum-saturated and preconditioned as per the recommendations of ASTM C1202 [134]. Further, they were sealed from the top and side surfaces with adhesive tape to allow water to penetrate from the bottom side only and prevent any evaporation. Each sample was weighed, and its unsealed surface was exposed to water by placing it on supports, as shown in Figure 8. The water reached 1 to 3 mm above the supports only. Subsequently, the sample's weight was recorded at 1, 5, 10, 15, 20, 30, and 60 minutes and then after every hour until 6 hours. The absorption was calculated using Equation (6) and plotted against the square root of time. The slope of the

best-fit relationship from 1 minute to 6 hours represented the initial sorptivity. The test was to be repeated if the regression coefficient, R^2, was less than 0.98, as per ASTM C1585 [133].

$$I \text{ (mm)} = \frac{\text{Change in mass at time t(g)}}{\text{Exposed area (mm}^2) \times \text{Density of water (g/mm}^3)} \qquad (6)$$
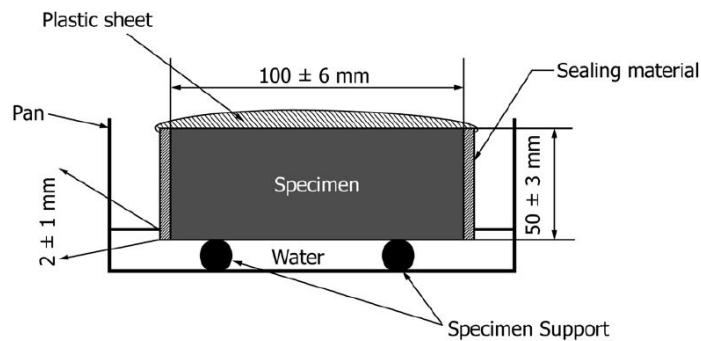
Figure 8: Schematic of Sorptivity Test Setup, ASTM C1585-13

3.6.7 Bulk Resistivity

Bulk resistivity is a non-destructive test that relates the concrete's ability to resist chloride ion diffusion under an electric current to its general quality, durability, and performance. The test was conducted using Giatec RCON2® equipment in accordance with ASTM C1876 [135], as shown in Figure 9. The concrete specimens used in this test were 28-day 100 mm × 200 mm (diameter × height) concrete cylinders. The bulk resistivity was calculated using Equation (7). Owing to their electrically conductive nature, steel fibers may give unrepresentative results. As such, only test results of plain geopolymer concrete samples were reported later. For every mix, three specimens were

tested to obtain an average. Table 5 shows the relationship between bulk resistivity of concrete and the level of corrosion protection.

$$\text{Bulk Resistivity } (\Omega.\text{cm}) = \frac{\text{Applied voltage (V)} \times (\text{Avg. sample diameter (mm)})^2}{1273.2 \times \text{Current at 1 minute (mA)} \times \text{Avg. sample length (mm)}} \qquad (7)$$

3.6.8 Ultra Pulse Velocity (UPV)

Ultrasonic pulse velocity is another nondestructive test of concrete. It is used to assess the general quality and integrity of the concrete by indirectly estimating the number of voids, cracks, and imperfections in the concrete structure. The direct UPV test was carried out on three cube samples (100 mm) per mix, according to ASTM C597 (Figure 10) [136]. The transit time of an ultrasonic pulse to travel between a transmitter and receiver is measured. It is inversely proportional to the density of concrete, i.e., the higher the density of concrete structure, the shorter the transit time will be. The results can be correlated to concrete quality grade using Table 6.

Figure 9: Bulk resistivity test setup

Table 5: Relationship between bulk resistivity and level of corrosion protection, ACI 222R-01

Bulk Resistivity (kΩ.cm)	Level of Corrosion Protection
< 5	Low
5 – 10	Moderate to Low
– 20	High
> 20	Very High
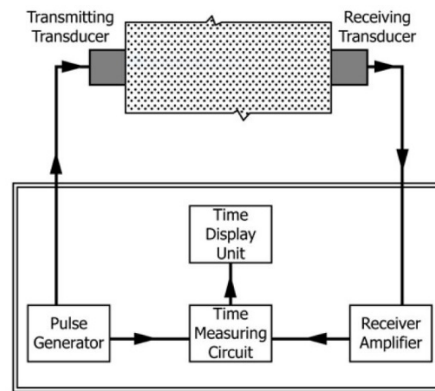
Figure 10: Schematic of Pulse Velocity Apparatus, ASTM C597-16

Table 6: Velocity Criterion for Concrete Quality Grading, IS:13311 part 1-1992

Pulse Velocity by Cross Probing (km/s)	Concrete Quality Grading
Above 4.5	Excellent
3.5 to 4.5	Good
3.0 to 3.5	Medium
Below 3.0	Doubtful

3.6.9 Abrasion Resistance

The abrasion resistance test was conducted to determine the ability of geopolymer concrete to resist impact and friction actions, providing an estimate of its general quality and durability. It is mainly dependent on the strength of the geopolymeric binding matrix and aggregate, in addition to the bond between these two components [137, 138]. The test was conducted using a Los Angeles (LA) abrasion testing machine shown in Figure 11 in accordance with the procedure of ASTM C1747 [139]. The mass of the 28-day test specimen (100 mm diameter x 50 mm height) was recorded before starting the test and

after each subsequent 100 revolutions. The mass loss percentage over 500 revolutions represented the geopolymer concrete abrasion resistance potential. The abrasion resistance was determined using Equation (8).

$$\text{Mass Loss (\%)} = \frac{\text{Final Mass - Initial Mass}}{\text{Initial Mass}} \times 100\% \tag{8}$$

Figure 11: LA abrasion test machine

Chapter 4: Experimental Results and Discussions

4.1 Introduction

After determining the properties of the as-received materials to be used in producing the geopolymer concrete, the feasibility of 100% RCA replacement alongside the addition of steel fibers is examined. This chapter offers a detailed experimental performance evaluation program to evaluate such feasibility by testing the 100% slag and slag-fly ash blended geopolymer concrete for compressive strength, splitting tensile strength, flexural performance, modulus of elasticity, water absorption, sorptivity, bulk resistivity, UPV, and abrasion resistance.

4.2 Compressive Strength

4.2.1 Cube Compressive Strength Development Profile

The cube compressive strength (f_{cu}) of 100% slag and slag-fly ash blended geopolymer concrete is measured at the ages of 1, 7, and 28 days to examine the development over time. Mixes were made with different RCA replacement percentages and steel fibers volume fractions. Figure 12 presents the results of 100% slag geopolymer concrete. The control mix S100R0F0 had 1-, 7-, and 28-day compressive strengths of 38.6, 46.4, and 47.5 MPa, respectively. As such, the increase from 1 to 7 days was 20% while that from 7 to 28 days was 2%, as shown in Table 7. Clearly, the geopolymerization reaction mainly took place during the first 7 days with 1- and 7-day strengths being 81 and 98% that at 28 days. This is due to the accelerated reaction of calcium-carrying compounds in slag to form calcium aluminosilicate hydrate (C-A-S-H) and calcium

silicate hydrate (C-S-H) gels [64, 140-142] and the high molarity of SH solution [143].
Yet, such a reaction seemed to slow down after 7 days.

The strength development profile of 100% slag concrete of mixes incorporating
RCA was also examined. Higher RCA replacement percentages led to higher increases in
strength from 1 to 7 days. Similar to the control mix, the main increase in strength was
within the first 7 days, while a lesser increase was noted from 7 to 28 days. However, the
increase in steel fiber volume fraction led to a decrease in the strength gain. In fact, the
cube compressive strength (f_{cu}) of mixes incorporating 0, 1, and 2% steel fibers, by
volume, increased by 45, 33, and 31%, on average, from 1 to 7 days. Conversely, the
strength increased by 11, 12, and 14%, on average, from 7 to 28 days. It seems that the
bond between the geopolymeric matrix and RCA improved over time.
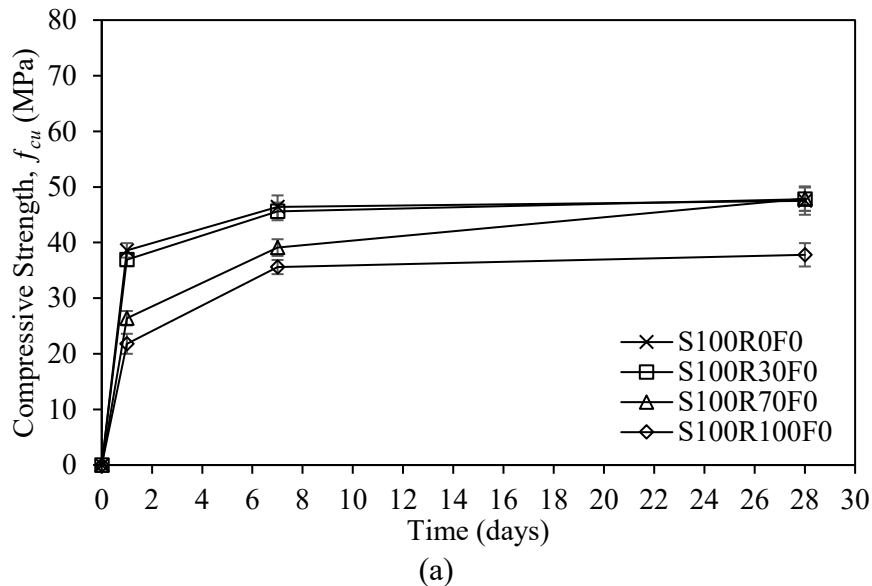
(a)

Figure 12: Development of cubic compressive strength of 100% slag geopolymer
concrete mixes: (a) SF 0%; (b) SF 1%; (c) SF 2%
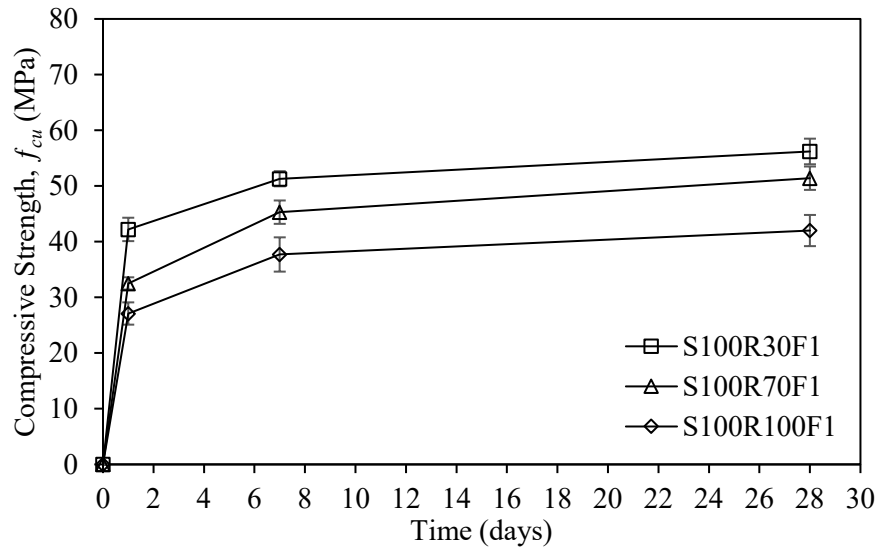
(b)
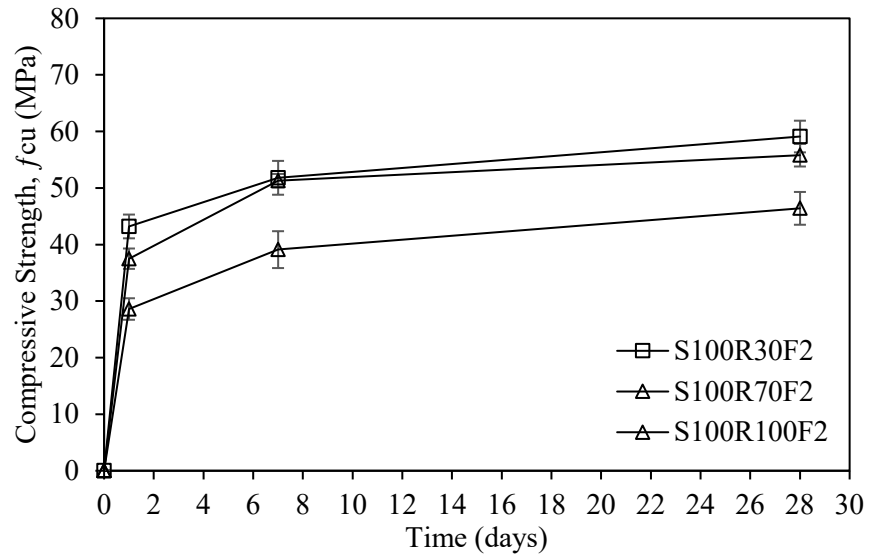
(c)

Figure 12: Development of cubic compressive strength of 100% slag geopolymer concrete mixes: (a) SF 0%; (b) SF 1%; (c) SF 2% (Continued)

Table 7: Development of compressive strength of 100% slag geopolymer concrete

Mix No.	Mix Designation	Increase[s] (%)	Increase[b] (%)
1	S100R0F0	20.2	2.4
2	S100R30F0	23.6	4.8
3	S100R30F1	21.6	9.6
4	S100R30F2	19.9	14.1
5	S100R70F0	48.1	22.5
6	S100R70F1	39.4	13.5
7	S100R70F2	36.8	8.8
8	S100R100F0	63.3	6.2
9	S100R100F1	39.1	11.4
10	S100R100F2	36.7	18.7

[a] Increase in f_{cu} from 1 to 7 days

[b] Increase in f_{cu} from 7 to 28 days

The development profiles of the cube compressive strength of slag-fly ash blended geopolymer concrete incorporating different amounts of steel fibers and various RCA replacement percentages are evaluated through Figure 13. The values shown represent the average of three specimens per mix. The control mix (S75R0F0) exhibited compressive strengths of 31.5, 44.2, and 56.8 MPa at the age of 1, 7, and 28 days, respectively, signifying increases of 40 and 29% from 1 to 7 days and 7 to 28 days. Also, the 1- and 7-day strengths are 55 and 78% that at 28 days. While most of the strength had developed within the first 7 days, the increase up to 28 days is indicative of the continuous reaction

of the fly ash to produce sodium aluminosilicate hydrate (N-A-S-H), as also reported by Ismail et al. [93]. However, such an increase in strength was more pronounced with the replacement of NA by RCA, as shown in Table 8. In fact, 30, 70, and 100% RCA replacement in plain blended geopolymer concrete led to respective increases of 59, 77, and 91%. It seems that the RCA had a more significant impact on 1 day. Yet, this negative impact, i.e., strength loss, could be reversed by the addition of steel fibers. The strength increase from 1 to 7 days was 75, 61, and 47%, on average, upon the incorporation of 0, 1, and 2% steel fiber volume fractions.
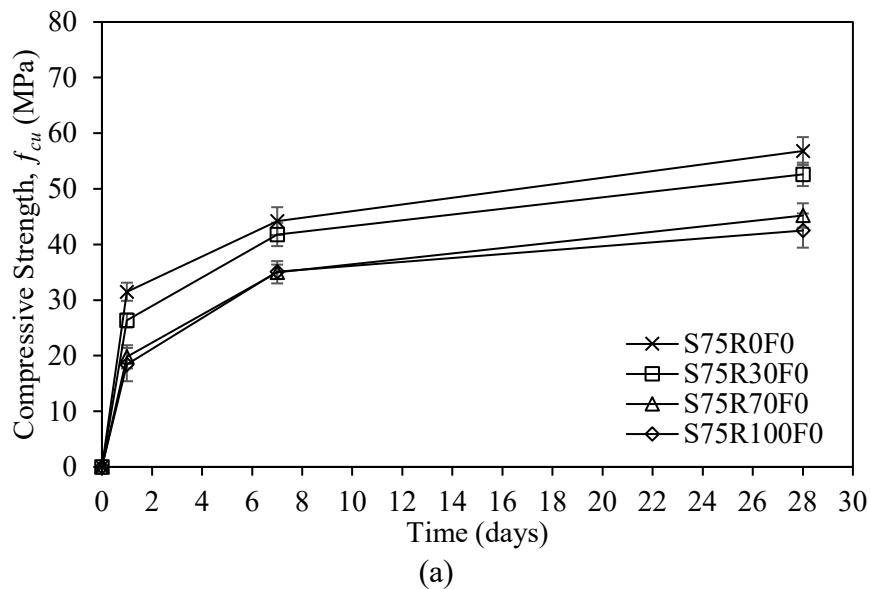
(a)

Figure 13: Development of cubic compressive strength of slag-fly ash blended geopolymer concrete mixes: (a) SF 0%; (b) SF 1%; (c) SF 2%
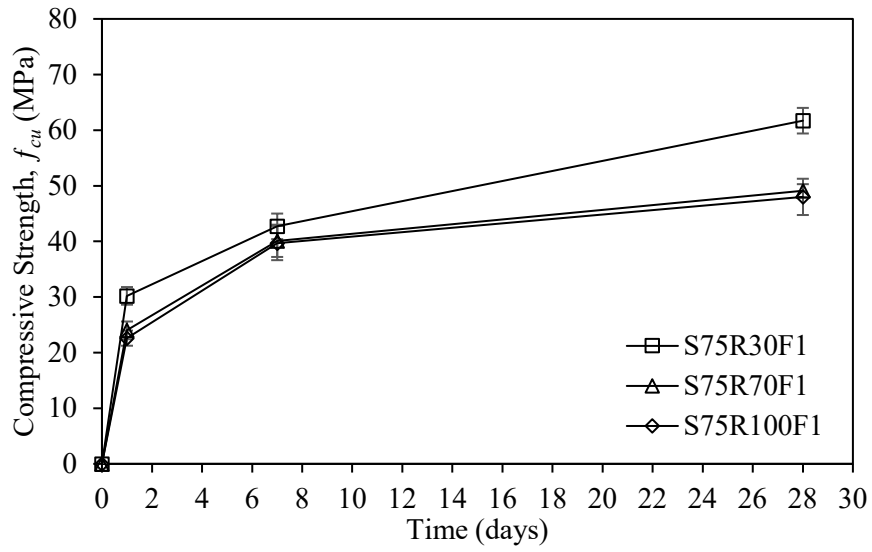
(b)
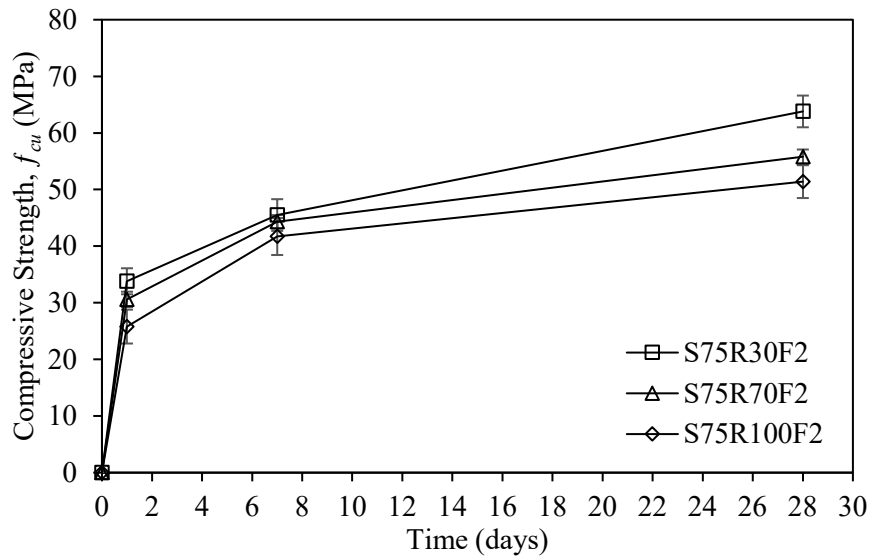
(c)

Figure 13: Development of cubic compressive strength of slag-fly ash blended geopolymer concrete mixes: (a) SF 0%; (b) SF 1%; (c) SF 2% (Continued)

Table 8: Development of compressive strength of slag-fly ash blended geopolymer concrete

Mix No.	Mix Designation	Increase[a] (%)	Increase[b] (%)
11	S75R0F0	40.3	28.5
12	S75R30F0	58.8	25.8
13	S75R30F1	41.4	44.5
14	S75R30F2	34.6	40.2
15	S75R70F0	76.8	29.1
16	S75R70F1	67.1	22.4
17	S75R70F2	44.8	26.0
18	S75R100F0	90.8	21.1
19	S75R100F1	75.7	20.9
20	S75R100F2	61.6	23.3

[a] Increase in f_{cu} from 1 to 7 days.

[b] Increase in f_{cu} from 7 to 28 days.

4.2.2 Effect of RCA and SF

Figure 14 shows the cube compressive strength of 100% slag geopolymer concrete made with different RCA replacement percentages and steel fiber volume fractions. At the age of 1 day, the replacement of 30% RCA had no impact on the strength, as presented in Figure 14(a). However, higher replacements of 70 and 100% reduced the strength from 38.6 MPa to 26.4 and 21.8 MPa, representing decreases of 32 and 44%, respectively. This is primarily owed to the weak interfacial bond between the geopolymeric matrix and RCA

alongside the porous nature of the RCA. Nevertheless, the addition of 1 and 2% steel fiber volume fractions could enhance the 1-day compressive strength by, on average, 21 and 30%, respectively, in comparison to the plain geopolymer concrete.

At the age of 7 and 28 days, the replacement of NA by RCA led to a loss in strength of up to 23 and 20%, respectively, as shown in Figures 14(b-c). Similar findings were reported in geopolymer concrete made with a single precursor, i.e., class C fly ash, class F fly ash, or ground granulated blast furnace slag [5, 98, 144]. Clearly, the impact of RCA replacement was most critical at an early age and became less apparent at a later age. The addition of steel fibers improved the respective 7- and 28-day strengths to up to 18 and 21%, on average, owing to the denser geopolymeric matrix and reduced pore space, which is attributed to the lower water absorption and sorptivity explained later in the thesis. Furthermore, the bridging effect of the steel fibers may have led to an enhancement in the structural integrity of the 100% slag geopolymer concrete. Analogous improvement in compressive strength was noted in other studies on steel fiber-reinforced NA-based geopolymer concrete [15, 38]. Compared to the values obtained at the age of 1 day, these are slightly lower, highlighting the superior effect of steel fibers at an early age. Accordingly, 100% slag geopolymer concrete mixes could be made with 100% RCA and 2% steel fiber volume fraction while sustaining insignificant loss (<3%) in 28-day cube compressive strength.
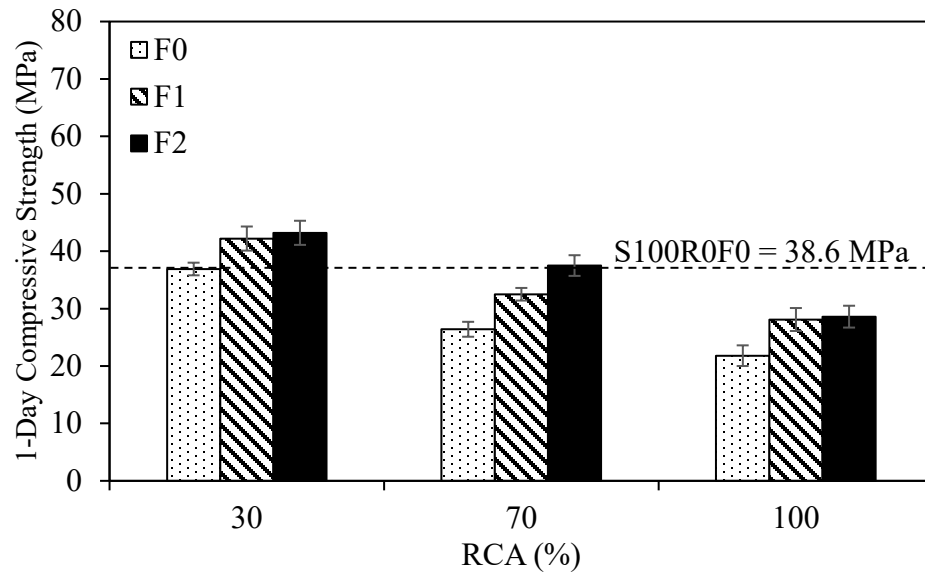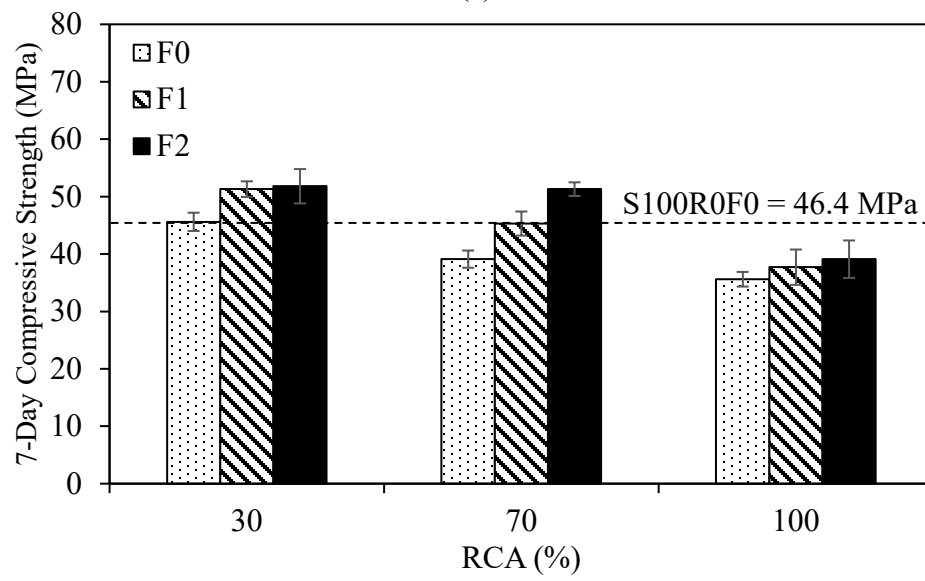
Figure 14: Cubic compressive strength for 100% slag geopolymer concrete at the age of (a) 1 day, (b) 7 days, and (c) 28 days

Figure 14: Cubic compressive strength for 100% slag geopolymer concrete at the age of (a) 1 day, (b) 7 days, and (c) 28 days (Continued)

Figure 15 presents the 1-, 7-, and 28-day compressive strengths of slag-fly ash blended geopolymer concrete while highlighting the RCA replacement percentage and steel fiber volume fraction. The replacement of NA by RCA has an adverse effect on the cube compressive strength. In fact, RCA replacement of 30, 70, and 100% decreased the 1-day strength by 16, 37, and 42%. Conversely, the 7-day strength was reduced by 5, 21, and 21%, and the 28-day strength was lower by 7, 20, and 25%. This reduction in strength could be associated with the weak interfacial bond between the aggregate and geopolymeric matrix as well as the rough porous nature of the RCA [95]. Yet, this negative impact of RCA was less pronounced at a later age, possibly due to a stronger matrix associated with the late reaction of fly ash. Nevertheless, the addition of steel fibers to slag-fly ash blended geopolymer concrete improved the compressive strength. Compared to the plain counterparts, the 1-, 7-, and 28-day strength increased, on average, by 20, 10,

and 13% upon adding 1% steel fibers, by volume, respectively, and by 41, 18, and 22% with 2% steel fiber volume fraction, respectively. Clearly, steel fibers could counter the negative effect of RCA replacement, especially at higher volume fractions. Indeed, it is possible to fully replace (100%) NA by RCA in producing a slag-fly ash geopolymer concrete incorporating 2% steel fibers, by volume, with a limited loss (< 10%) in the 28-day cube compressive strength.
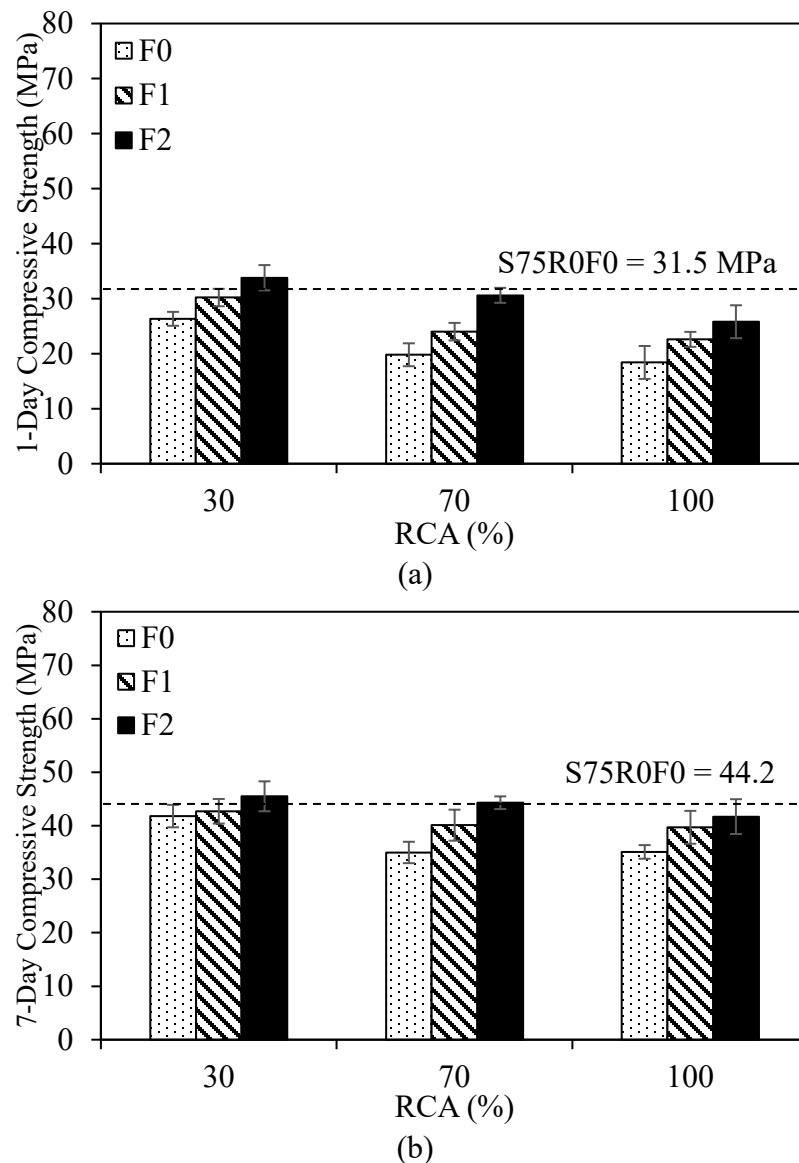
(a)

(b)

Figure 15: Cubic compressive strength for concrete mixes (75% S) for (a) 1 day, (b) 7 days, and (c) 28 days
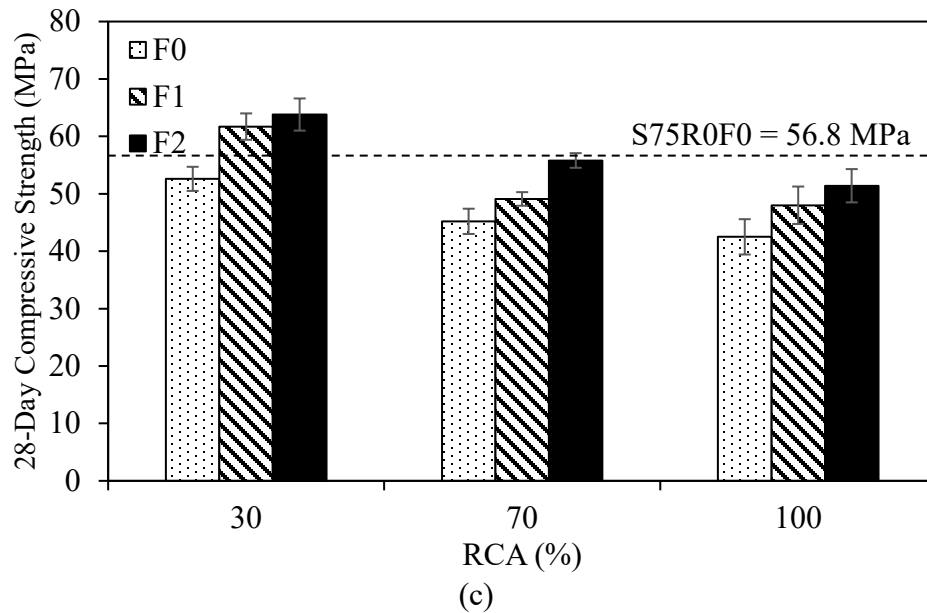
Figure 15: Cubic compressive strength for concrete mixes (75% S) for (a) 1 day, (b) 7 days, and (c) 28 days (Continued)

4.2.3 Cylinder Compressive Strength

Figure 16 highlights the effect of RCA replacement and steel fiber incorporation on the 28-day cylinder compressive strength (f'_c) of 100% slag geopolymer concrete. An increase in the RCA replacement percentage to 30, 70, and 100% led to respective decreases of 5, 5, and 21% in f'_c, owing to a weak interface between the aggregate and geopolymeric paste. It is also possibly attributed to the poor quality and presence of voids and cracks in the RCA [16]. Compared to the 28-day cube compressive strengths, the loss in cylinder strength was more pronounced, especially for 30 and 70% RCA replacement. The addition of 1 and 2% steel fibers, by volume, enhanced f'_c of the plain RCA geopolymer concrete by up to 14 and 21%, respectively, thus providing evidence to the ability to reverse the negative impact of RCA replacement using steel fibers.
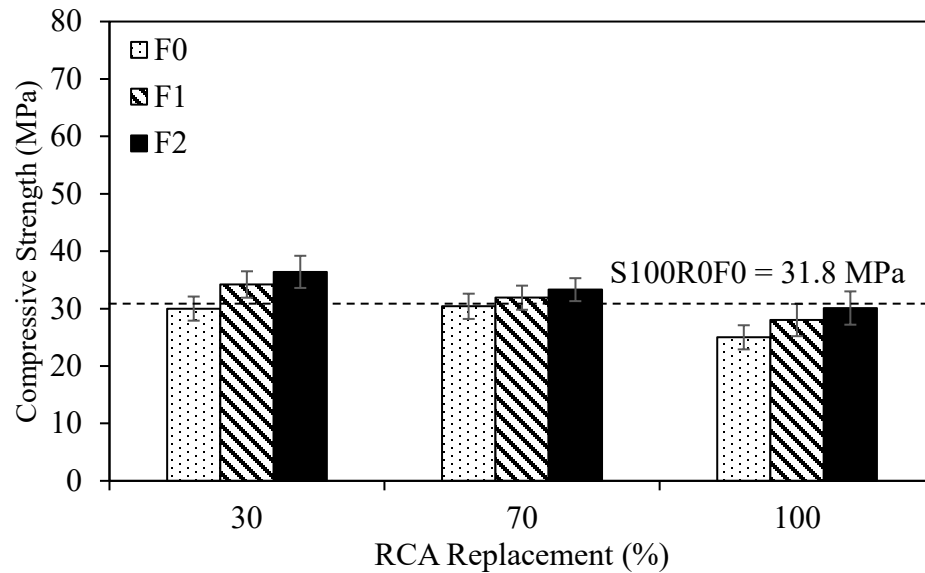
Figure 16: Cylinder compressive strength (MPa) for 100% slag geopolymer concrete

The effect of RCA replacement and steel fiber incorporation on the 28-day cylinder compressive strength (f'_c) of slag-fly ash blended geopolymer concrete is presented in Figure 17. It can be clearly seen that the replacement of NA by RCA resulted in a decrease in the strength. Indeed, 30, 70, and 100% RCA replacement led to a reduction of 10, 42, and 50% in f'_c, respectively. These values are much higher than those reported for cube compressive strength, especially for 70 and 100% RCA replacement, signifying a possible compounded effect of specimen geometry and RCA replacement. Nevertheless, the addition of 1 and 2% steel fibers volume fractions could enhance the cylinder compressive strength by up to 69 and 101%, respectively. As such, slag-fly ash blended geopolymer concrete mixes made with 100% RCA and 2% steel fibers, by volume, could substitute NA-based counterparts with no loss in mechanical performance.
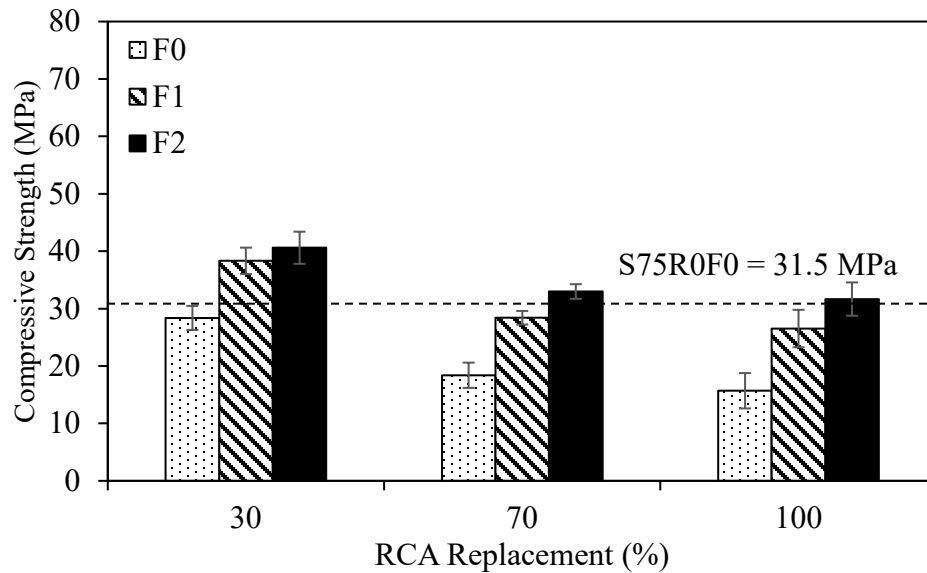
Figure 17: Cylinder compressive strength (MPa) for slag-fly ash blended geopolymer concrete mixes

4.2.4 Relationship Between f'_c and f_{cu}

Table 9 shows the f'_c-to-f_{cu} ratio of 100% slag geopolymer concrete. The control mix S100R0F0 had a ratio of 0.67. The replacement of NA by 30 and 70% RCA seemed to decrease the ratio while 100% replacement generally had a limited impact. On the other hand, the addition of steel fibers did not significantly affect the ratio with values being in the range of plain counterparts. Based on these findings, it is apparent that the 28-day cylinder and cube compressive strengths of 100% slag geopolymer concrete can be correlated. The relationship between these properties is illustrated in Figure 18 and presented in Equations 9 and 10. Using these analytical relationships and with respective correlation coefficients, $R^2 = 0.95$ and $R^2 = 0.85$, it is possible to predict f'_c from f_{cu} (or vice versa) with reasonable to high accuracy.

$$f'_c = 0.48f_{cu} + 7.70 \tag{9}$$

$$f'_c = 0.63f_{cu} \tag{10}$$

Table 9: Cylinder and cube compressive strength of 28-day 100% slag geopolymer concrete

Mix #	Mix Name	f'_c (MPa)	f_{cu} (MPa)	f'_c/f_{cu}
1	S100R0F0	31.8	47.5	0.67
2	S100R30F0	30.0	47.8	0.63
3	S100R30F1	34.2	56.2	0.61
4	S100R30F2	36.4	59.1	0.62
5	S100R70F0	30.4	47.9	0.63
6	S100R70F1	31.9	51.4	0.62
7	S100R70F2	33.3	55.8	0.60
8	S100R100F0	25.0	37.8	0.66
9	S100R100F1	28.0	42.0	0.67
10	S100R100F2	30.1	46.4	0.65
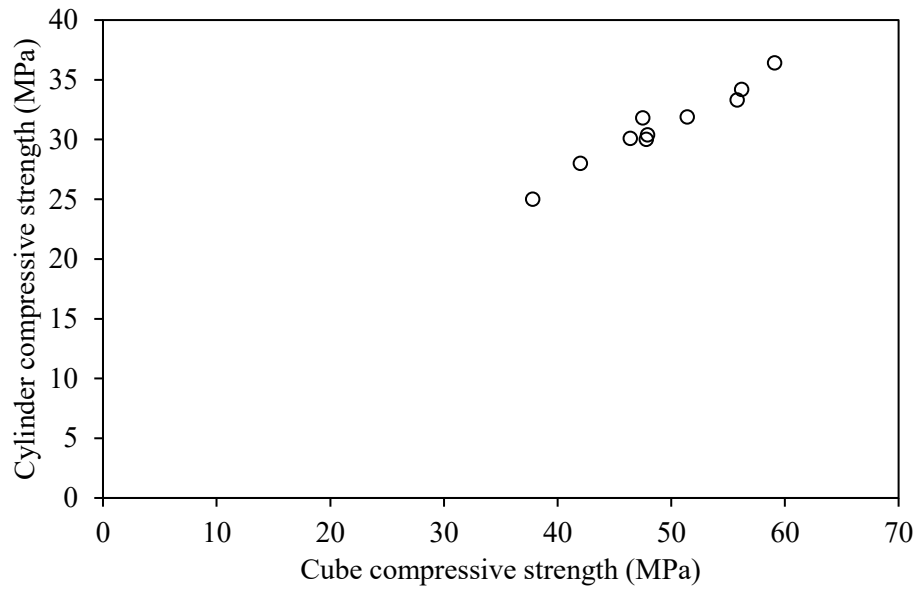
Figure 18: Relationship between cube and cylinder compressive strengths of 100% slag geopolymer concrete

The f'_c/f_{cu} ratio of slag-fly ash blended geopolymer concrete is shown in Table 10. For the control mix, the ratio was 0.55. Yet, this value decreased to 0.54, 0.41, and 0.37 as RCA replacement increased to 30, 70, and 100%. This shows that the effect RCA was more pronounced in the cylinder samples, signifying a more critical impact of the confinement effect of cubes under compression with RCA replacement. Furthermore, the addition of 1 and 2% steel fibers, by volume, increased the f'_c/f_{cu} ratio to 0.58 and 0.62, respectively. These results highlight a possible relationship between f'_c and f_{cu} as shown in Figure 19 and Equations 11 and 12. With these analytical relations, it is possible to predict one property from the other with reasonable ($R^2 = 0.91$) and moderate accuracy ($R^2 = 0.70$). Yet, for Equation 11, the value of f_{cu} is limited to at least 30 MPa.

$$f'_c = 1.08f_{cu} - 27.54 \tag{11}$$

$$f'_c = 0.56f_{cu} \tag{12}$$

Table 10: Cylinder and cube compressive strength of 28-day slag-fly ash blended geopolymer concrete

Mix No.	Mix Designation	f'_c (MPa)	f_{cu} (MPa)	f'_c/f_{cu}
11	S75R0F0	31.5	56.8	0.55
12	S75R30F0	28.4	52.6	0.54
13	S75R30F1	38.3	61.7	0.62
14	S75R30F2	40.6	63.8	0.64
15	S75R70F0	18.4	45.2	0.41
16	S75R70F1	28.4	49.1	0.58
17	S75R70F2	33.0	55.8	0.59
18	S75R100F0	15.7	42.5	0.37
19	S75R100F1	26.5	48.0	0.55
20	S75R100F2	31.7	51.4	0.62
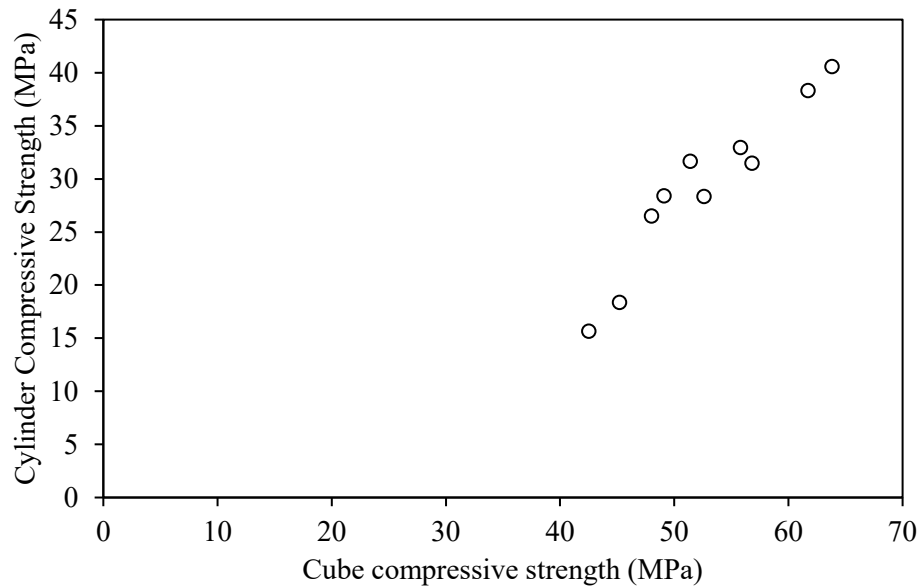
Figure 19: Relationship between cube and cylinder compressive strengths of slag-fly ash blended geopolymer concrete

4.3 Compressive Stress-Strain Response

Figure 20 illustrates compression stress-strain curves of 100% slag geopolymer concrete mixes made with constant RCA replacement and variation in the steel fiber volume fractions. For respective mixes made with 30, 70, and 100% RCA, the peak stress was, on average, 11, 22, and 20% higher with every 1% steel fiber added, by volume. In turn, the peak strain (strain at peak load) increased by, on average, 147% with the addition of 1 and 2% steel fiber volume fractions. In addition, slag-fly ash blended geopolymer concrete mixes showed similar trends as slag-based counterparts. Figure 21 shows that, for every 1% increase in steel fibers, by volume, the peak stress of slag-fly ash blended geopolymer concrete mixes made with 30, 70, and 100% RCA increased by, on average, 14, 24, and 21%, respectively, while the respective peak strains increased by 16, 26, and 37%. Based on these results, it is clear that the incorporation of steel fibers increased the

deformability of 100% slag and slag-fly ash blended geopolymer concrete made with RCA while also enhancing the compressive stress. Yet, it is worth noting that, despite the fact that steel fibers resulted in concrete with similar peak strains, the tail part of the compressive stress-strain curve was longer with higher steel fiber volume fractions, highlighting the enhanced energy absorption capacity.
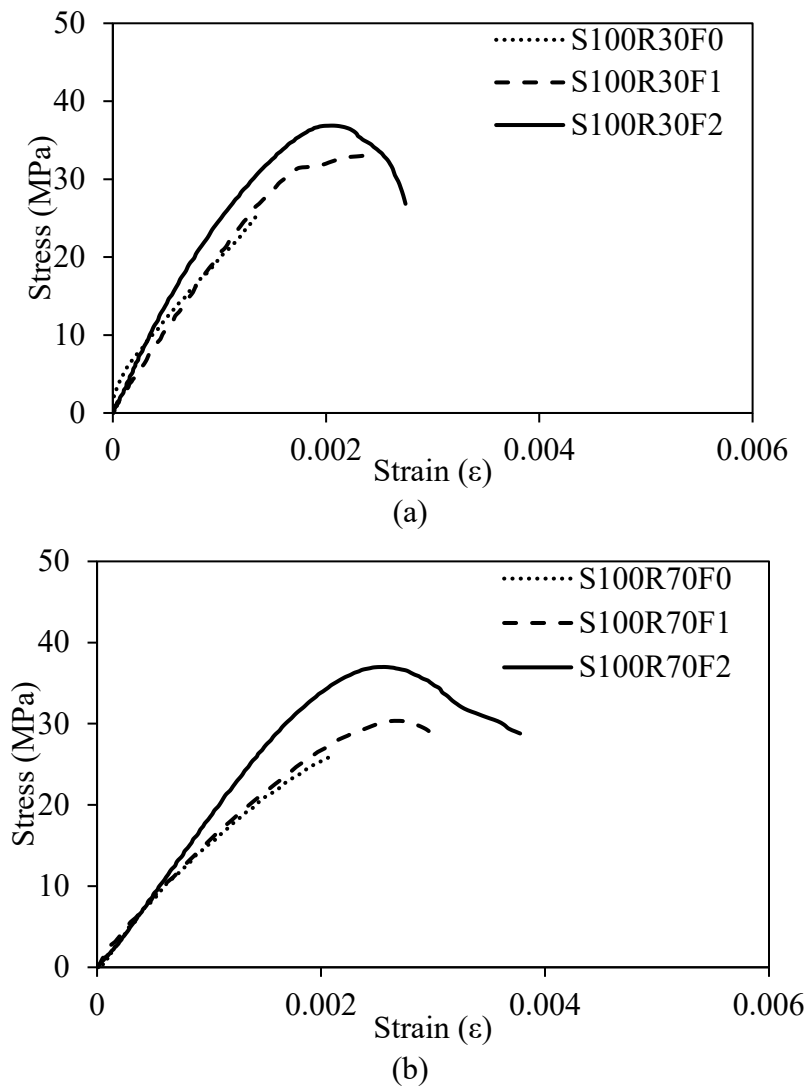
Figure 20: Typical compression stress-strain curves of 100% slag geopolymer concrete mixes with RCA replacement of (a) 30%, (b) 70%, and (c) 100%

(c)

Figure 20: Typical compression stress-strain curves of 100% slag geopolymer concrete mixes with RCA replacement of (a) 30%, (b) 70%, and (c) 100% (Continued)

(a)
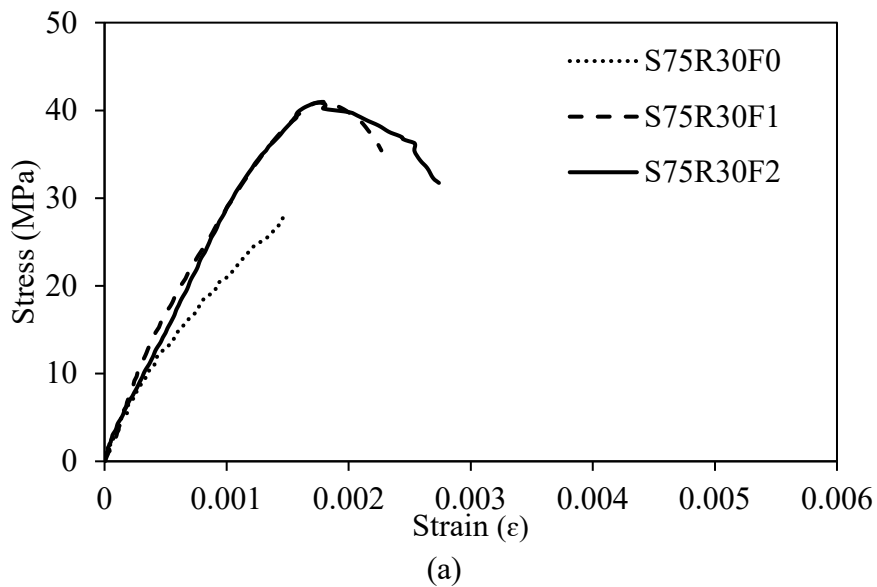
Figure 21: Typical compression stress-strain curves of slag-fly ash blended geopolymer concrete mixes with RCA replacement of (a) 30%, (b) 70%, and (c) 100%

Figure 21: Typical compression stress-strain curves of slag-fly ash blended geopolymer concrete mixes with RCA replacement of (a) 30%, (b) 70%, and (c) 100% (Continued)

Figure 22 examines the effect of different RCA replacement percentages on the compressive stress-strain behavior of 100% slag geopolymer concrete mixes. A decrease in peak stress was noted as more RCA was replaced in the mix. In fact, mixes made with 0, 1, and 2% steel fibers showed decreases of 2.5, 1.8, and 1.3% for every 10% RCA

replaced in the mixes, owing to the general weaker and porous nature of RCA. Conversely, the respective peak strains increased by, on average, 11, 5, and 4%. Furthermore, the influence of RCA replacement on the compression behavior of slag-fly ash geopolymer concrete mixes is highlighted in Figure 23. Higher RCA replacement percentages led to a major decrease in the peak stress and a slight increase in the peak strain. In conclusion, it is noted that the effect of steel fiber addition on the peak strain was more significant than the RCA replacement, while the latter was more influential on the peak stress than the former.
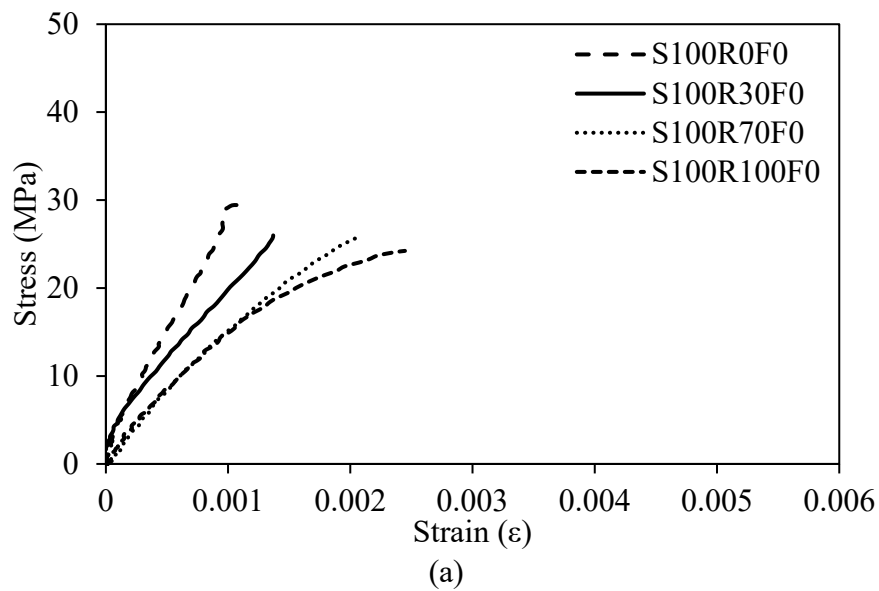
(a)

Figure 22: Typical compression stress-strain curves of 100% slag geopolymer concrete mixes with steel fiber volume fractions of (a) 0%, (b) 1%, and (c) 2%
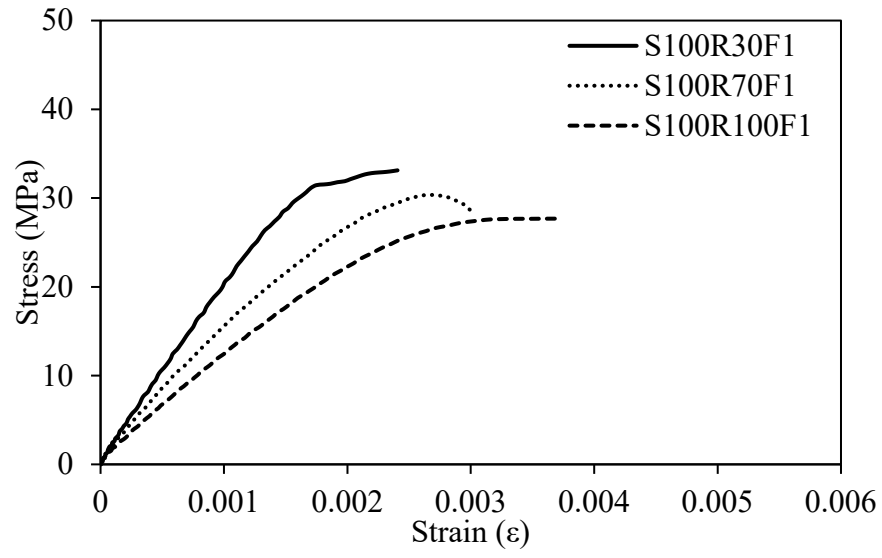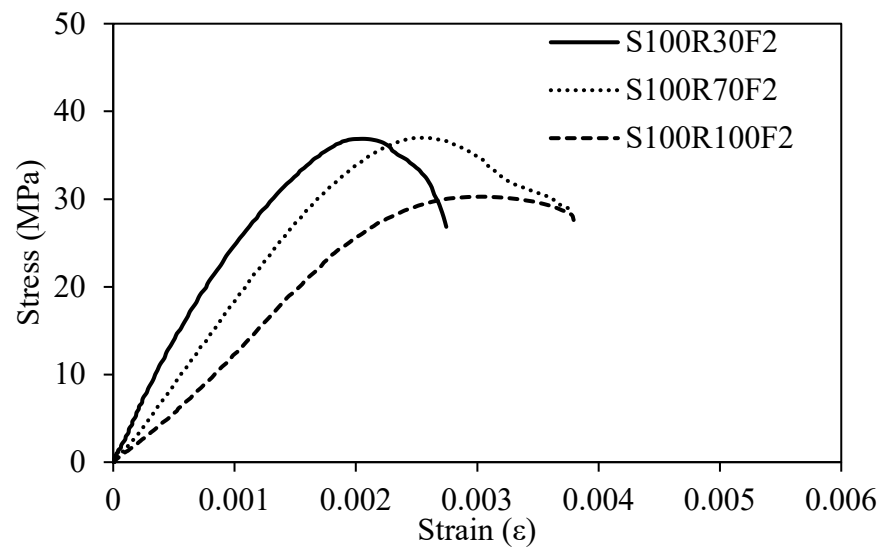
Figure 22: Typical compression stress-strain curves of 100% slag geopolymer concrete mixes with steel fiber volume fractions of (a) 0%, (b) 1%, and (c) 2% (Continued)
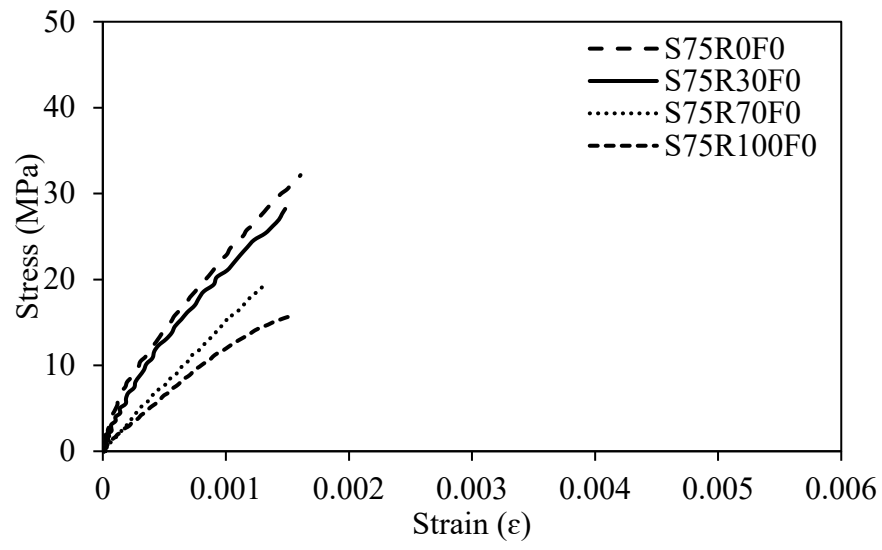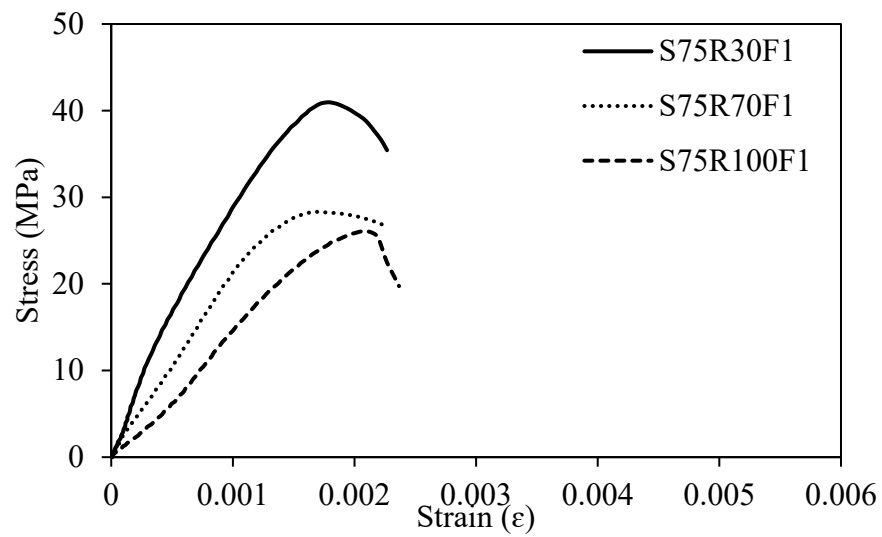
Figure 23: Typical compression stress-strain curves of slag-fly ash blended geopolymer concrete mixes with steel fiber volume fractions (a) 0%, (b) 1%, and (c) 2%
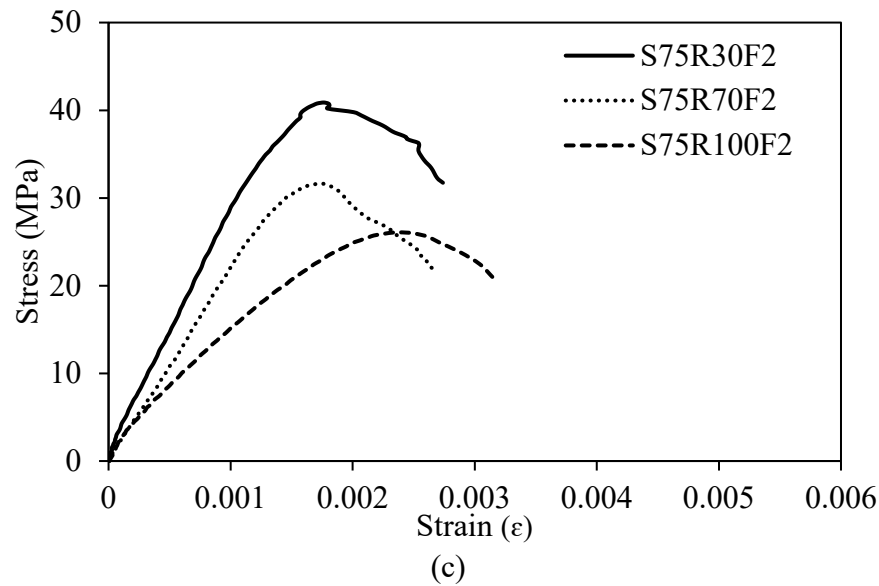
Figure 23: Typical compression stress-strain curves of slag-fly ash blended geopolymer concrete mixes with steel fiber volume fractions (a) 0%, (b) 1%, and (c) 2% (Continued)

4.4 Modulus of Elasticity

The modulus of elasticity, E_c (in GPa), of 28-day 100% slag geopolymer concrete is presented in Figure 24. The replacement of NA by RCA led to a decrease in the values of E_c. Plain geopolymer concrete mixes made with 30, 70, and 100% RCA had 42, 44, and 56% lower E_c than the control mix, respectively, due to the weak interfacial bond between the aggregate and old mortar and porous structure of the RCA. Nevertheless, steel fiber inclusion could counter this reduction in modulus of elasticity. In fact, the addition of 1% steel fiber, by volume, to mixes made with 30, 70, and 100% RCA led to respective increases in E_c of 13, 11, and 28%, while 2% steel fiber volume fraction increased E_c by 43, 36, and 32%, respectively. Nevertheless, none of the mixes incorporating RCA and steel fibers could attain the modulus of elasticity of the control mix, S100R0F0. This

shows that while steel fibers could enhance the modulus of elasticity, the adverse effect of RCA replacement was more pronounced.
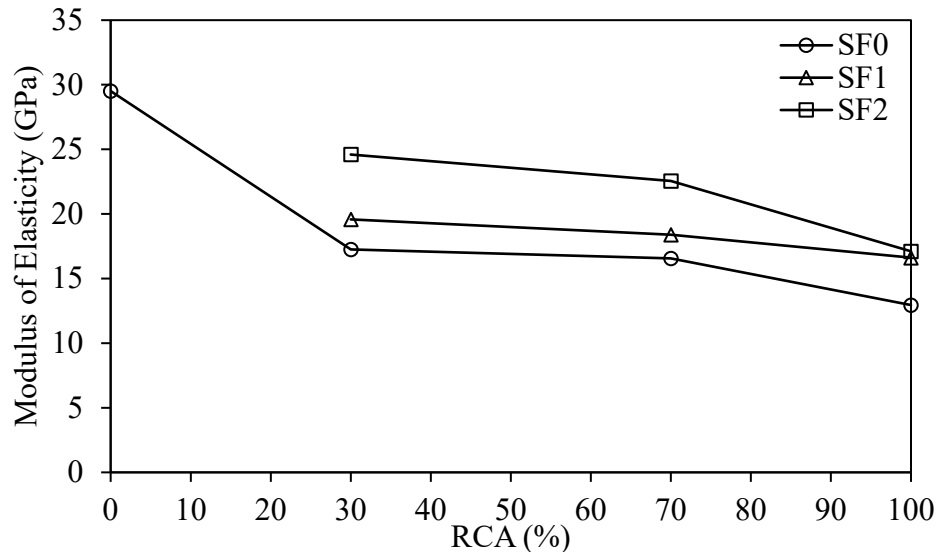
Figure 24: Modulus of elasticity of 100% slag geopolymer concrete mixes with different RCA replacement percentages and SF volume fractions

Figure 25 shows the modulus of elasticity of slag-fly ash blended geopolymer concrete made with different RCA and steel fiber proportions. Decreases of 28, 43, and 52% in E_c were noted when NA was replaced by 30, 70, and 100% RCA, respectively. Similar results were reported in fly ash-based geopolymer concrete [99]. On the other hand, average increases in E_c of 38, 28, and 44% were noted for every 1% steel fiber, by volume, added to 30, 70, and 100% RCA concrete. Accordingly, slag-fly ash geopolymer concrete mixes made with RCA and steel fibers were between 53% lower and 18% higher than that of the control mix S75R0F0, signifying that steel fibers cannot only reverse the negative impact of RCA but could also enhance the modulus of elasticity to the extent of exceeding that of the control mix in some mixes.
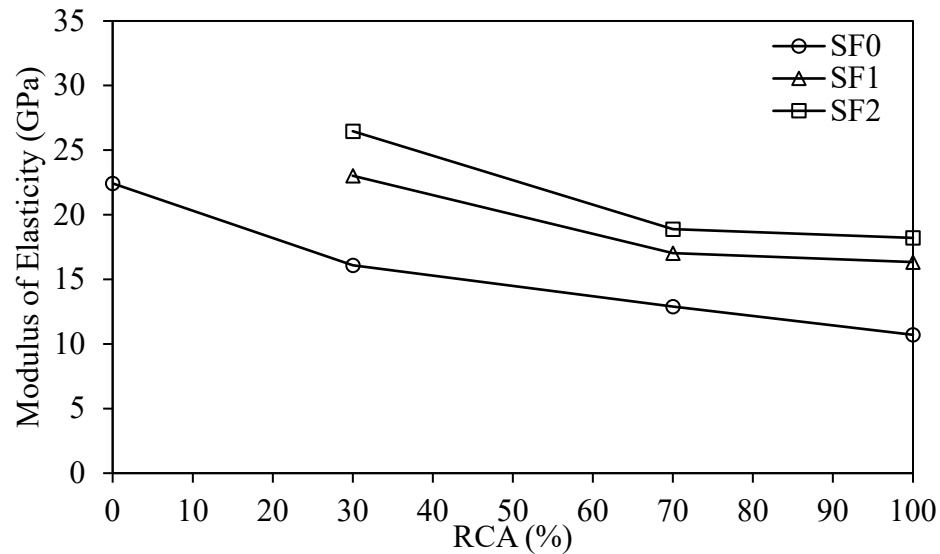
Figure 25: Modulus of elasticity of slag-fly ash blended geopolymer concrete mixes with different RCA replacement percentages and SF volume fractions

The modulus of elasticity and 28-day cylinder compressive strength of 100% slag geopolymer concrete were correlated. A linear regression model was developed using the scatter form of Figure 26 and formulated into Equation 13. The low correlation coefficient, R^2, of 0.25 signifies a relatively high scatter between the two properties. As such, a multivariable linear regression model was proposed in the form of Equation 14 to include the effect of RCA and steel fibers (SF). From Equation 14, it can be noted that the modulus of elasticity was proportional to the 28-day cylinder compressive strength and the steel fiber volume fraction but was inversely proportional to the RCA replacement. This is indicative of the respective positive and negative effects of steel fibers and RCA on E_c of 100% slag geopolymer concrete.

A similar analysis was carried out for slag-fly ash blended geopolymer concrete. The first analytical model (Equation 15) developed using the scatter plot of Figure 27 showed a moderate correlation ($R^2 = 0.72$) between E_c and f'_c. Accordingly, the RCA and

steel fiber volume fraction were incorporated into the model to formulate Equation 16. Evidenced by the modulus of elasticity analysis presented earlier, the coefficients indicate a positive impact of f'_c and steel fiber volume fraction and a negative impact of RCA on E_c.

$$E_c = 3.52\sqrt{f'_c} \tag{13}$$

$$E_c = 4.24\sqrt{f'_c} - 0.09\text{RCA} + 1.10\text{SF} \tag{14}$$

$$E_c = 3.44\sqrt{f'_c} \tag{15}$$

$$E_c = 3.78\sqrt{f'_c} - 0.05\text{RCA} + 1.16\text{SF} \tag{16}$$
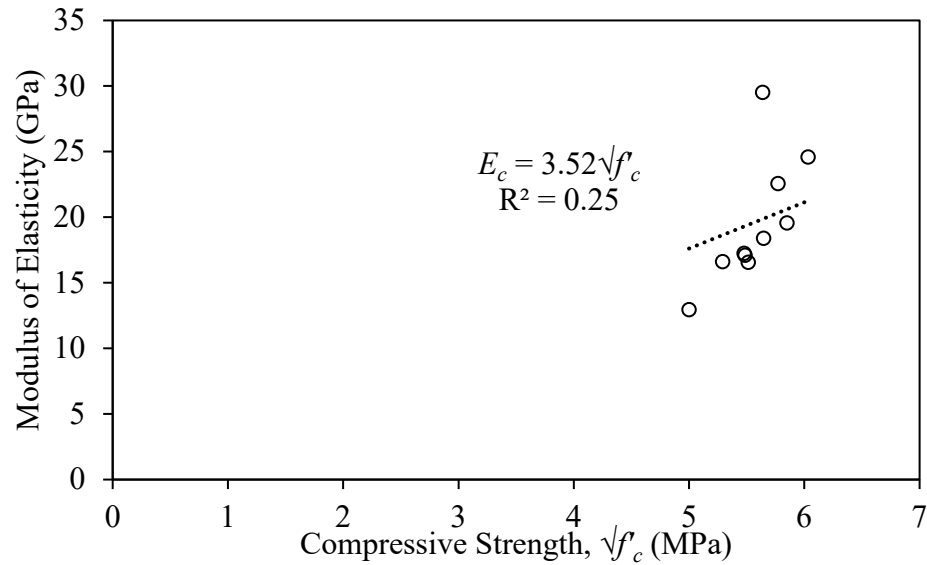
Figure 26: Modulus of elasticity of 100% slag geopolymer concrete mixes as a function of compressive strength
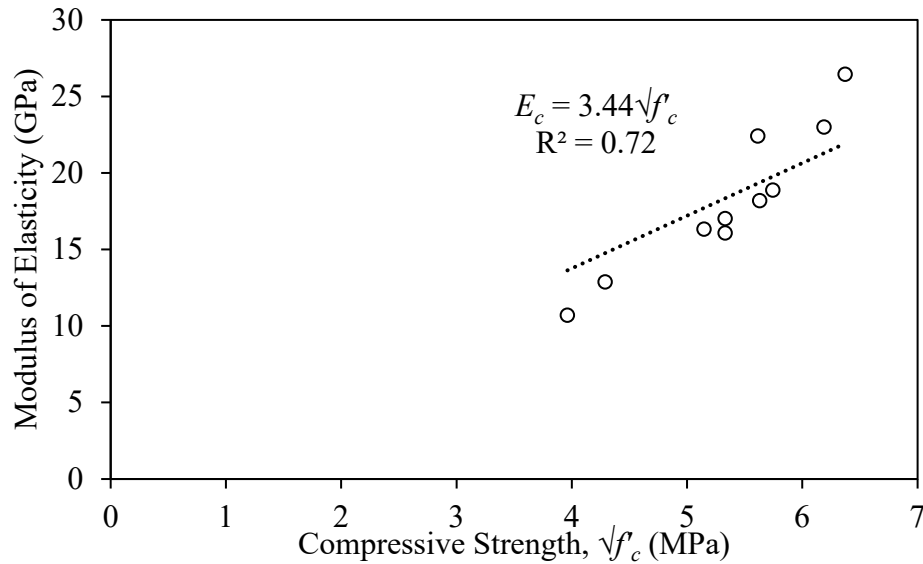
Figure 27: Modulus of elasticity of slag-fly ash blended geopolymer concrete mixes as a function of compressive strength

The modulus of elasticity can be typically predicted from codified equations, including those of ACI Committee 318 [84], CEB-FIP [145], and AS3600 [83]. The feasibility of using these equations is evaluated while also considering the newly-developed relationship in Equation 14. Figure 28 shows that the equations of ACI Committee 318 [84] and CEB-FIP [145] over-estimate the values of E_c for 100% slag geopolymer concrete, while that of AS3600 [83] provides a more accurate prediction for E_c up to 20 GPa, beyond which the accuracy is significantly reduced. Nevertheless, Equation 14 proved to be most accurate at predicting E_c with scatter plots converging around the 45°-line. As such, it can be concluded that only the codified equation of AS3600 [83] can be used to a certain extent to predict E_c of 100% slag geopolymer concrete while the other equations were deemed unsuitable.

Figure 29 plots the experimental and predicted modulus of elasticity of slag-fly ash blended geopolymer concrete. Equation 16 developed herein is compared to codified

equations of ACI Committee 318 [84], CEB-FIP [145], and AS3600 [83]. With values mainly converging around the 45°-line, it is clear that Equation 16 is the most accurate among the employed equations. Yet, it is worth noting that the AS3600 [83] provides predictions with acceptable accuracy for E_c between 15 and 20 GPa, but deviates from the experimental result for E_c outside this range. Indeed, the error between the experimental and predicted E_c was in the range of 3 to 30%. Conversely, the error associated with utilizing the ACI Committee 318 [84] and CEB-FIP [145] reached up to 87 and 133%, respectively. Accordingly, some modifications to the codified equations are needed to accurately predict the modulus of elasticity of slag-fly ash blended geopolymer concrete.
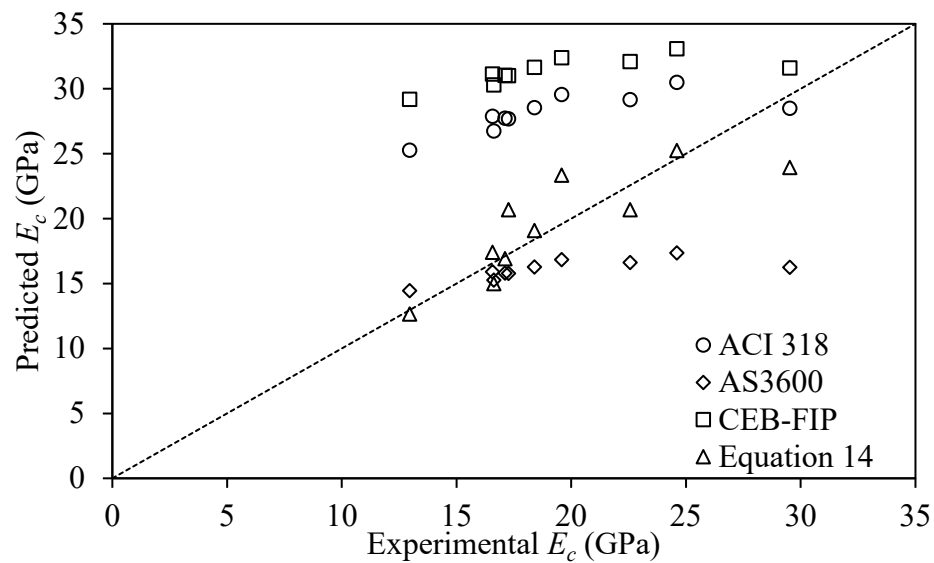
Figure 28: Experimental versus predicted modulus of elasticity of 100% slag geopolymer concrete
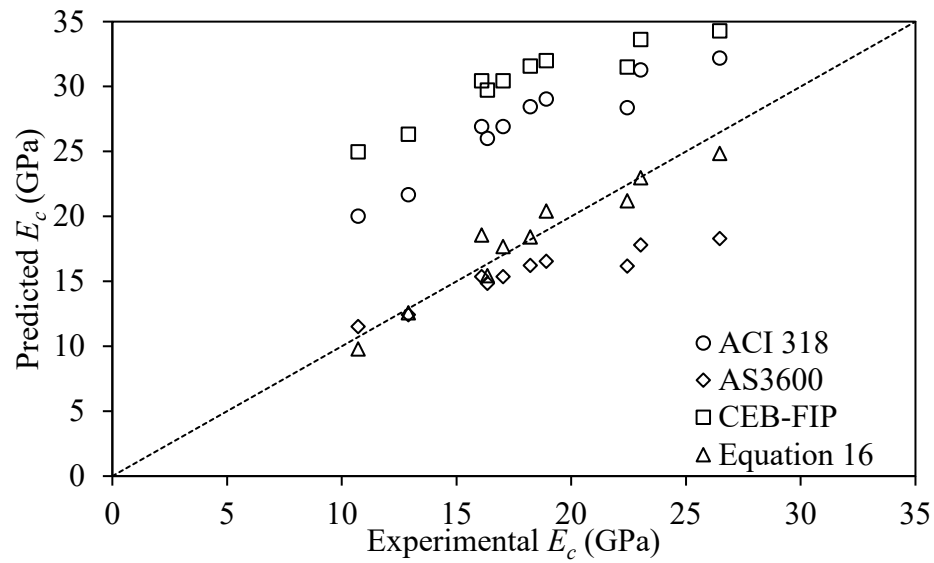
Figure 29: Experimental versus predicted modulus of elasticity of slag-fly ash blended geopolymer concrete

4.5 Tensile Splitting Strength

The tensile properties of 100% slag geopolymer concrete were indirectly evaluated using the 28-day splitting tensile strength (f_{sp}), as shown in Figure 30(a). An increase in RCA replacement to 30, 70, and 100% led to 23, 23, and 25% lower f_{sp}. This adverse effect of RCA is similar to that described earlier for f'_c. However, similar replacement percentages resulted in decreases in f'_c of 5, 5, and 21%, respectively. This signifies that f_{sp} was more influenced by RCA replacement than f'_c, which is evidenced by the decrease in the f_{sp}-to-f'_c ratio in Table 11. Figure 30(a) also presents the effect of steel fiber addition on the splitting tensile strength. Compared to those of the plain concrete mixes, f_{sp} increased by, on average, 98 and 193%, when 1 and 2% steel fibers were added, by volume, respectively, with values reaching up to 7.4 MPa. Similar enhancements in f_{sp} were noted in other work that incorporated steel fibers to NA-based geopolymer concrete

[15, 38, 105]. This shows that the adverse effect of RCA cannot only be countered by steel fiber addition but can also surpass that of the control mix made with NA (3.0 MPa), owing to the fibers' bridging effect and ability to increase the energy required for crack propagation. Furthermore, while the positive effect of steel fibers on f_{sp} was analogous with that on f'_c, the extent of improvement was superior. From Table 11, the ratio of f_{sp}-to-f'_c increased with steel fiber addition. This shows that it was more influential on f_{sp} than f'_c.

Figure 30(b) illustrates the effect of RCA replacement and steel fiber incorporation on the 28-day splitting tensile strength of slag-fly ash blended geopolymer concrete. The replacement of NA by 30, 70, and 100% RCA resulted in 13, 31, and 35% respective losses in f_{sp}. These losses were generally lower than those noted in f'_c (9, 41, and 50%). As such, it should be noted that the negative impact of RCA was generally more pronounced on f'_c than f_{sp}, which is also evidenced by the increase in the ratio of f_{sp}-to-f'_c of Table 11. Nevertheless, such an adverse effect of RCA can be reversed by the addition of steel fibers. In fact, incorporating 1 and 2% steel fibers, by volume, increased f_{sp} by 87 and 194%, respectively. Such enhancement surpasses that experienced by f'_c, resulting in higher f_{sp}-to-f'_c ratios, as shown in Table 11. This signifies the more prominent impact of steel fiber addition on f_{sp} rather f'_c of slag-fly ash blended geopolymer concrete.
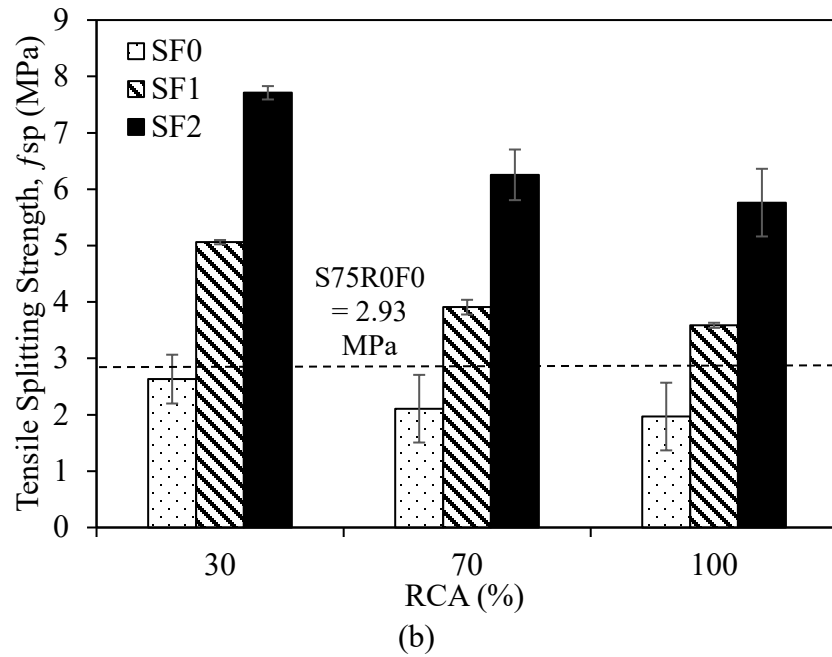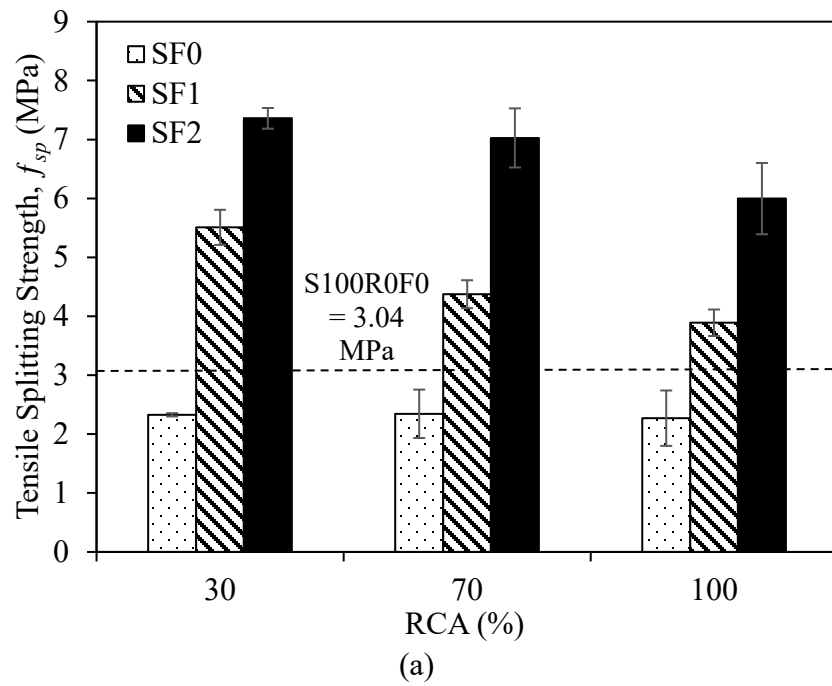
Figure 30: Splitting tensile strength of 28-day geopolymer concrete made with (a) 100% slag and (b) 3:1 slag:fly ash ratio

Table 11: Ratio of splitting tensile strength to compressive strength

Mix No.	Mix designation	f'_c (MPa)	f_{sp} (MPa)	f_{sp} / f'_c (%)
1	S100R0F0	31.8	3.0	9.6
2	S100R30F0	30.0	2.3	7.8
3	S100R30F1	34.2	5.5	16.1
4	S100R30F2	36.4	7.4	20.2
5	S100R70F0	30.4	2.3	7.7
6	S100R70F1	31.9	4.4	13.7
7	S100R70F2	33.3	7.0	21.1
8	S100R100F0	25.0	2.3	9.1
9	S100R100F1	28.0	3.9	13.9
10	S100R100F2	30.1	6.0	19.9
11	S75R0F0	31.5	2.9	9.3
12	S75R30F0	28.4	2.6	9.3
13	S75R30F1	38.3	5.1	13.2
14	S75R30F2	40.6	7.7	19.0
15	S75R70F0	18.4	2.1	11.5
16	S75R70F1	28.4	3.9	13.8
17	S75R70F2	33.0	6.3	19.0
18	S75R100F0	15.7	2.0	12.5
19	S75R100F1	26.5	3.6	13.5
20	S75R100F2	31.7	5.8	18.2

Codified equations are typically employed in predicting the splitting tensile strength of concrete. Yet, a linear model was developed to relate f_{sp} to f'_c. It is illustrated in the scatter plot of Figure 31(a) and presented in the form of Equation 17. However, the low correlation coefficient, $R^2 = 0.16$, shows that it is difficult to predict f_{sp} from f'_c with good accuracy. As such, Equation 18 was proposed as a multivariable linear regression relationship that incorporates steel fiber volume fraction (SF) as an additional parameter to enhance the accuracy of the prediction with R^2 of 0.97.

A similar approach was adopted for slag-fly ash blended geopolymer concrete. Equation 19 and Figure 31(b) show the relationship between f_{sp} and f'_c. With a low R^2 value of 0.41, the prediction capability of Equation 20 was limited. As such, Equation 18 was developed to predict f_{sp} from f'_c and steel fiber volume fraction. The accuracy significantly increased with R^2 reaching 0.95.

$$f_{sp} = 0.82\sqrt{f_c} \tag{17}$$

$$f_{sp} = 0.55\sqrt{f_c} - 0.01\text{RCA} + 2.13\text{SF} \tag{18}$$

$$f_{sp} = 0.80\sqrt{f_c} \tag{19}$$

$$f_{sp} = 0.89\sqrt{f_c} - 0.01\text{RCA} + 1.83\text{SF} \tag{20}$$
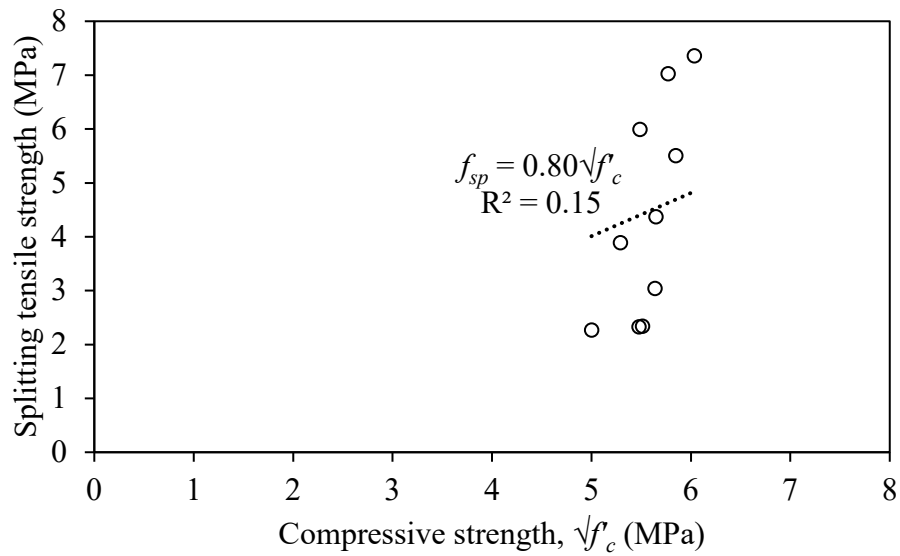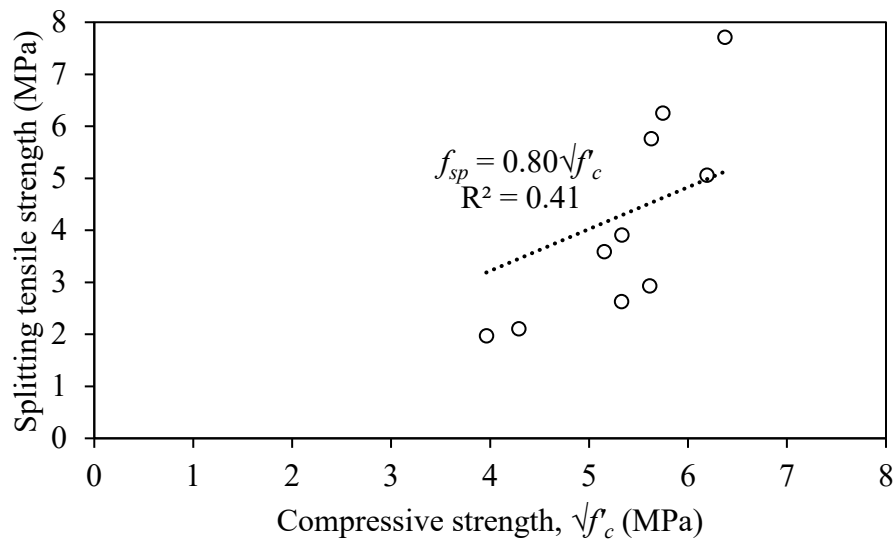
Figure 31: Correlation between tensile splitting strength and compressive strength of (a) 100% slag and (b) slag-fly ash blended geopolymer concrete

Figure 32(a) depicts the experimental versus predicted splitting tensile strength. In addition to Equation 16, codified equations of ACI 318, AS3600, and CEB-FIP [83, 84, 145] were utilized to assess their feasibility to predict f_{sp}. It is clear that the codified equations can predict f_{sp} with reasonable accuracy for values ranging between 2 and 3

MPa, beyond which the accuracy was significantly reduced. This is because these equations do not account for the effect of steel fibers. As such, such equations cannot be employed in providing a prediction of f_{sp} for 100% slag geopolymer concrete. Similar findings and conclusions are noted for slag-fly ash blended geopolymer concrete in Figure 32(b).
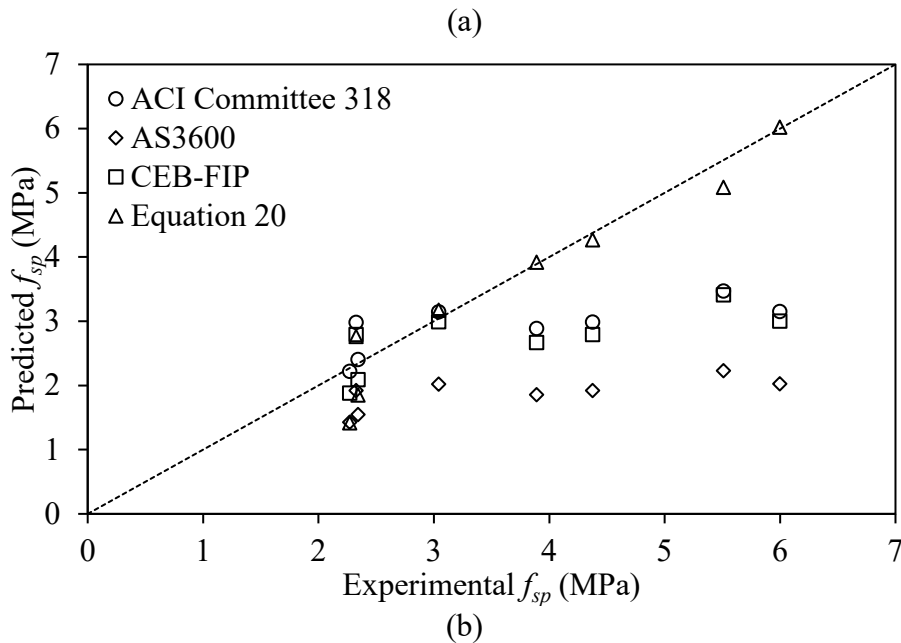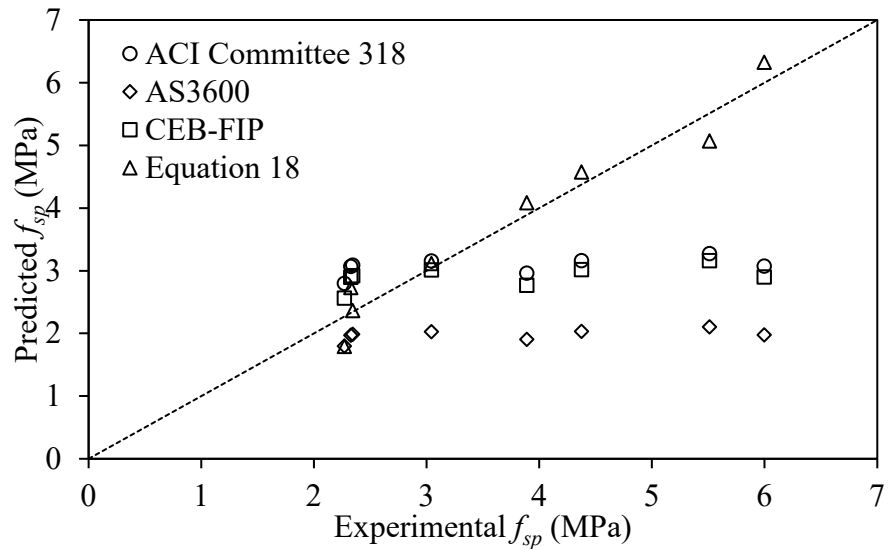
Figure 32: Correlation between Experimental and predicted tensile splitting strength of (a) 100% slag and (b) slag-fly ash blended geopolymer concrete

Table 12: Flexural performance test results of geopolymer concrete

Mix No.	Mix Designation	f_p MPa	δ_p mm	f_{600}^{100} MPa	f_{150}^{100} MPa	T_{150}^{100} J	$R_{T,150}^{100}$ %
1	S100R0F0	6.3	0.20	-	-	2.0	0.47
2	S100R30F0	5.6	0.35	-	-	2.3	0.62
3	S100R30F1	6.6	0.43	4.8	2.0	24.0	5.46
4	S100R30F2	9.0	1.00	-	8.4	33.2	5.54
5	S100R70F0	4.4	0.46	-	-	2.4	0.82
6	S100R70F1	5.4	0.53	4.9	1.9	22.3	6.20
7	S100R70F2	8.4	1.42	-	5.8	31.5	5.56
8	S100R100F0	3.1	0.52	-	-	4.0	1.93
9	S100R100F1	4.6	1.00	-	1.0	20.5	6.70
10	S100R100F2	8.1	2.20	-	4.3	31.1	5.75
11	S75R0F0	6.1	0.25	-	-	1.6	0.39
12	S75R30F0	4.4	0.35	-	-	2.4	0.82
13	S75R30F1	6.3	0.52	5.4	2.2	25.8	6.14
14	S75R30F2	9.7	0.68	9.5	7.4	49.8	7.70
15	S75R70F0	3.6	0.46	-	-	2.5	1.04
16	S75R70F1	5.6	0.67	5.4	2.0	25.2	6.75
17	S75R70F2	7.3	1.15	-	4.9	39.5	8.12
18	S75R100F0	2.9	0.81	-	-	3.2	1.66
19	S75R100F1	3.9	1.84	-	1.5	21.9	8.42
20	S75R100F2	6.0	2.05	-	3.3	28.0	8.57

4.6 Flexural Performance

The flexural performance of 100% slag and slag-fly ash blended geopolymer concrete mixes made with different proportions of RCA and steel fiber volume fractions is evaluated using the flexural (peak) strength, deflection at peak (peak deflection), residual strength, flexural toughness, and equivalent flexural strength ratio. Table 12 summarizes the results, which are discussed in more detail in the following sections.

4.6.1 Load-Deflection Curves

4.6.1.1. Effect of RCA Replacement

The load-deflection curves of 100% slag geopolymer concrete made with different RCA replacement percentages are presented in Figure 33. Although three samples were tested per mix, a representative curve for each mix is shown throughout this section. Figure 33(a) shows the load-deflection curves of plain geopolymer concrete. The applied load increased until failure in a pseudo-elastic mode for all mixes. Yet, a decrease in slope can be noted with RCA replacement. Actually, 30, 70, and 100% RCA replacement resulted in 33, 34, and 87% decreases in the slope compared to the control mix S100R0F0. This is primarily due to the lower modulus of elasticity.

Figure 33(b-c) depicts the load-deflection curves of 100% slag steel fiber-reinforced geopolymer concrete. Unlike those of plain concrete, these curves comprise two phases. The first phase is characterized by an increase in load until the peak load is reached and is governed by E_c. Irrespective of steel fiber volume fraction, the change in RCA replacement percentage did not have a significant impact on the slope. Furthermore,

the second phase represents the post-peak flexural softening behavior. It was due to the bridging effect of steel fibers and their capacity to reduce crack development and propagation. The slope of this part of the curve was not significantly impacted by the RCA replacement percentage; yet, the residual strength was, as noted in later sections.
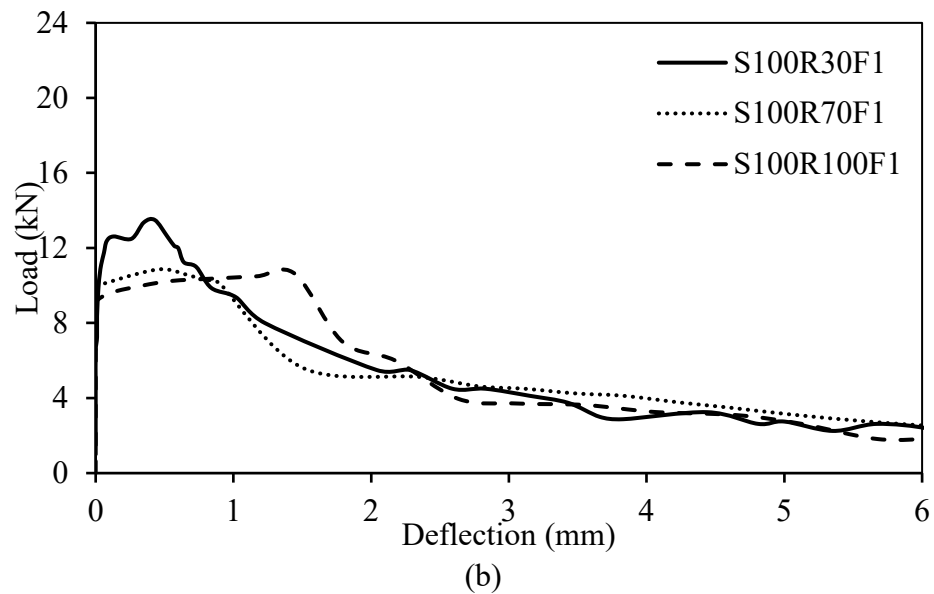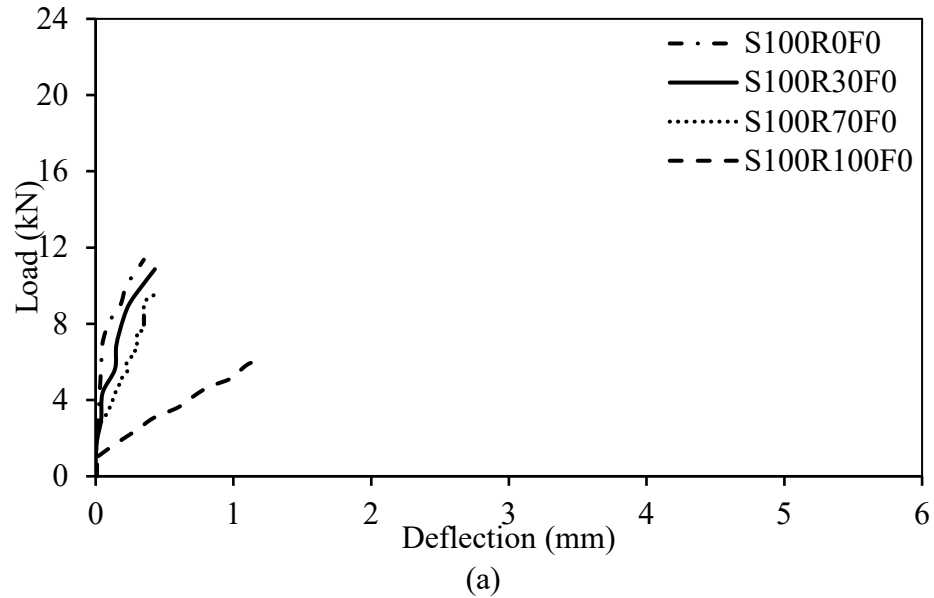
Figure 33: Typical load-deflection curves of 100% slag geopolymer concrete mixes with (a) SF 0%, (b) SF 1%, and (c) SF 2%
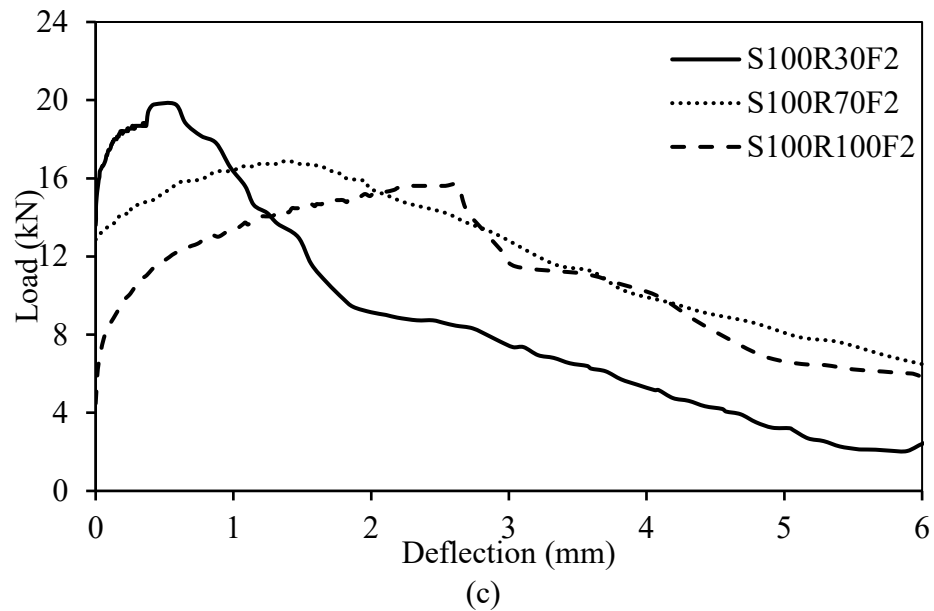
Figure 33: Typical load-deflection curves of 100% slag geopolymer concrete mixes with (a) SF 0%, (b) SF 1%, and (c) SF 2% (Continued)

Figure 34 demonstrates the effect of RCA replacement on the load-deflection curves of slag-fly ash blended geopolymer concrete. For plain concrete mixes [Figure 34(a)], the replacement of NA by 30, 70, and 100% RCA decreased the slope of the ascending part of the load-deflection curve by 25, 64, and 84%, respectively, compared to the control mix S75R0F0. Similar but less significant reductions in the slope were noted when 1 and 2% steel fiber, by volume, were added to the mix, as shown in Figure 34(b-c). Furthermore, the slope of the descending post-peak part of the curves was similar for 70 and 100% RCA replacement but was more intense for mixes made with 30% RCA.
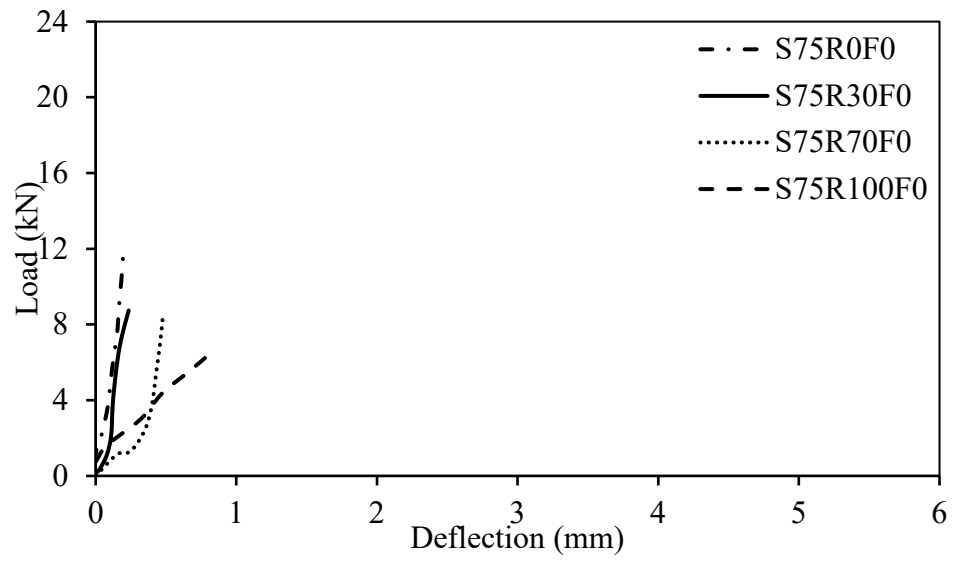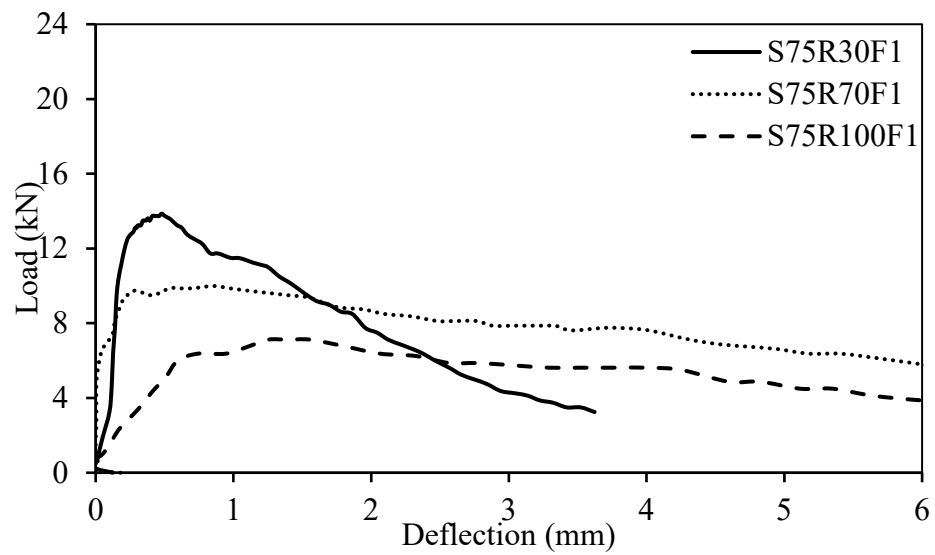
Figure 34: Typical load-deflection curves of slag-fly ash blended geopolymer concrete mixes with (a) SF 0%, (b) SF 1%, and (c) SF 2%
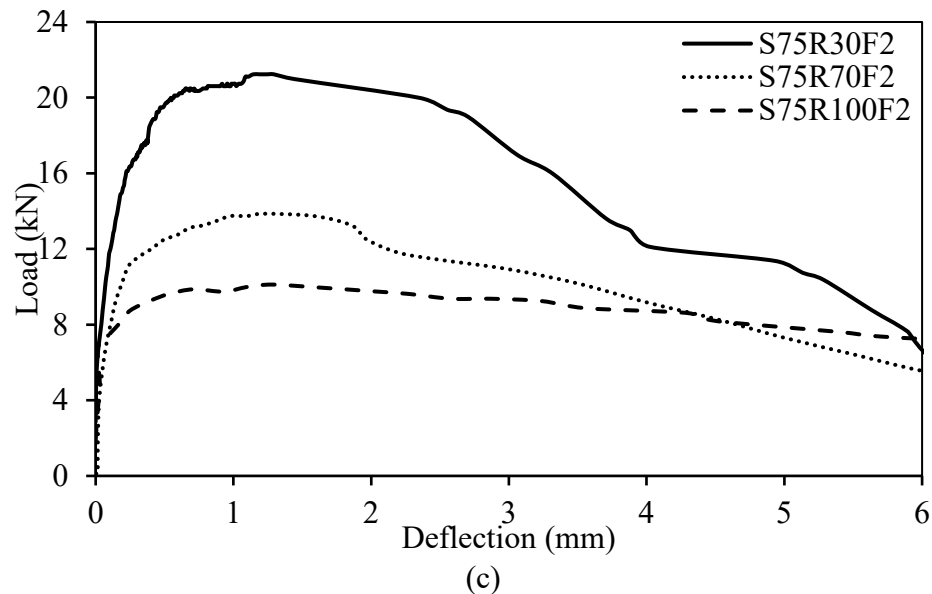
Figure 34: Typical load-deflection curves of slag-fly ash blended geopolymer concrete mixes with (a) SF 0%, (b) SF 1%, and (c) SF 2% (Continued)

4.6.1.2 Effect of Steel Fiber Addition

To evaluate the effect of steel fiber addition on the flexural load-deflection curves of 100% slag geopolymer concrete, Figures 35(a-c) are considered. For every 1% steel fiber added, by volume, the slope of mixes made with 30, 70, and 100% RCA increased by, on average, 1.7, 3.2, and 11.4 times, respectively. This is primarily due to the increase in the modulus of elasticity of the concrete upon the incorporation of steel fibers. It is also possible that the bond between the steel fibers and binding matrix may have hindered crack development when the applied load was lower than the peak load [146, 147]. After this point, i.e., the applied load exceeded the peak load, the steel fibers bridged the cracks and delayed their propagation. This is evident by the post-peak tail in steel fiber-reinforced geopolymer concrete mixes in Figures 35(a-c). Also, the post-peak load decreased at a

generally faster rate for mixes made with 2% steel fibers, by volume, despite having a higher peak load. In conclusion, the negative impact of RCA on the flexural performance of 100% slag geopolymer concrete could not only be reversed by the addition of steel fibers but also enhanced to the extent of exceeding that of the control mix made with natural aggregates only.
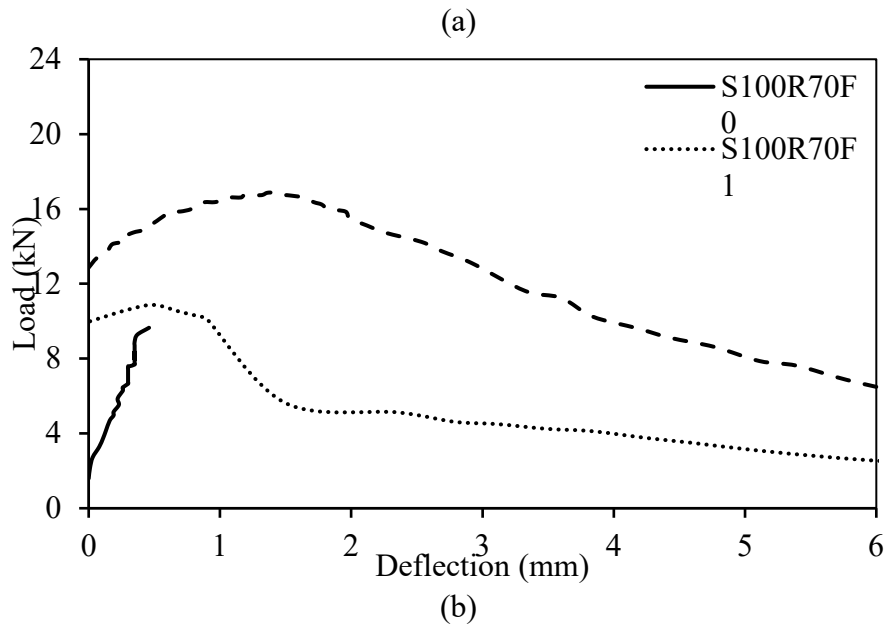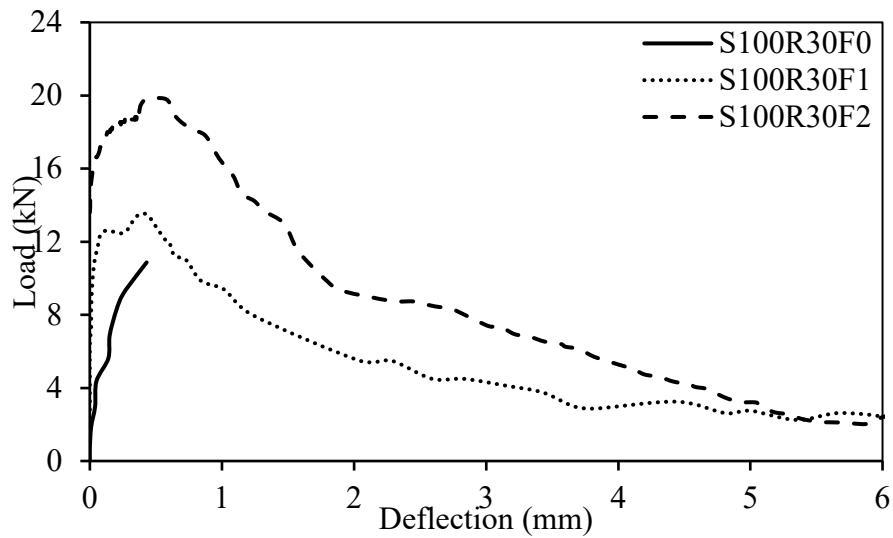
Figure 35: Typical load-deflection curves of 100% slag geopolymer concrete specimens with RCA (a) 30%, (b) 70%, and (c) 100%
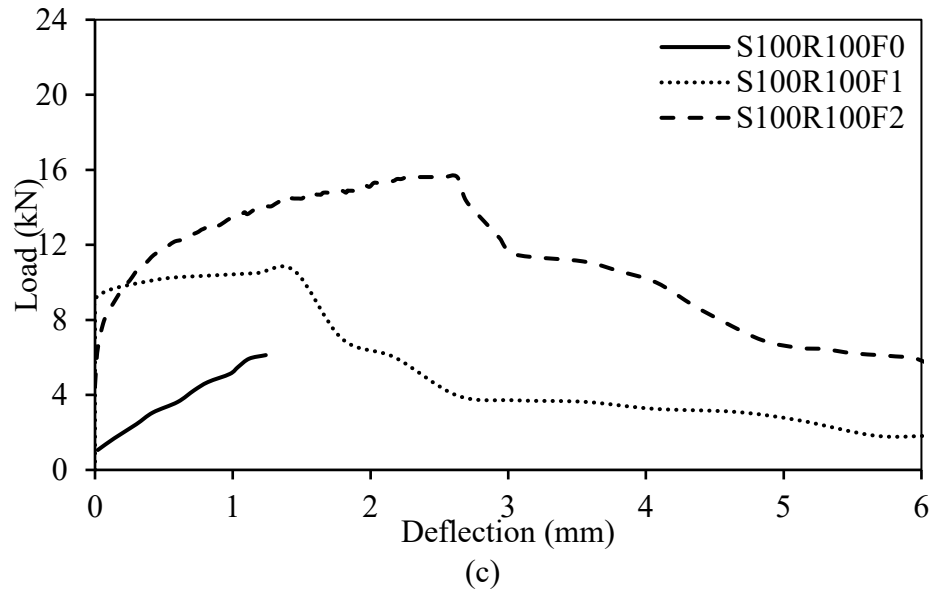
Figure 35: Typical load-deflection curves of 100% slag geopolymer concrete specimens with RCA (a) 30%, (b) 70%, and (c) 100% (Continued)

Figure 36(a-c) illustrates the effect of steel fiber addition on the load-deflection curve of slag-fly ash blended geopolymer concrete made with different RCA replacement percentages. For every 1% steel fiber added, by volume, the slope of the ascending part of the curve of blended geopolymer mixes incorporating 30, 70, and 100% RCA increased by, on average, 2.5, 3.0, and 3.5 times, respectively, owing to an associated increase in the modulus of elasticity. Conversely, the slope of the descending part for mixes made with 1 and 2% steel fibers was either the same or slightly higher for the latter. This post-peak tail developed because of the bridging effect associated with the incorporation of steel fibers. Thus, it can be concluded that the addition of steel fibers improved the flexural performance of slag-fly ash blended geopolymer made with 100% RCA to exceed that of the control mix (S75R0F0).
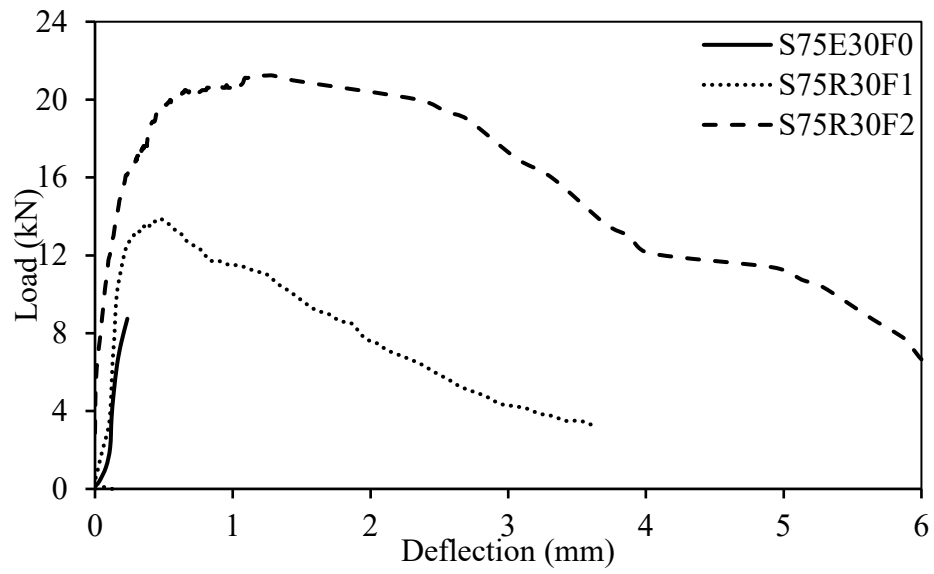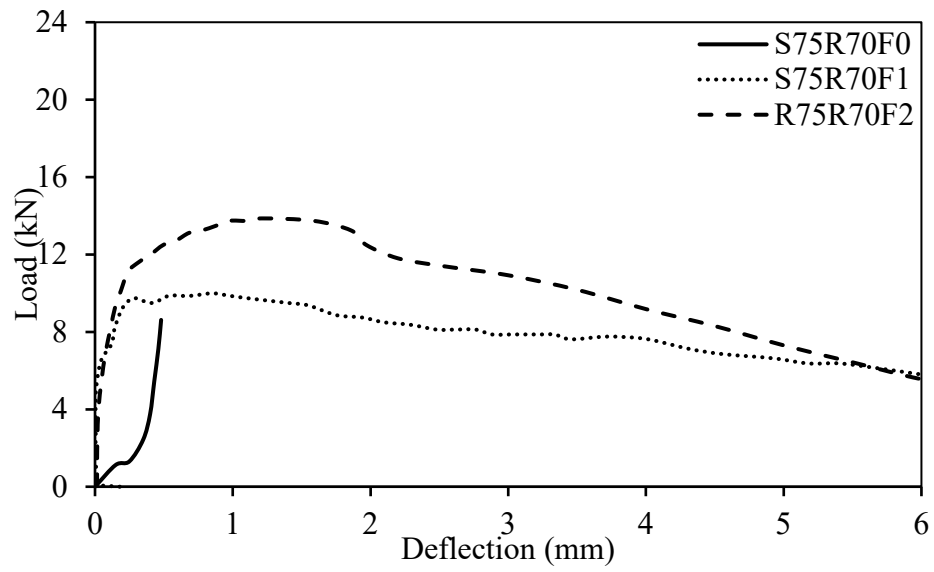
Figure 36: Typical load-deflection curves of slag-fly ash blended geopolymer concrete specimens with (a) RCA 30%, (b) RCA 70%, and (c) RCA 100%
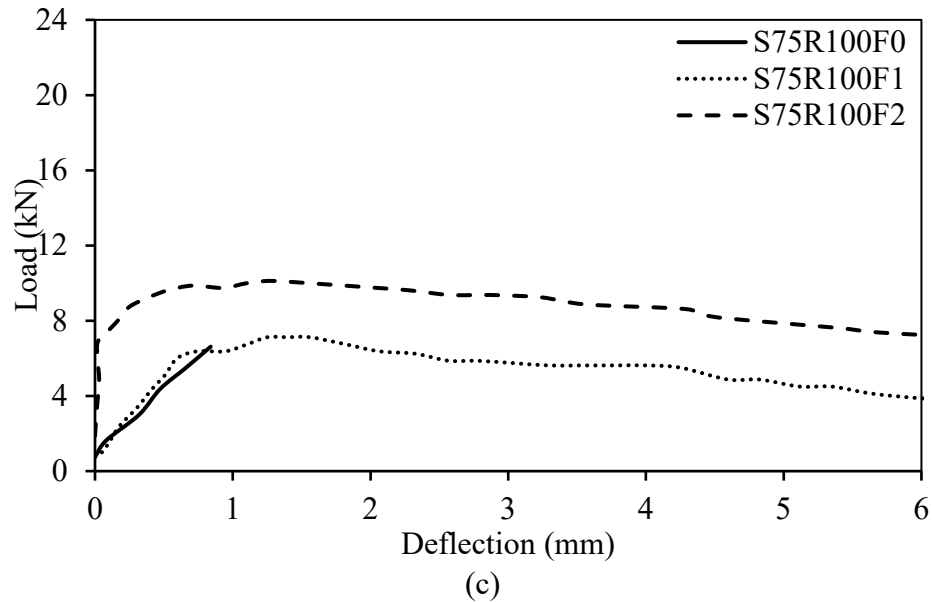
Figure 36: Typical load-deflection curves of slag-fly ash blended geopolymer concrete specimens with (a) RCA 30%, (b) RCA 70%, and (c) RCA 100% (Continued)

4.6.2 Flexural Strength

The flexural strength (f_r) of 28-day 100% slag geopolymer concrete made with different RCA replacement percentages and steel fiber volume fractions is shown in Figure 37(a). Replacing NA by 30, 70, and 100% RCA in plain geopolymer concrete led to reductions in f_r by 11, 29, and 51%, respectively. In comparison, the corresponding values of f'_c decreased by 5, 5, and 21%. This signifies that the RCA replacement has a more prominent effect on the flexural strength. As such, the f_r-to-f'_c ratio decreased, as shown in Table 13. Furthermore, the addition of 1 and 2% steel fibers, by volume, increased the flexural strength by, on average, 30 and 105%, respectively, compared to plain geopolymer counterparts. Such findings are analogous to those reported in steel fiber-reinforced slag-based or slag-fly ash blended geopolymer concrete made with

natural aggregates only [15, 38, 105, 106]. Also, the incorporation of steel fibers seemed to be more impactful on f_r rather than f'_c, evidenced by the increase in the f_r-to-f'_c ratio in Table 13. Based on the results, it is apparent that the addition of 2% steel fiber, by volume, could promote the production of 100% slag RCA geopolymer concrete with superior flexural strength than the NA-based control mix (S100R0F0).

Figure 37(b) presents the flexural strength of slag-fly ash geopolymer concrete incorporating RCA and steel fibers. The results show that every 10% RCA replacement caused average reductions in f_r of 6.7%. While a similar trend was noted for f'_c, the corresponding decrease was 4.8%. With such a slight difference, it can be noted that the replacement of NA by RCA has a somewhat similar effect on f_r and f'_c, evidenced by the relatively similar f_r-to-f'_c ratios of these mixes in Table 13. Conversely, the addition of steel fibers had a different effect on the flexural strength of slag-fly ash geopolymer concrete. For every 1% steel fiber added to the mix, the value of f_r increased by, on average, 55%. Such an increase is sufficient to counter the negative impact of RCA. In addition, f_r increased more than f'_c upon the incorporation of steel fibers, which can be clearly seen in the increase in f_r-to-f'_c ratios in Table 13.
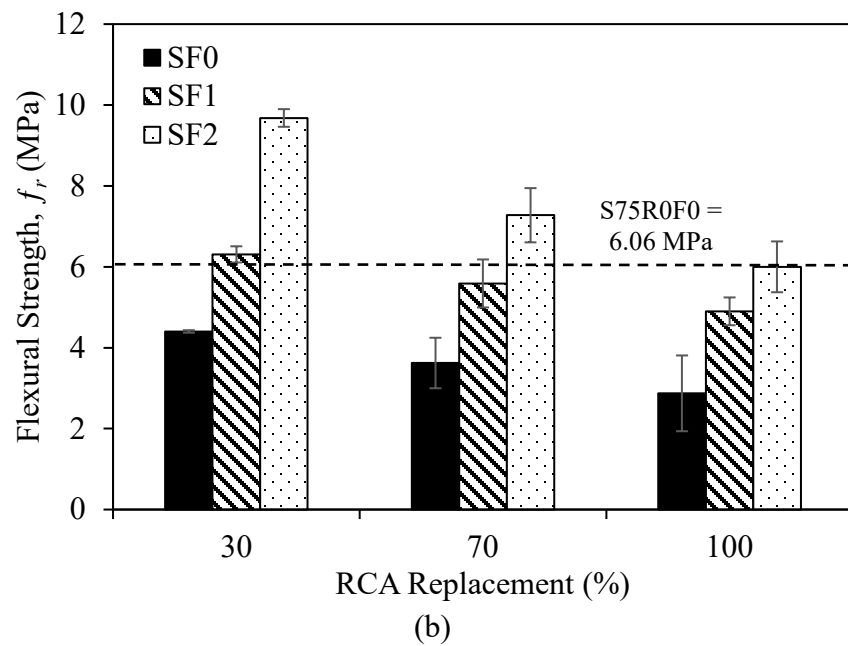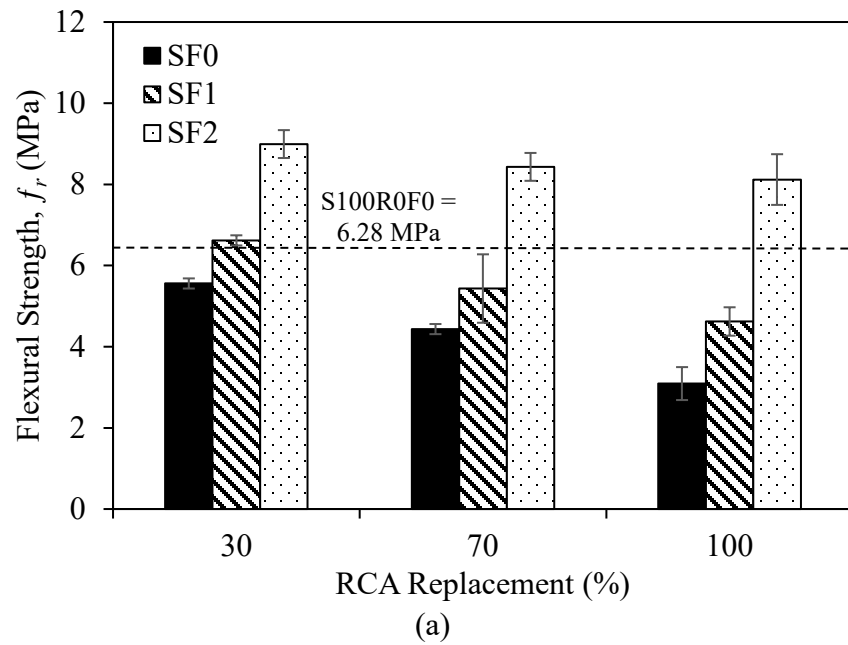
Figure 37: Flexural strength of 28-day (a) 100% slag and (b) slag-fly ash blended geopolymer concrete

Table 13: Ratio of flexural strength to compressive strength

Mix No.	Mix designation	f'_c (MPa)	f_r (MPa)	f_r/f'_c (%)
1	S100R0F0	31.8	6.3	19.7
2	S100R30F0	30.0	5.6	18.5
3	S100R30F1	34.2	6.6	19.4
4	S100R30F2	36.4	9.0	24.7
5	S100R70F0	30.4	4.4	14.6
6	S100R70F1	31.9	5.4	17.0
7	S100R70F2	33.3	8.4	25.3
8	S100R100F0	25.0	3.1	12.4
9	S100R100F1	28.0	4.6	16.5
10	S100R100F2	30.1	8.1	27.0
11	S75R0F0	31.5	6.1	19.2
12	S75R30F0	28.4	4.4	15.5
13	S75R30F1	38.3	6.3	16.5
14	S75R30F2	40.6	9.7	23.8
15	S75R70F0	18.4	3.6	19.7
16	S75R70F1	28.4	5.6	19.7
17	S75R70F2	33.0	7.3	22.1
18	S75R100F0	15.7	2.9	18.3
19	S75R100F1	26.5	4.9	18.5
20	S75R100F2	31.7	6.0	19.0

As noted earlier, the values of f_r and f'_c were affected by RCA replacement and steel fiber addition. Accordingly, the two properties were correlated using a linear regression model, as shown in Figure 38(a) and presented in the form of Equation 21. However, with a low correlation coefficient, R^2, of 0.25, it provides a predicted value of f_r with low accuracy. As such, a multivariable regression model comprising f'_c, steel fiber volume fraction (SF), and RCA replacement percentage was developed as Equation 22 with $R^2 = 0.91$. A similar approach was adopted for slag-fly ash blended geopolymer concrete. As a result, Equation 23 was developed based on the scatter plot of Figure 38(b). With a low correlation coefficient, R^2, of 0.57, Equation 24 was proposed to enhance the accuracy of predicting f_r by including f'_c, SF, and RCA. The resultant value of R^2 was 0.89. Based on the coefficients of Equations 22 and 24, it can be mentioned that f_r is proportional to f'_c and SF and inversely proportional to RCA.

The feasibility of using codified equations of ACI 318, AS3600, and CEB-FIP [83, 84, 145] is evaluated through Figure 39. For 100% slag and slag-fly ash blended geopolymer concrete, the equations of ACI 318 [84] and AS3600 [83] underestimated the value of f_r, while that of CEB-FIP [145] provided a more accurate prediction. Indeed, the average respective errors associated with these three codified equations were 39, 41, and 26%. On the other hand, the newly-developed Equation 20 was more suitable for predicting the values of f_r for 100% slag geopolymer concrete with an error of 7%. Similarly, for slag-fly ash geopolymer concrete, the errors attributed to the three codified equations were 35, 37, and 18%, respectively, while that of Equation 22 was less than 10%. As such, codified equations cannot be used in their current form to predict the flexural strength of geopolymer concrete made with RCA and steel fibers.

$$f_r = 1.12\sqrt{f_c} \tag{21}$$

$$f_r = 1.04\sqrt{f_c} - 0.02\text{RCA} + 1.79\text{SF} \tag{22}$$

$$f_r = 1.08\sqrt{f_c} \tag{23}$$

$$f_r = 1.07\sqrt{f_c} - 0.02\text{RCA} + 1.12\text{SF} \tag{24}$$
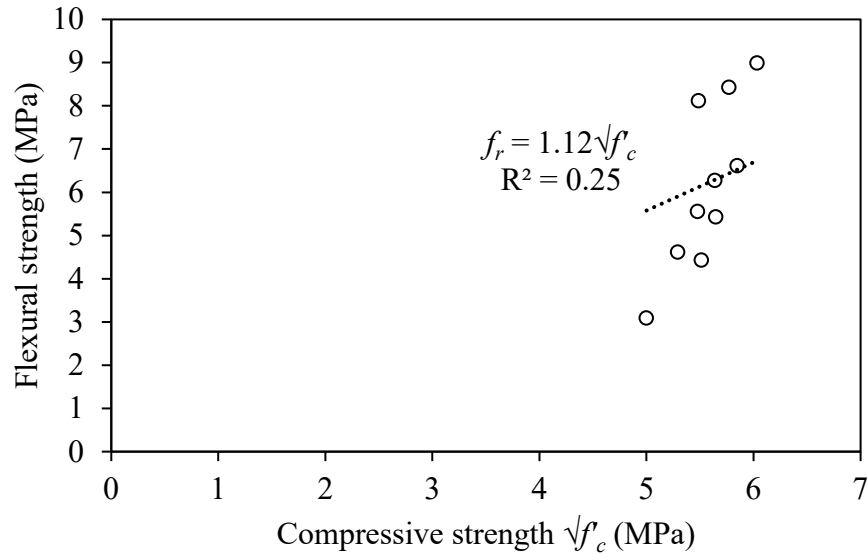
(a)
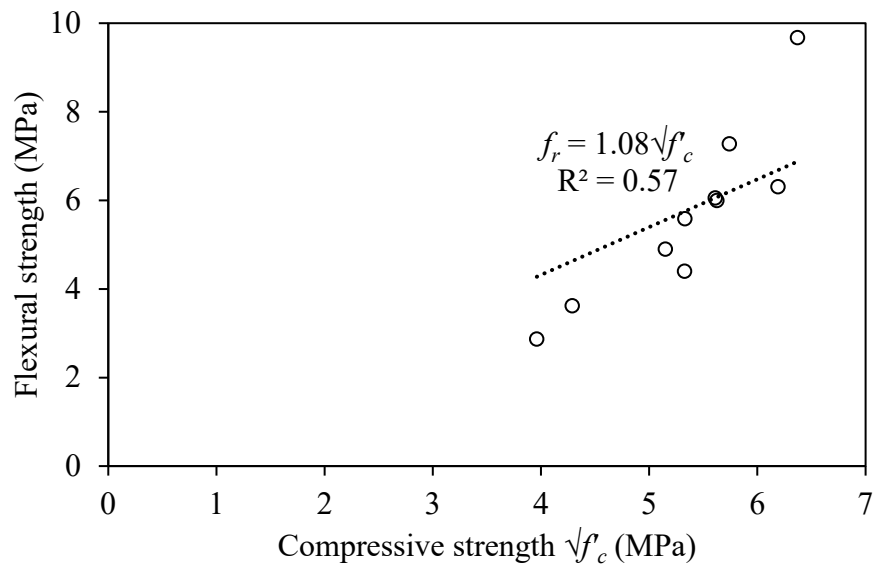
(b)

Figure 38: Relationship between flexural and cylinder compressive strength of 28-day (a) 100% slag and (b) slag-fly ash blended geopolymer concrete
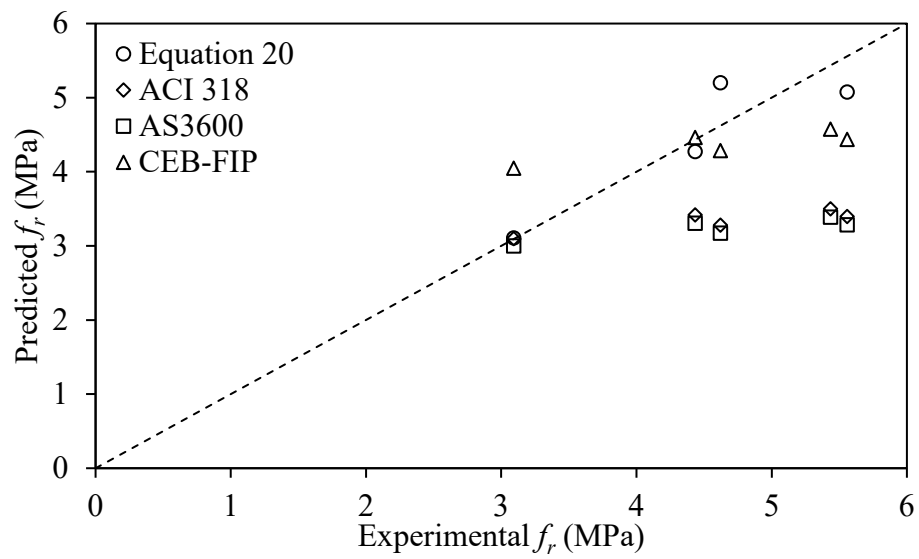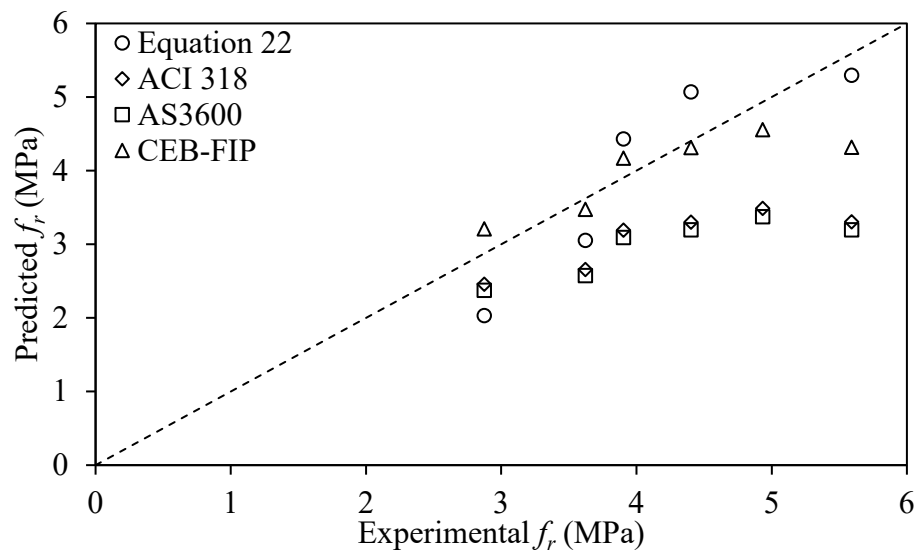
Figure 39: Experimental versus predicted flexural strength of (a) 100% slag and (b) slag-fly ash blended geopolymer concrete

4.6.3 Deflection

The mid-span deflection of 100% slag geopolymer concrete mixes made with different RCA and steel fiber proportions was measured. Although ASTM C1609 [131] notes that the first and peak deflection associated with the first and peak load are typically required, the load-deflection curves of Figure 33-36 show that the first load and deflection cannot be detected in all mixes. To maintain comparability of the mixes, the deflection referred to herein is that at the peak load and is denoted as δ_p. Figure 40(a) presents the peak deflection as a function of RCA replacement percentage and steel fiber volume fraction with values ranging from 0.2 to 2.2 mm. In plain geopolymer concrete, the replacement of NA by 30, 70, and 100% RCA increased δ_p by 75, 130, and 160%, respectively. A similar increasing trend was noticed with steel fiber-reinforced mixes. Furthermore, the addition of steel fibers led to higher peak deflections. In fact, adding 1 and 2% steel fiber volume fractions increased the deflection by, on average, 43 and 239%, respectively. Similar results were reported in cement-based concrete and were attributed to the bridging effect of steel fibers and their ability to diminish crack propagation [9].

The change in peak deflection (δ_p) as a function of 28-day cylinder compressive strength is presented in Figure 40(b). For plain 100% slag geopolymer concrete, the deflection ranged between 0.20 and 0.52 mm with higher deflections being associated with mixes with lower f'_c and higher RCA replacement. On the other hand, the deflection of steel fiber-reinforced geopolymer concrete made with 1 and 2% steel fiber, by volume, were in the ranges of 0.43-1.00 mm and 1.00-2.20 mm, respectively. Moreover, it is worth noting that the inclusion of steel fibers significantly increased the deflection for a specific compressive strength. For instance, mixes incorporating 0, 1, and 2% steel fiber volume

fractions with a compressive strength of around 31 MPa had respective deflections of 0.20, 0.53, and 1.20 mm. Such an increase in δ_p highlights steel fibers-reinforced geopolymer concrete's ability to maintain a certain compressive strength while enhancing the deflection capacity.
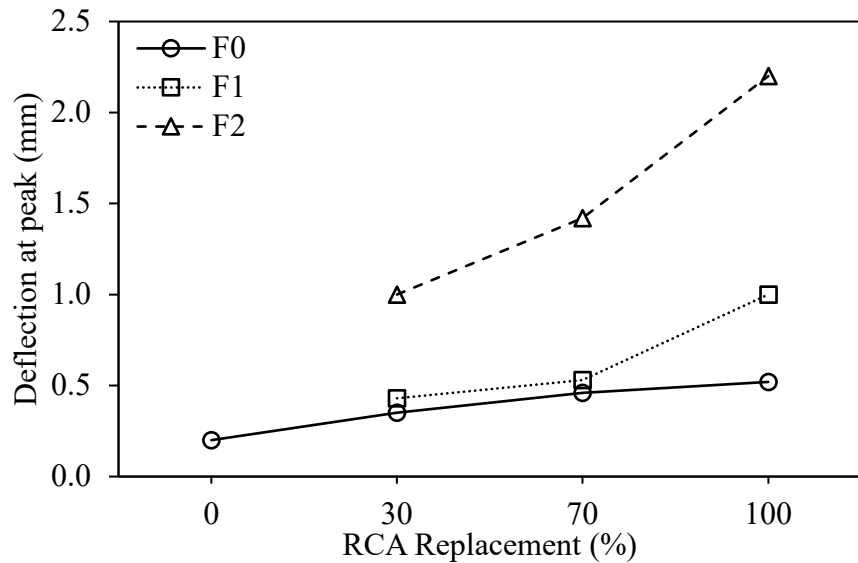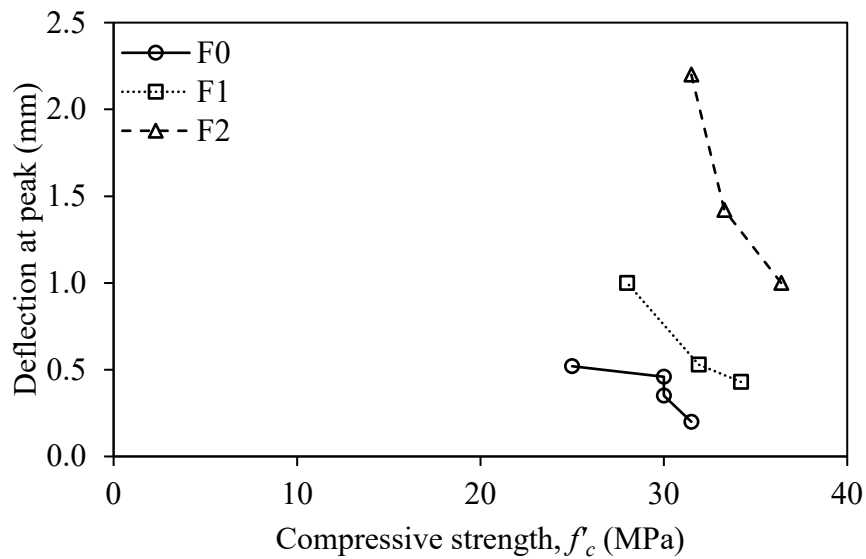
Figure 40: Deflection at peak load of 100% slag geopolymer concrete with various (a) RCA replacement percentage and SF volume fractions and (b) cylinder compressive strength.

Figure 41(a) illustrates the influence of RCA replacement and steel fiber addition on the peak deflection of slag-fly ash blended geopolymer concrete. An increase in the RCA replacement percentage to 30, 70, and 100% led to respective increases in δ_p of 43, 112, and 178%. Similarly, the addition of 1 and 2% steel fibers, by volume, increased the deflection by, on average, 44 and 195%, respectively. Furthermore, the change in δ_p as a function of 28-day cylinder compressive strength is depicted in Figure 41(b). For plain slag-fly ash blended geopolymer concrete, the peak deflection reached up to 0.68 mm, while that of counterparts incorporating 1 and 2% steel fiber volume fractions could reach up to 1.15 and 2.05 mm, respectively. Yet, such values were impacted by the values of f'_c. In fact, higher compressive strength, associated with lower RCA replacement, resulted in lower δ_p. Accordingly, it can be concluded that for both types of geopolymer concrete, i.e. 100% slag and slag-fly ash blended, the peak deflection is proportional to RCA replacement and steel fiber addition but inversely proportional to the compressive strength. Similar findings were reported for steel fiber-reinforced RCA cement-based concrete incorporating steel fibers [8, 9, 147, 148].

Figure 41: Deflection at peak load of slag-fly ash blended geopolymer concrete with various (a) RCA replacement percentage and SF volume fractions and (b) cylinder compressive strength

4.6.4 Residual Strength

The residual strength of concrete represents its capacity to maintain strength after cracking [131]. Table 12 shows the residual strength at two deflection points, L/600 and L/150. Since plain geopolymer concrete mixes did not experience any post-peak behavior, their residual strength was not reported and left blank. Further, mixes with peak deflections larger than L/600 (0.75 mm) were also left empty. Accordingly, the residual strength reported in this thesis is mainly focused on that at L/150 denoted by f_{150}^{100}.

The residual strengths at L/150 of 100% slag geopolymer concrete made with different RCA replacement percentages and steel fiber volume fractions are shown in Figure 42(a). Increasing the RCA replacement from 30 to 70 and 100% reduced f_{150}^{100} by, on average, 19 and 51%, respectively. With a similar flexural strength retention rate, mixes with higher RCA had lower flexural strength, resulting in lower residual strength. Moreover, the inclusion of steel fibers in 100% slag geopolymer concrete mixes resulted in a significant increase in f_{150}^{100}. In fact, increasing the steel fiber volume fraction from 1 to 2% increased f_{150}^{100} by, on average, 3.86 times. Also, the correlation between f'_c and f_{150}^{100} was investigated in Figure 42(b). Regardless of steel fiber volume fraction, an increase in compressive strength led to an increase in residual strength. Yet, this increase was more apparent in mixes incorporating 2% steel fiber volume fraction. Indeed, for every 1 MPa increase in f'_c, the value of f_{150}^{100} for mixes made with 1 and 2% steel fiber, by volume, increase by an average 0.16 and 0.84 MPa, respectively.
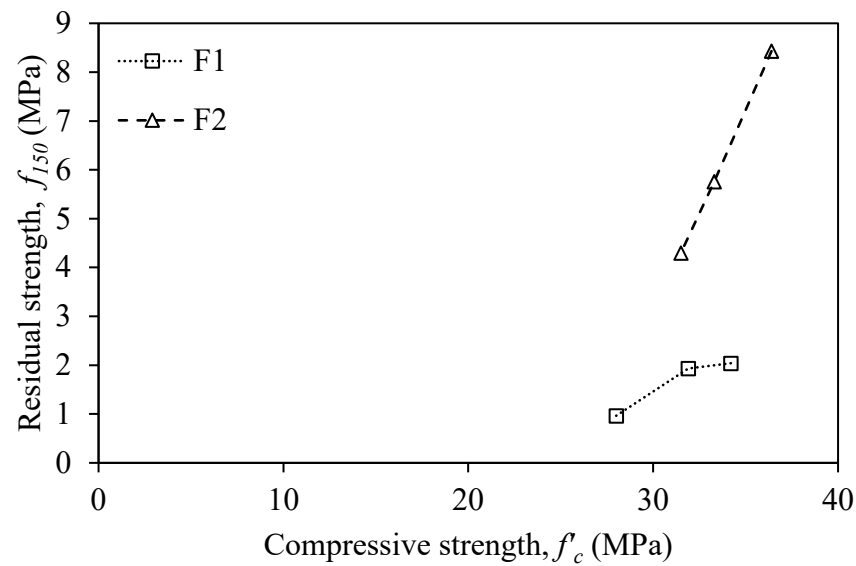
Figure 42: Residual strength of 100% slag geopolymer concrete with various (a) RCA replacement percentage and SF volume fractions and (b) cylinder compressive strength

Figure 43(a) presents the residual strength as a function of RCA replacement and steel fiber volume fraction. Increasing the RCA replacement percentage from 30 to 100% reduced f_{150}^{100} for mixes made with 1 and 2% steel fibers, by volume, from 2.22 to 1.48

MPa and 7.36 to 3.27 MPa. Clearly, the decrease in f_{150}^{100} was more significant in the latter

mixes. Nevertheless, the addition of steel fibers increased f_{150}^{100}. In fact, mixes with 30, 70,

and 100% RCA replacement experienced 2.3, 2.5, and 2.2 times higher f_{150}^{100} when steel

fiber volume fraction increased from 1 to 2%. Furthermore, the effect of f'_c on f_{150}^{100} is

presented in Figure 43(b). As f'_c increased by 1 MPa, f_{150}^{100} increased by, on average, 0.12

and 0.69 MPa for mixes reinforced with 1 and 2% steel fibers, by volume. These findings

highlight that f_{150}^{100} is proportional to steel fiber volume fraction and f'_c and inversely

proportional to RCA replacement. Similar conclusions were noted in cement-based

concrete made with RCA and steel fibers [8, 9, 148].

(a)

Figure 43: Residual strength of slag-fly ash blended geopolymer concrete with various (a) RCA replacement percentage and SF volume fractions and (b) cylinder compressive strength

Figure 43: Residual strength of slag-fly ash blended geopolymer concrete with various (a) RCA replacement percentage and SF volume fractions and (b) cylinder compressive strength (Continued)

4.6.5 Flexural Toughness

The concrete's energy absorption capacity is characterized by its flexural toughness. The influence of RCA replacement and steel fiber addition on T_{150} is shown in Figure 44(a). For plain 100% slag geopolymer concrete, the replacement of NA by RCA had little to no impact on T_{150}. However, the results were different when steel fibers were incorporated into the geopolymer mixes. For mixes made with 1% steel fiber, by volume, the toughness decreased from 24 to 20 J (14% drop) when RCA replacement increased from 30 to 100%, respectively. Conversely, the toughness of mixes incorporating 2% steel fiber volume fraction decreased from 33 to 31 J (6% drop). Clearly, replacing NA with RCA had a limited impact on T_{150}. Furthermore, the addition of 1 and 2% steel fibers, by volume, increased the value of T_{150} by, on average, 8.3 and 14.5 times, respectively. Such

an increase is due to the steel fibers' bridging effect and ability to diminish crack propagation and enhance flexural performance.

Figure 44(b) presents the change in T_{150} as a function of 28-day cylinder compressive strength. A limited change in T_{150} was noted when f'_c increased in plain 100% slag geopolymer concrete. This was not the case for steel fiber-reinforced counterparts. Indeed, for every 1 MPa increase in f'_c, the toughness of mixes made with 1 and 2% steel fiber volume fractions increased by, on average, 0.6 and 0.4 J, respectively. Also, it should be noted that, for a specific compressive strength, the toughness changed with steel fiber incorporation. For instance, concrete mixes incorporating 0, 1, and 2% steel fiber, by volume, with a compressive strength of around 31 MPa had respective toughness values of 2.0, 22.3, and 31.5 J. Accordingly, it is clear that toughness was more impacted by steel fiber addition than RCA replacement.
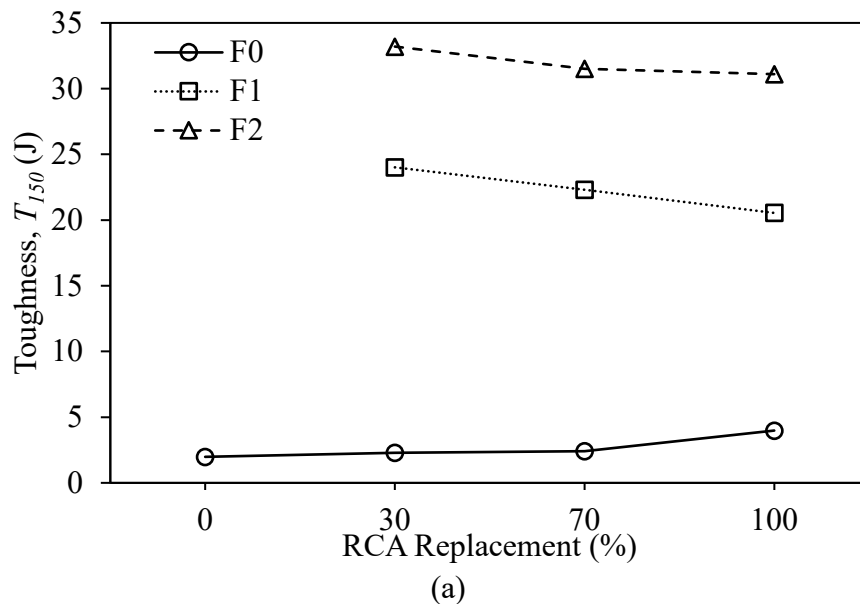
(a)

Figure 44: Flexural toughness of 100% slag geopolymer concrete with various (a) RCA replacement percentage and SF volume fractions and (b) cylinder compressive strength
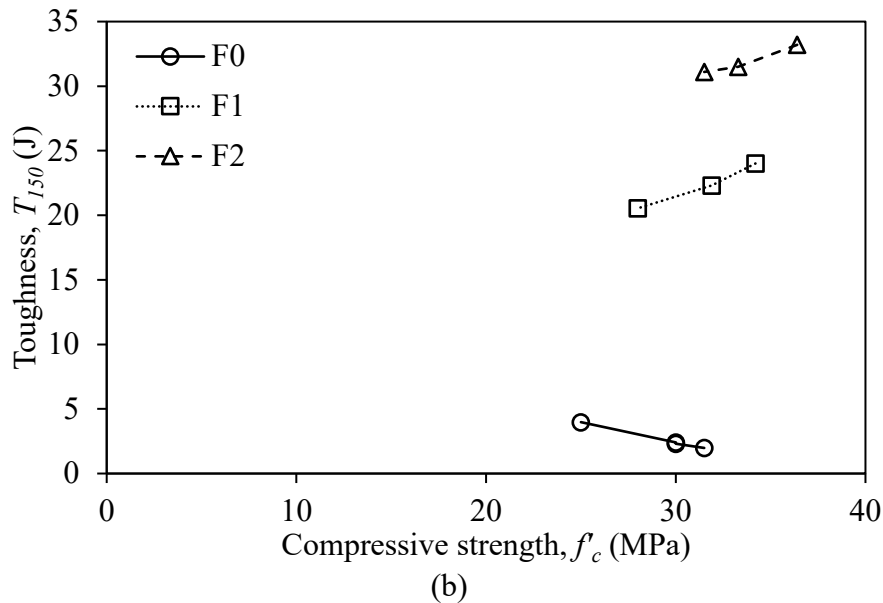
Figure 44: Flexural toughness of 100% slag geopolymer concrete with various (a) RCA replacement percentage and SF volume fractions and (b) cylinder compressive strength (Continued)

The flexural toughness of slag-fly ash blended geopolymer concrete made with different RCA and steel fiber proportions is shown in Figure 45(a). While T_{150} did not significantly change due to RCA replacement in plain geopolymer concrete mixes, respective reductions of up to 15 and 44% were noted for those incorporating 1 and 2% steel fiber, by volume. Yet, this adverse effect could be countered by steel fiber addition. In fact, T_{150} increased by, on average, 9.2 and 19.6 times when 1 and 2% steel fiber fractions were added to the mix, respectively. However, the positive impact of steel fiber addition diminished with RCA replacement. Furthermore, the relationship between T_{150} and f'_c is shown in Figure 45(b). The toughness did not experience significant change as f'_c of plain slag-fly ash blended geopolymer concrete increased. However, for mixes reinforced with 1 and 2% steel fiber, it increased by 0.7 and 4.2 J for every 1 MPa increase

in f'_c. A similar finding to that reported in 100% slag geopolymer concrete is noted here, whereby the toughness increased when steel fibers were added to the mix even though the compressive strength was the same.
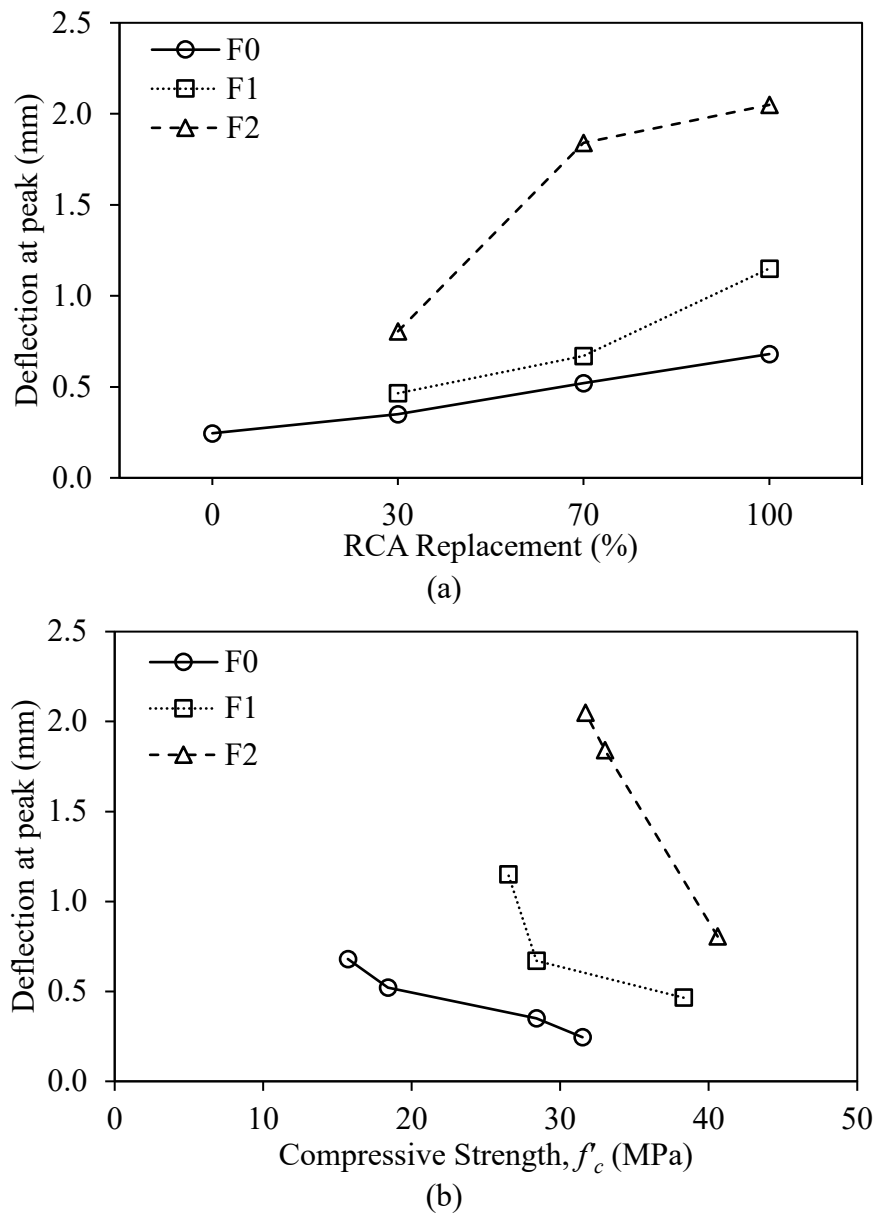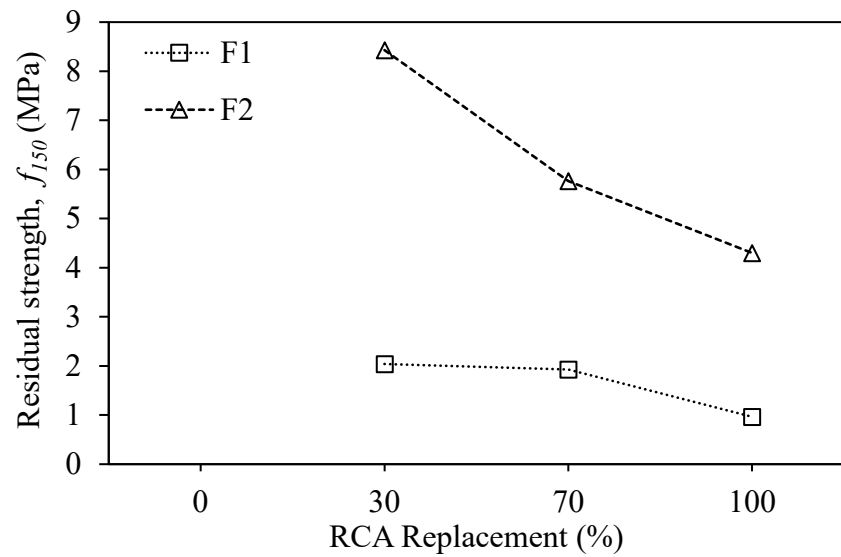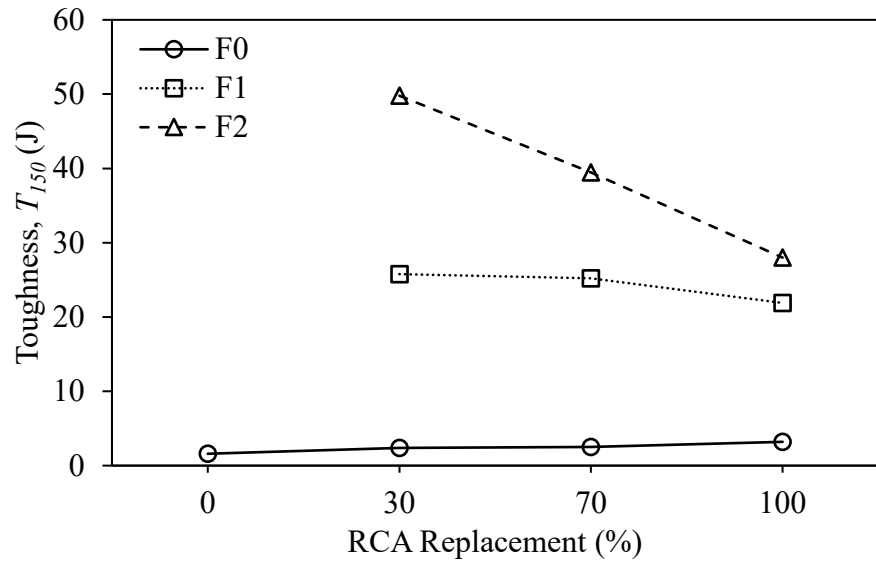

(a)
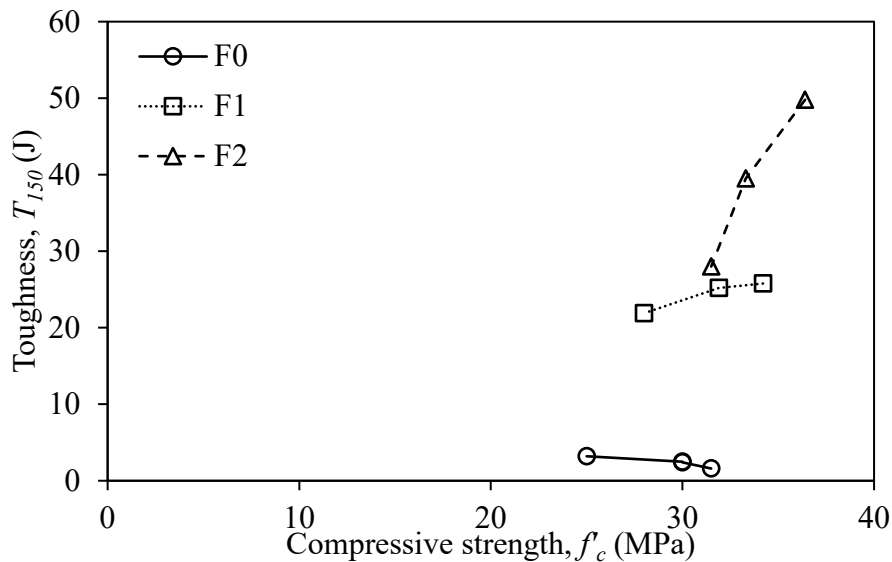
(b)

Figure 45: Flexural toughness of slag-fly ash blended geopolymer concrete with various (a) RCA replacement percentage and SF volume fractions and (b) cylinder compressive strength

4.6.6 Equivalent Flexural Strength Ratio

The equivalent flexural strength ratio ($R_{T,150}^{100}$) of 100% slag geopolymer concrete is shown in Figure 46(a). For plain concrete mixes, 30, 70, and 100% RCA replacement increased the ratio by 32, 75, and 311%, respectively. Despite such increases, the values ranged from 0.5 to 1.9%. The impact of RCA was less significant for steel fiber-reinforced geopolymer concrete, as mixes made with 1 and 2% steel fiber, by volume, experienced 23 and 3% respective increases in $R_{T,150}^{100}$ when RCA replacement increased from 30 to 100%. This enhancement in the equivalent flexural strength ratio is owed to the slight increase in toughness and obvious decrease in peak load. Furthermore, steel fiber addition of 1 and 2%, by volume, increased $R_{T,150}^{100}$ by, on average, 6.6 and 12.1 times with a more pronounced increase at lower RCA replacement.

Figure 46(b) presents the relationship between $R_{T,150}^{100}$ and f'_c. The two properties are clearly inversely proportional. In fact, the value of $R_{T,150}^{100}$ decreased by, on average, 0.26, 0.22, and 0.04% for every 1 MPa increase in f'_c of mixes made with 0, 1, and 2% steel fiber volume fractions. This shows that the effect of f'_c on $R_{T,150}^{100}$ was reduced as more steel were are included in the mix. It is also worth noting that different $R_{T,150}^{100}$ were noted for mixes having the same compressive strength but different steel fiber volume fractions. For instance, a 31-MPa concrete incorporating 0, 1, and 2% steel fibers, by volume, had equivalent flexural strength ratios of 0.5, 6.2, and 7.4%, respectively. As such, it can be concluded that steel fiber incorporation had a more significant impact on $R_{T,150}^{100}$ than RCA replacement.
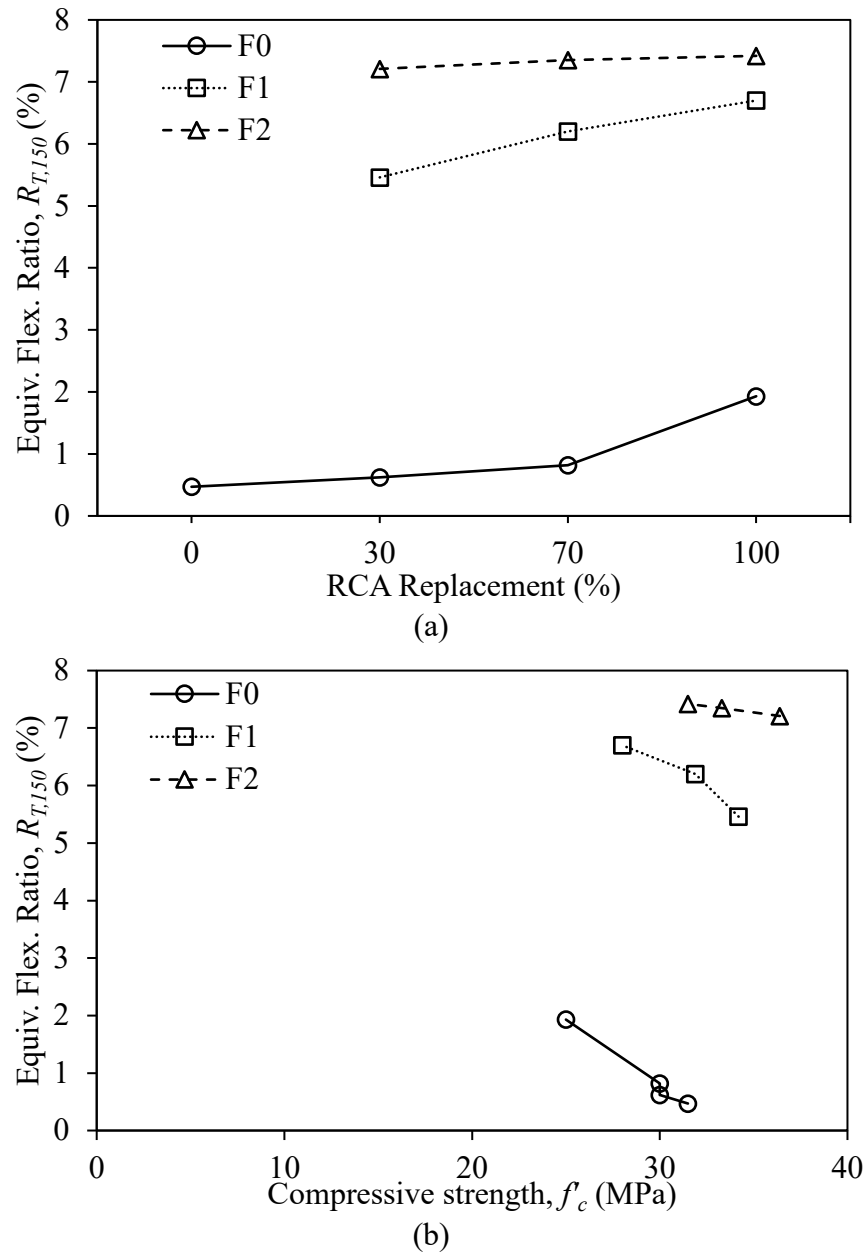
Figure 46: Equivalent flexural ratio of 100% slag geopolymer concrete with various (a) RCA replacement percentage and SF volume fractions and (b) cylinder compressive strength

The equivalent flexural strength ratio of slag-fly ash blended geopolymer concrete is depicted in Figure 47(a). Compared to the NA-based control mix, RCA replacement of 30, 70, and 100% increased $R_{T,150}^{100}$ by 110, 167, and 326%, respectively. Yet, such

increases were much lower in steel fiber-reinforced counterparts with 37% higher $R_{T,150}^{100}$ being associated with an increase in RCA from 30 to 100%. In contrast, steel fiber addition was much more influential on $R_{T,150}^{100}$. Indeed, 1 and 2% steel fiber volume fractions increased $R_{T,150}^{100}$ by, on average, 6.4 and 12.6 times, respectively. This can also be noted for mixes having the same compressive strength but higher $R_{T,150}^{100}$ upon fiber addition, as shown in Figure 47(b). Furthermore, for mixes made with 0, 1, and 2% steel fiber, by volume, $R_{T,150}^{100}$ decreased by an average of 0.06, 0.38, and 0.17% for every 1 MPa increase in f'_c. Thus, the inclusion of steel fibers had a more prominent impact on the equivalent flexural strength ratio of slag-fly ash blended geopolymer concrete than RCA replacement.
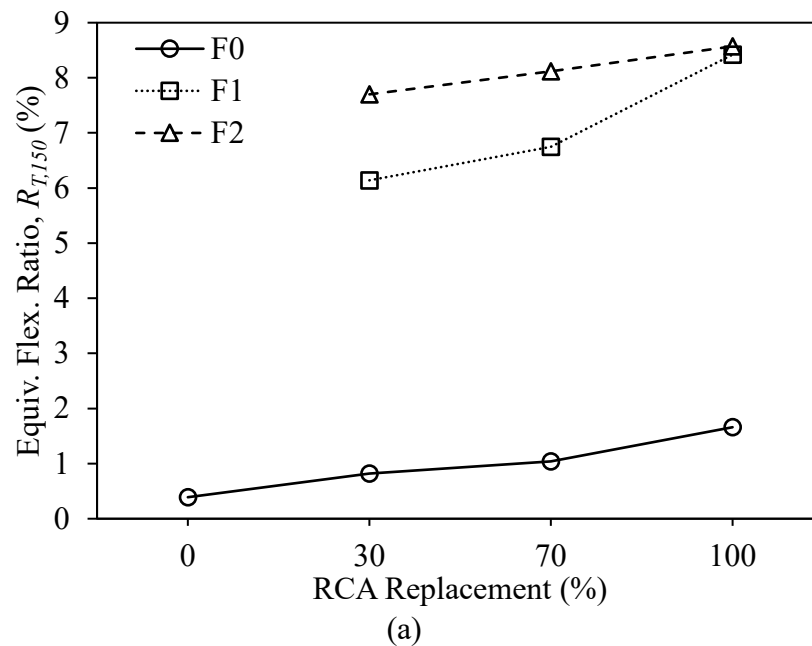
Figure 47: Equivalent flexural ratio of slag-fly ash blended geopolymer concrete with various (a) RCA replacement percentage and SF volume fractions and (b) cylinder compressive strength

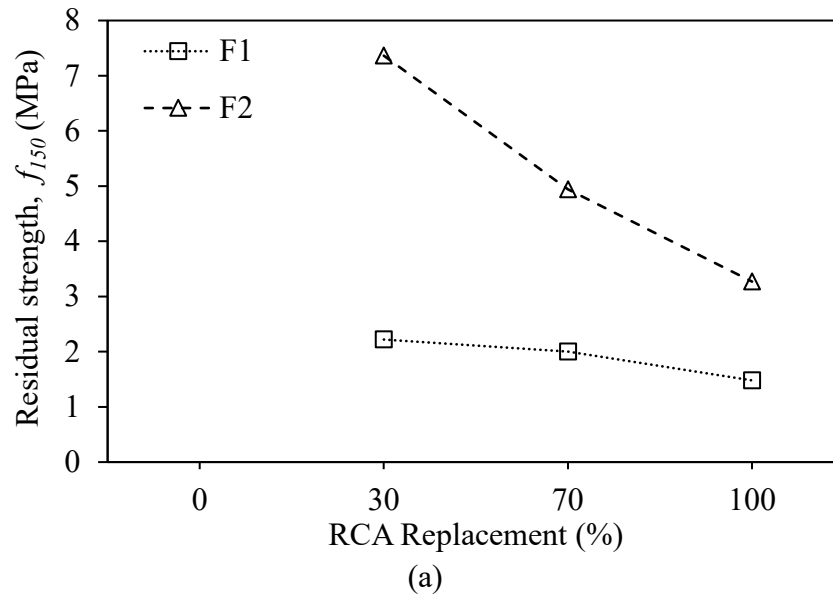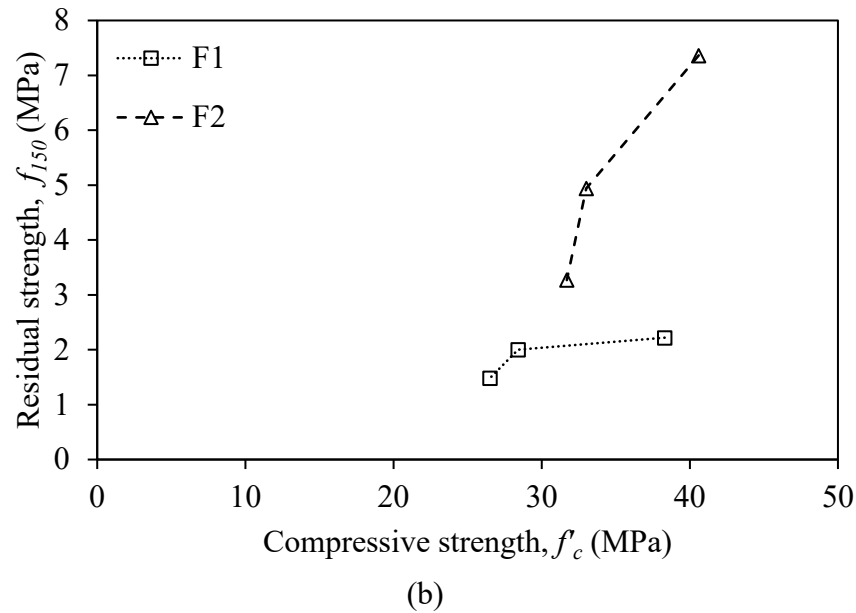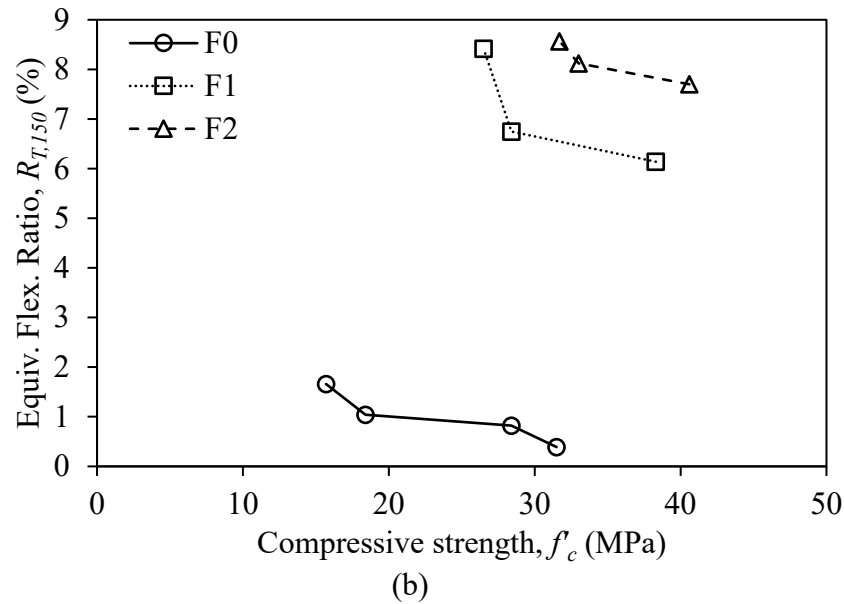Figure 47: Equivalent flexural ratio of slag-fly ash blended geopolymer concrete with various (a) RCA replacement percentage and SF volume fractions and (b) cylinder compressive strength (Continued)

4.7 Water Absorption

The durability of concrete is affected by the concrete's resistance to penetration of damaging ions. Since water is the main carrier of these aggressive ions, the water absorption capacity of concrete can indicate its durability [29]. Figure 48 shows the water absorption of 100% slag geopolymer concrete at the age of 28 days. The control mix (S100R0F0) had a water absorption of 2.1%, while those of plain mixes incorporating 30, 70, and 100% RCA were 3.3, 5.8, and 7.5%, respectively. These represent a 58, 173, and 255% increase over that of the control mix. In fact, every 10% RCA replacement led to, on average, a 23% increase in water absorption, owing to the porous nature of the RCA and the adhered mortar. This finding is well-correlated and provides evidence of the

decrease in mechanical properties, including compressive, splitting tensile, and flexural strength.

Figure 48 also highlights the impact of steel fiber addition on the water absorption of 100% slag geopolymer concrete. Generally, an increase in steel fiber volume fraction led to a decrease in water absorption. In fact, it was reduced by, on average, 25 and 43% upon the incorporation of 1 and 2% steel fibers, by volume, compared to plain counterparts. Accordingly, it can be concluded that steel fiber inclusion can densify the geopolymer matrix, thereby reducing the water absorption and enhancing the mechanical performance. Similar findings have been reported in 100% slag geopolymer concrete made with natural aggregates [105].
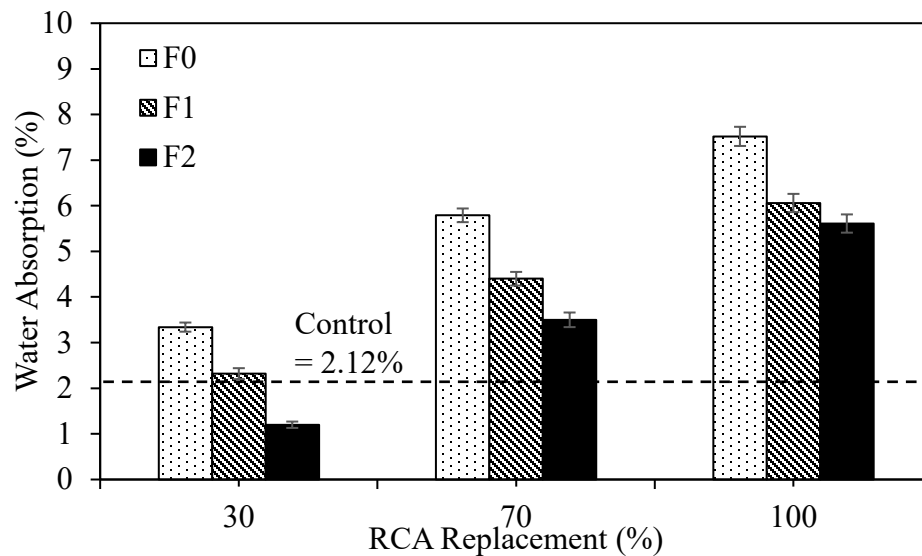
Figure 48: Water absorption of 100% slag geopolymer concrete mixes

Figure 49 presents the water absorption of 28-day slag-fly ash blended geopolymer concrete mixes. The control mix had the lowest water absorption of 2.2%. Conversely,

plain concrete made with 30, 70, and 100% RCA had water absorption of 3.7, 5.8, and 8.2%, respectively, representing 65, 158, and 262% respective increases. This shows that the water absorption increased by an average of 23.5% for every 10% NA replaced by RCA. Additionally, the effect of incorporating steel fibers in slag-fly ash blended geopolymer concrete mixes is examined in Figure 49. An increase in steel fiber volume fraction led to a reduction in water absorption. Indeed, the addition of 1 and 2% steel fiber, by volume, decreased the absorption by, on average, 11 and 34%, respectively, in comparison to the corresponding plain concrete mixes. In conclusion, RCA replacement had a negative impact on the water absorption of slag-fly ash blended geopolymer concrete. Yet, it could be somewhat countered through the addition of steel fibers.
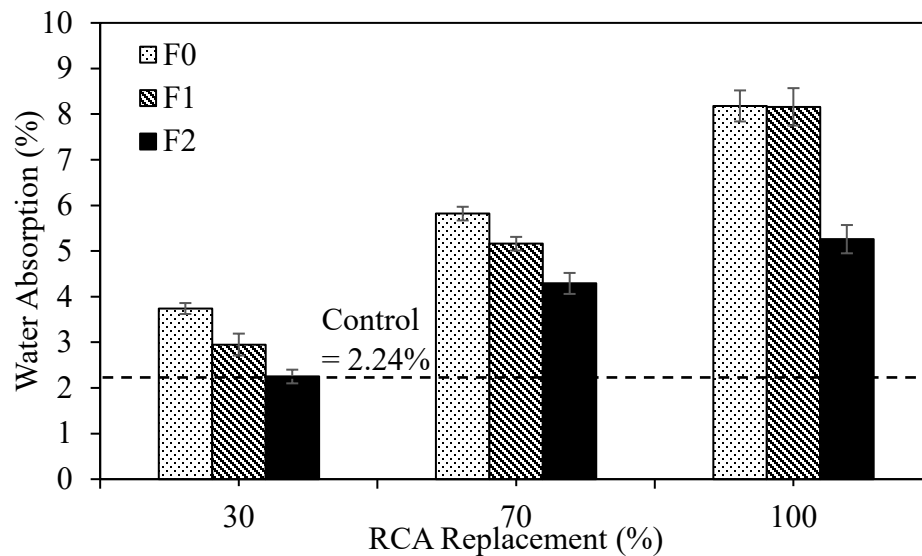
Figure 49: Water absorption of slag-fly ash blended geopolymer concrete mixes

4.8 Sorptivity

Sorptivity represents the concrete's tendency to absorb and transport water into its microstructure through capillary action, making it an indirect tool to assess the durability of concrete. It depends on the permeability and porosity of concrete as well as the strength of the capillary forces and size and distribution of the pores [29, 149]. Large capillary and small gel pores control the sorptivity. It is because of the different sizes of these pores that two types of sorptivity are analyzed, namely initial and secondary sorptivity [150]. As the former pores are larger than the latter, water occupies them faster, causing the initial sorptivity to be larger than the secondary sorptivity. As such, this thesis only focuses on the initial sorptivity.

Figure 50 presents the plot of absorption over time and is used to find the rate of absorption or sorptivity of 100% slag geopolymer concrete. For plain mixes in Figure 50(a), the slope of the sorptivity curve changes with time and is a function of RCA replacement. In fact, mixes made with 0, 30, 70, and 100% RCA maintain the same slope for up to 15, 90, 135, and 240 minutes before the slope decreases. This shows that the higher the RCA replacement, the more time it takes to fill the large pores present in the RCA, which may be cracks or fissures that developed during the production of RCA. In addition, RCA replacement was found to be proportional to the absorption at 360 minutes. Moreover, Figure 50(b) shows the sorptivity of mixes incorporating 1% steel fiber, by volume. Compared to the plain concrete mixes, the slope of the absorption curves did not significantly vary due to steel fiber incorporation while the 360-minute absorption value experienced little to no change. Conversely, mixes with a 2% steel fiber volume fraction

exhibited a decrease in the slope compared to plain counterparts. Also, the slope changed at 3, 90, and 240 minutes for mixes made with 30, 70, and 100% RCA, respectively. As such, steel fiber-reinforced geopolymer mixes filled the larger pores faster than plain mixes due to steel fibers' ability to restrict water movement and occupy void space in the geopolymer structure. Other work reported similar findings in conventional cement-based steel fiber-reinforced concrete [151, 152].

Figure 50: Capillary sorptivity of 100% slag geopolymer concrete mixes over time: (a) SF 0%; (b) SF 1%; (c) SF 2%.

Figure 50: Capillary sorptivity of 100% slag geopolymer concrete mixes over time: (a) SF 0%; (b) SF 1%; (c) SF 2%. (Continued)

Figure 51(a) shows the absorption of plain slag-fly ash blended geopolymer concrete as a function of time. Mixes made with 0, 30, 70, and 100% maintained the same initial slope up to 33, 60, 135, and 240 minutes, after which the slope decreased. This shows that the higher RCA replacement required more time to reach absorption stability due to the presence of voids in RCA. Additionally, higher RCA content resulted in higher absorption at 360 minutes. Figures 51(b-c) present the absorption of steel fiber-reinforced slag-fly ash blended geopolymer concrete as a function of time. While 1% steel fiber volume fraction did not have a major impact on the slope and absorption, 2% steel fiber volume fraction caused a significant reduction in the slope. This signifies a slower absorption rate with steel fiber incorporation owing to their ability to restrict water movement and occupy larger void space in the geopolymer structure.

(a)

(b)

Figure 51: Capillary sorptivity of slag-fly ash blended geopolymer concrete mixes over time: (a) SF 0%; (b) SF 1%; (c) SF 2%

(c)
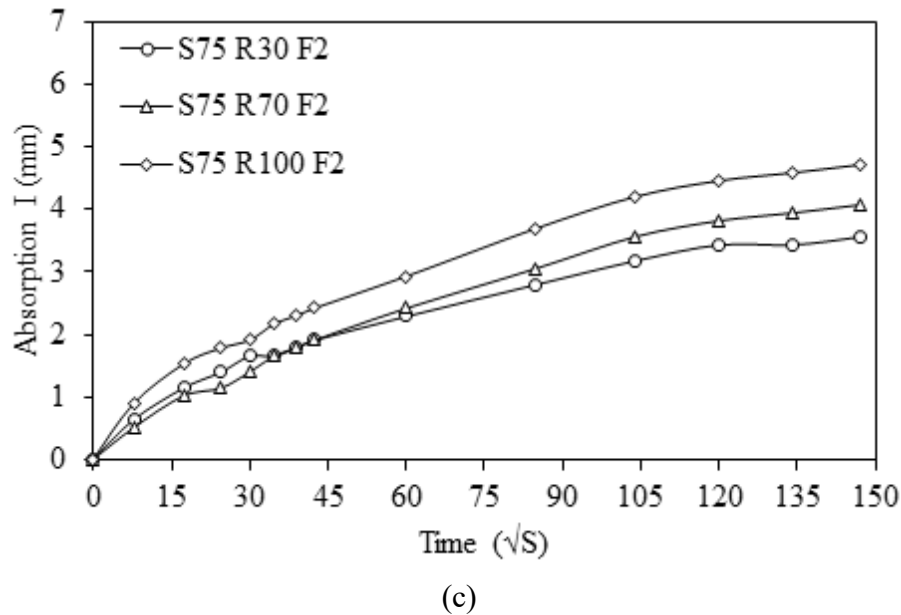
Figure 51: Capillary sorptivity of slag-fly ash blended geopolymer concrete mixes over time: (a) SF 0%; (b) SF 1%; (c) SF 2% (Continued)

The sorptivity results of 28-day geopolymer concrete mixes are summarized in Table 14. The replacement of NA by RCA increased the sorptivity. For 100% slag geopolymer concrete, 30, 70, and 100% RCA led to 111, 256, and 356% higher sorptivity, respectively. Conversely, slag-fly ash blended geopolymer concrete experienced respective increases in sorptivity of 38, 80, and 125%. Nevertheless, steel fiber incorporation decreased the sorptivity of RCA geopolymers. In fact, the addition of 1 and 2% steel fiber volume fractions to 100% slag geopolymer concrete reduced the sorptivity by, on average, 7.4 and 11.6%, respectively. The respective average reductions were 5.1 and 14.4% for slag-fly ash blended geopolymer. Such a decrease with steel fiber inclusion may be due to an improvement in the bond within the binding matrix [18]. Similar conclusions were noted upon reinforcing cement-based concrete with steel fibers [151-153].

Table 14: Initial sorptivity of geopolymer concrete mixes

Mix No.	Mix Designation	RCA (%)	Steel Fibers (%)	Sorptivity x 10^{-2} (mm/√s)
1	S100R0F0	0	0	0.86
2	S100R30F0	30	0	1.86
3	S100R30F1	30	1	1.70
4	S100R30F2	30	2	1.56
5	S100R70F0	70	0	3.15
6	S100R70F1	70	1	2.94
7	S100R70F2	70	2	2.85
8	S100R100F0	100	0	4.12
9	S100R100F1	100	1	3.96
10	S100R100F2	100	2	3.75
11	S75R0F0	0	0	1.58
12	S75R30F0	30	0	2.17
13	S75R30F1	30	1	1.99
14	S75R30F2	30	2	1.83
15	S75R70F0	70	0	2.91
16	S75R70F1	70	1	2.78
17	S75R70F2	70	2	2.48
18	S75R100F0	100	0	3.58
19	S75R100F1	100	1	3.49
20	S75R100F2	100	2	3.21

4.9 Bulk Resistivity

The concrete durability can be indirectly assessed using bulk electric resistivity or simply bulk resistivity. While 20 mixes were carried out in this thesis, those incorporating steel fibers were discarded. This is because steel fibers are electrically conductive, rendering the results incomparable and unrepresentative of true durability. Figure 52(a) presents the bulk resistivity results of 100% slag geopolymer concrete. While the control mix with 0% RCA had a resistivity of 8.5 kΩ.cm, those of mixes incorporating 30, 70,

and 100% RCA were 6.1, 5.5, and 4.9 kΩ.cm, respectively. This represents respective decreases of 28, 35, and 42%, which are owed to the increase in pore space in the geopolymeric binder matrix.

Furthermore, the bulk resistivity of slag-fly ash blended geopolymer concrete is shown in Figure 52(b). Values of mixes made with 0, 30, 70, and 100% RCA were 8.2, 5.9, 3.7, and 3.6 kΩ.cm. The respective reductions in resistivity are 28, 55, and 56%. In this case, the replacement of 70% RCA caused a significant impact on the resistivity to the extent that 100% RCA did not cause much further reduction.
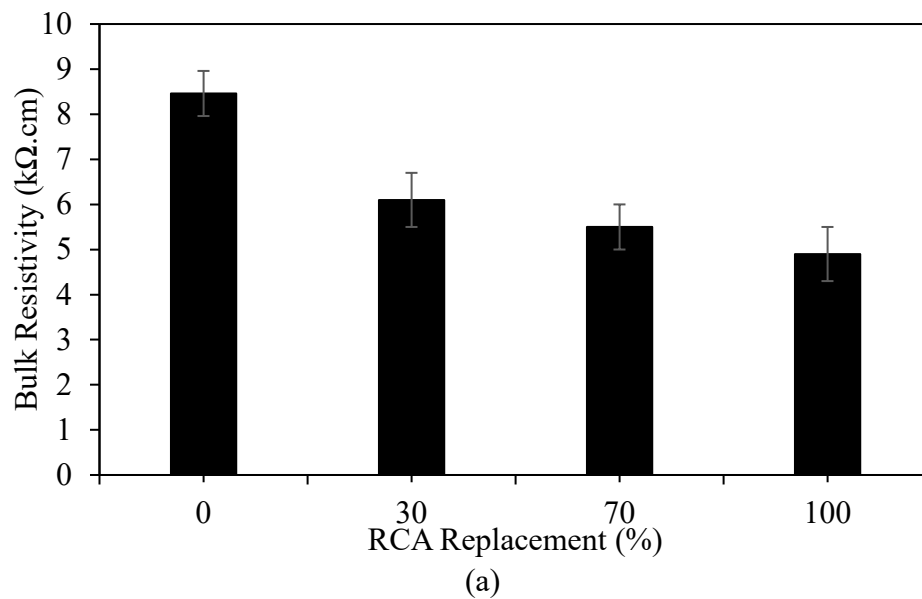
(a)

Figure 52: Bulk resistivity of (a) 100% slag and (b) slag-fly ash blended geopolymer concrete mixes
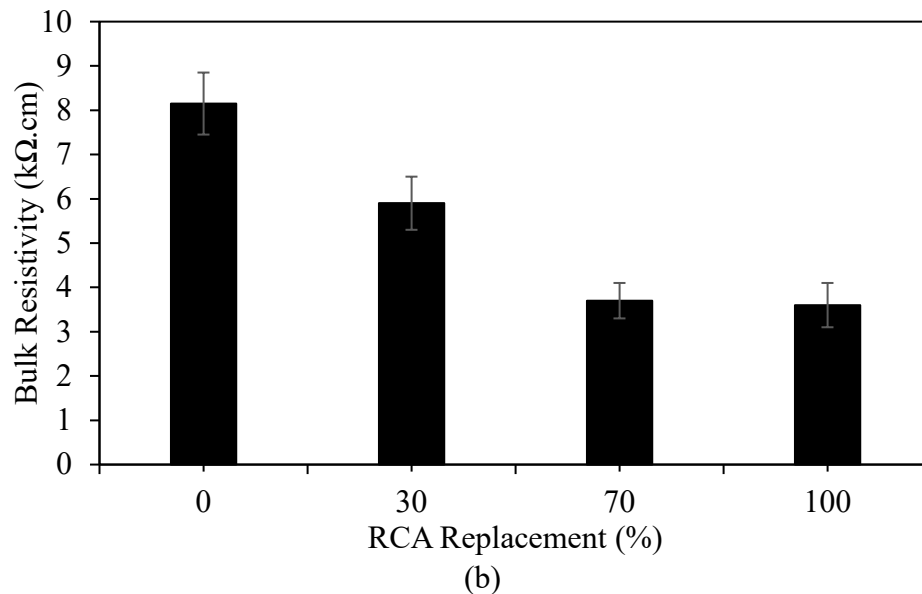
Figure 52: Bulk resistivity of (a) 100% slag and (b) slag-fly ash blended geopolymer concrete mixes (continued)

4.10 Ultrasonic Pulse Velocity

The concrete quality and durability can be indirectly assessed by the ultrasonic pulse velocity test. Similar to bulk resistivity, steel fiber-reinforced geopolymer concrete mixes were omitted. Figure 53(a) shows the results of 100% slag geopolymer concrete. An increase in RCA from 0 to 30, 70, and 100% led to 5.6, 15.9, and 22.7% decreases in UPV, respectively. Nevertheless, values of mixes S100R0F0, S100R30F0, and S100R70F0 were above 4.5 km/s, signifying excellent concrete quality based on IS 13311-1 [154]. The mix made with 100% RCA was classified to have good quality. Similarly, these RCA replacements reduced respective UPV values of slag-fly ash blended geopolymer by 7.3, 15.0, and 19.9%, as depicted in Figure 52(b). With reference to the quality grading of IS 13311-1 [154], mixes S75R0F0 and S75R30F0 were categorized as "Excellent", while S75R70F0 and S75R100F0 were considered "Good".
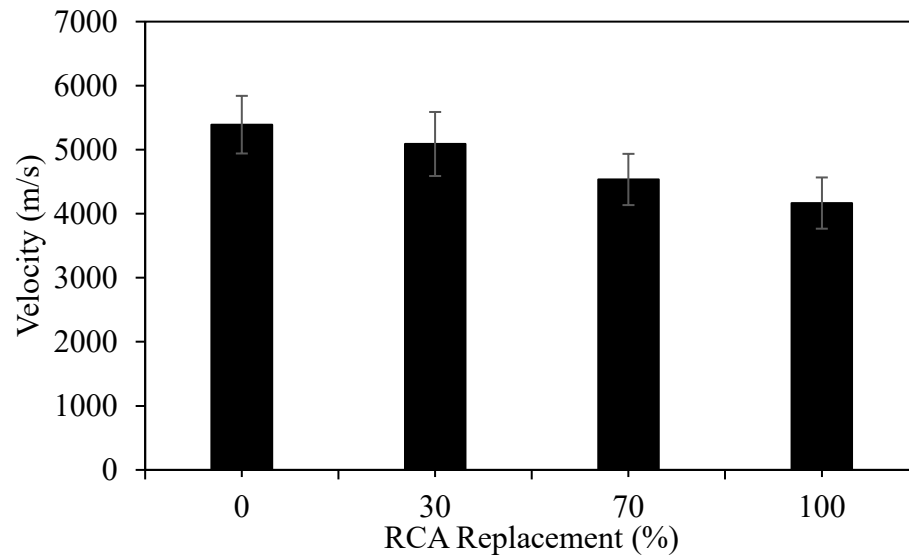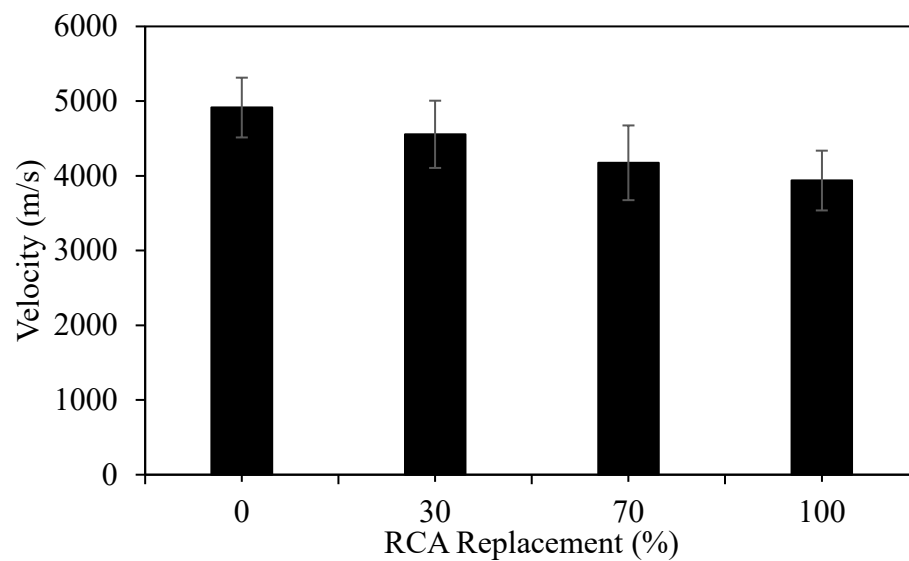
Figure 53: Ultrasonic pulse velocity of (a) 100% slag and (b) slag-fly ash blended geopolymer concrete mixes

4.11 Abrasion Resistance

The mechanical properties of the concrete and the hardness of the aggregates govern its abrasion resistance. In this thesis, the mass loss due to abrasive forces was recorded every 100 revolutions for up to 500 revolutions to determine the mass loss

profile. The abrasion resistance of 100% slag geopolymer concrete is shown in Figure 54. For plain mixes made with 30, 70, and 100% RCA, the mass loss was mainly within the first 400 revolutions, while counterparts made with 0% RCA had a uniform mass loss during the 500 revolutions. In fact, the control mix had a mass loss of 33%, while mixes having 30, 70, and 100% NA replaced by RCA had losses of 92, 97, and 100%, respectively. Such higher mass losses are associated with the inferior properties of RCA, in addition to the weak interfacial bond between the old mortar and new paste. Similar findings were noted in conventional concrete made with RCA [153, 155]. Figures 54(b-c) show the abrasion mass loss of steel fiber-reinforced 100% slag geopolymer concrete. While the effect of RCA replacement was similar to that of plain counterparts, the mass loss values were much lower, indicating a much less pronounced influence of RCA on the abrasion resistance of steel fiber-reinforced 100% slag geopolymer concrete.

The influence of steel fiber addition on the abrasion mass loss of 100% slag geopolymer concrete was also investigated in Figure 54. On average, the inclusion of 1 and 2% steel fiber decreased the abrasion mass loss by 53 and 68%, respectively. This is owed to the steel fibers' bridging effect and ability to improve the geometric integrity and densify the geopolymer matrix, thereby increasing the abrasion resistance. Indeed, mixes incorporating 2% steel fiber volume fractions had comparable abrasion resistance as that of the NA-based control mix.
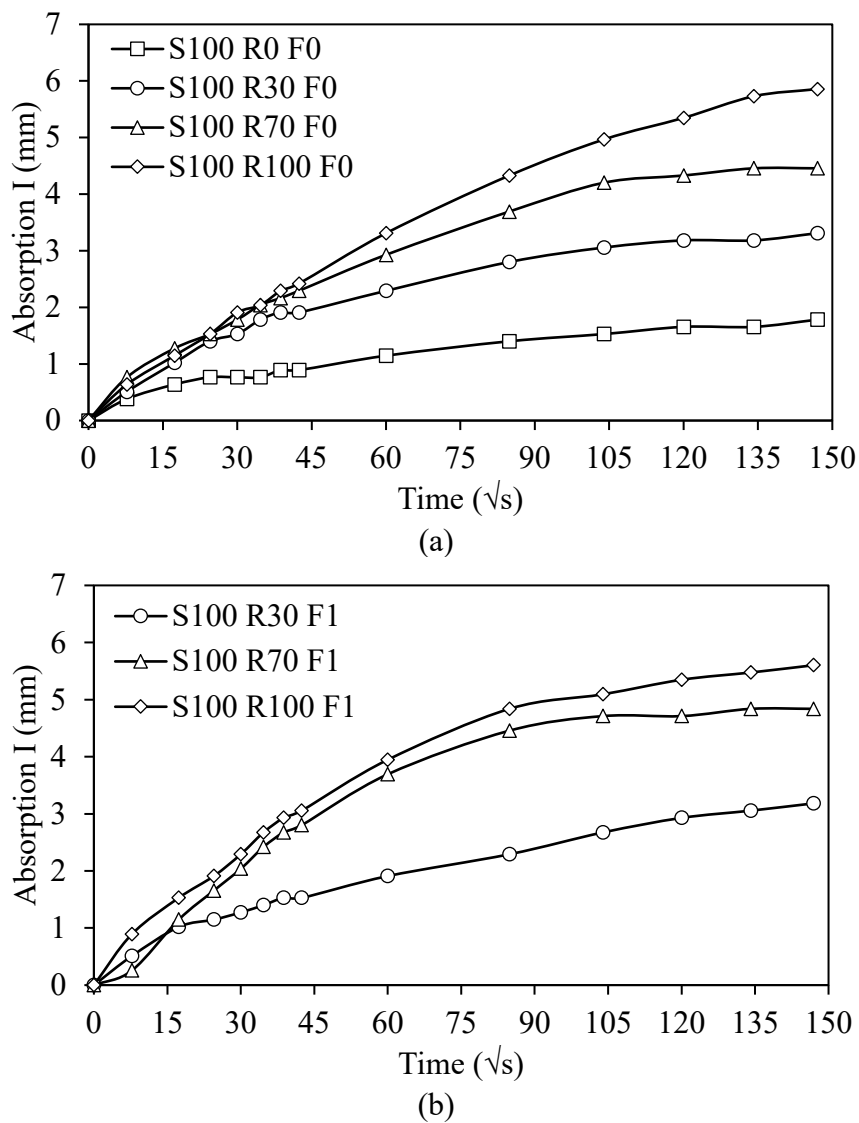
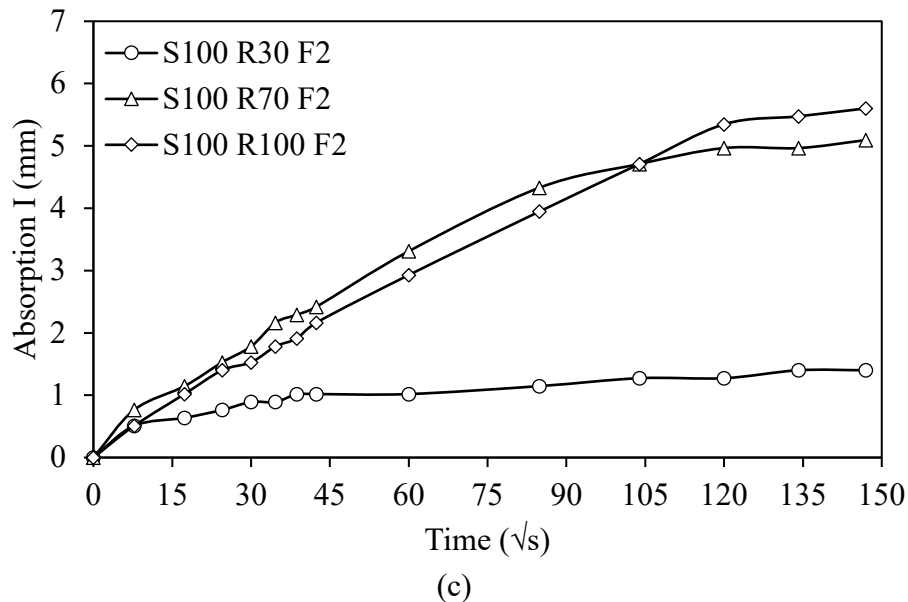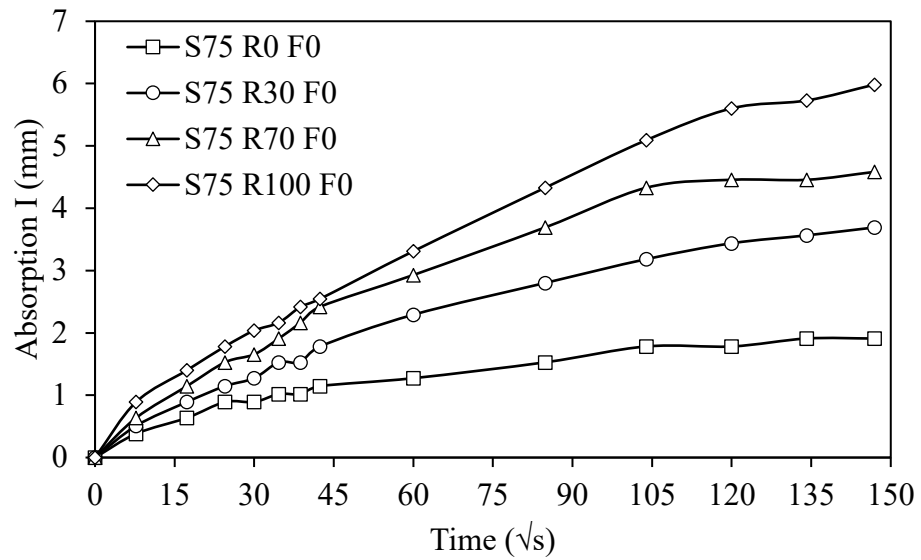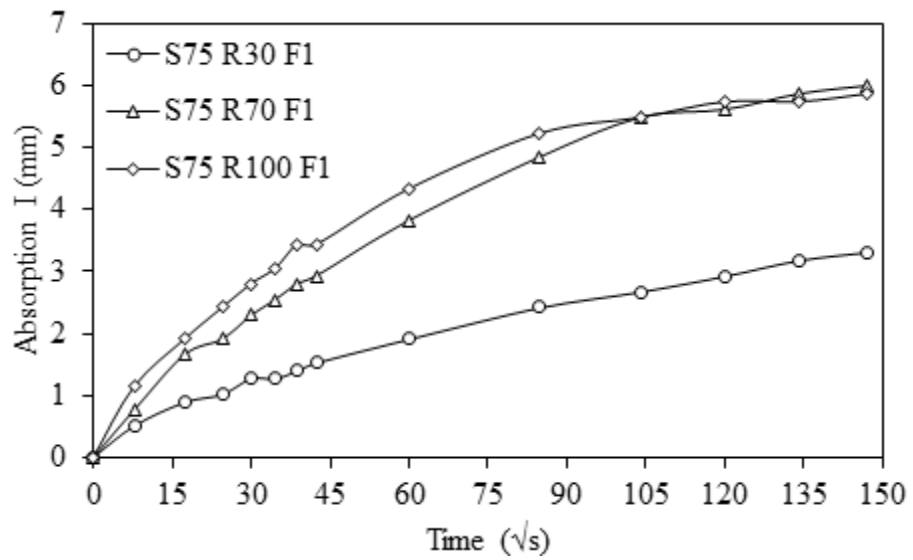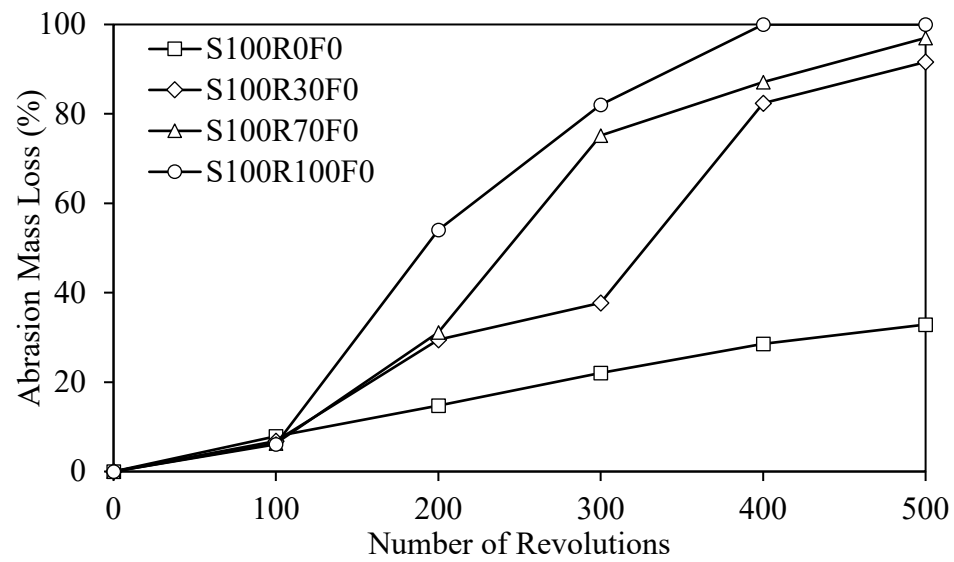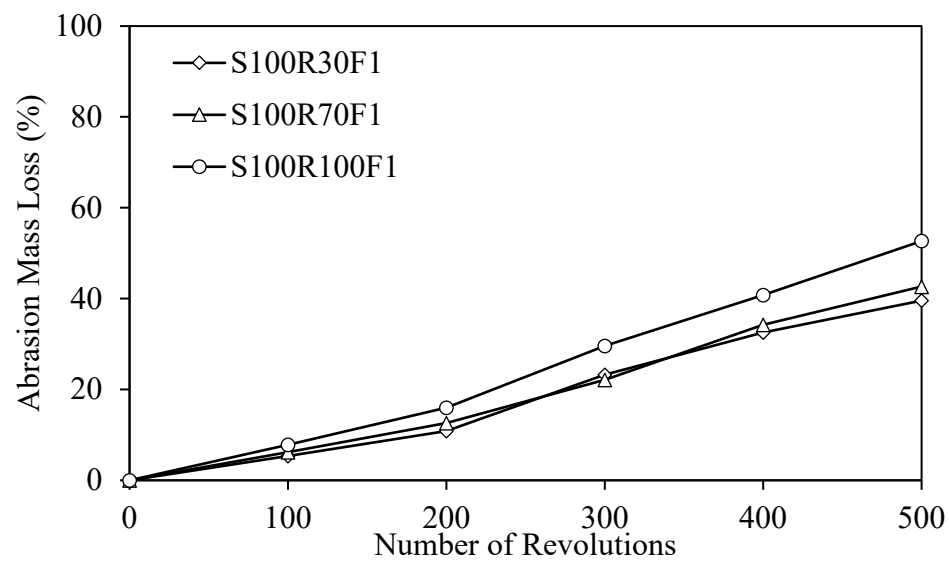Figure 54: Abrasion resistance of 100% slag geopolymer concrete mixes over time: (a) SF 0%; (b) SF 1%; (c) SF 2%
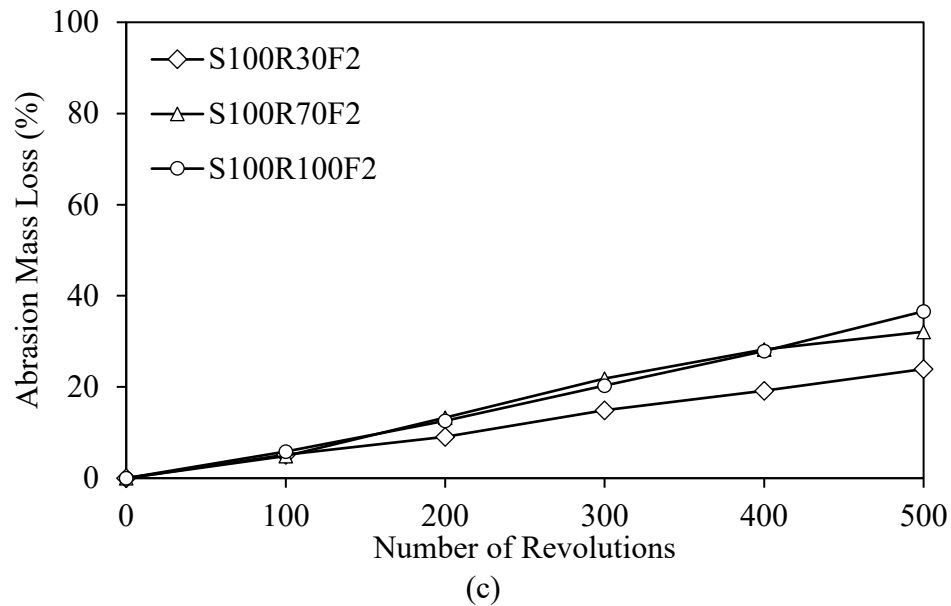
Figure 54: Abrasion resistance of 100% slag geopolymer concrete mixes over time: (a) SF 0%; (b) SF 1%; (c) SF 2% (Continued)

Figure 56 shows the abrasion mass loss of slag-fly ash blended geopolymer concrete. Mixes made with 0 and 30% RCA had a nearly linear increase in the mass loss as a function of the number of revolutions. Yet, this was not the case with higher RCA replacement, where the slope of mass loss increased around 300 revolutions. As a result, the mass loss of 0, 30, 70, and 100% RCA mixes were 35, 43, 73, and 88%, respectively. Furthermore, steel fiber-reinforced mixes noted a similar trend but the mass loss values were lower. Indeed, mixes incorporating 1% steel fiber, by volume, and 30, 70, and 100% RCA had mass losses of 27, 57, and 67%, respectively. In turn, 2% steel fiber volume fraction addition led to respective mass losses of 26, 34, and 36%, highlighting the less significant impact of RCA replacement on the abrasion resistance of steel fiber-reinforced slag-fly ash blended geopolymer concrete.

The abrasion resistance of slag-fly ash blended geopolymer concrete as a function of steel fiber inclusion was also examined. The addition of 1 and 2% steel fiber, by volume, decreased the mass loss by, on average, 27 and 51%, respectively. Apparently, the incorporation of steel fibers enhanced the abrasion resistance of slag-fly ash blended geopolymer concrete to the extent that the mix made with 100% RCA and 2% steel fiber, by volume, was comparable to that of the control.
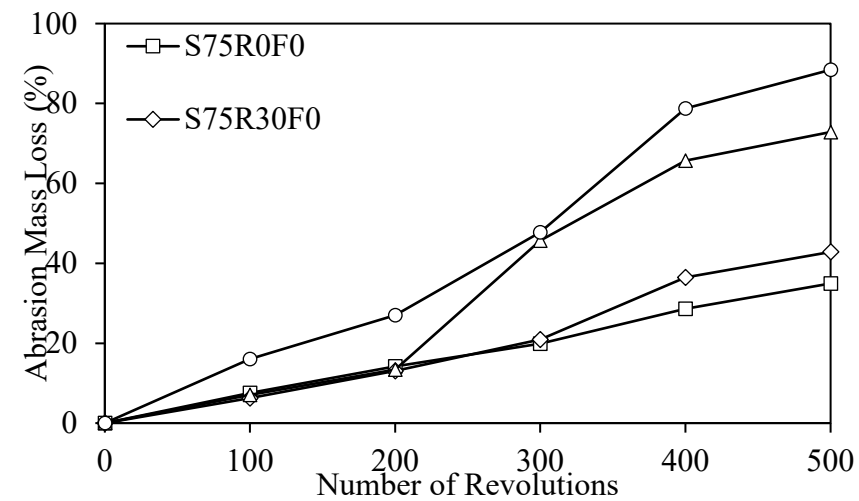
(a)
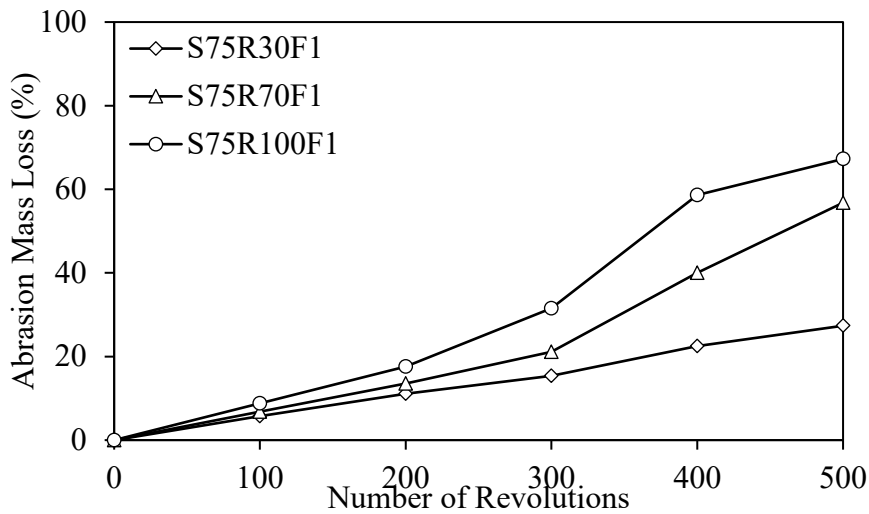
(b)

Figure 56: Abrasion resistance of slag-fly ash blended geopolymer concrete mixes over time: (a) SF 0%; (b) SF 1%; (c) SF 2%

(c)
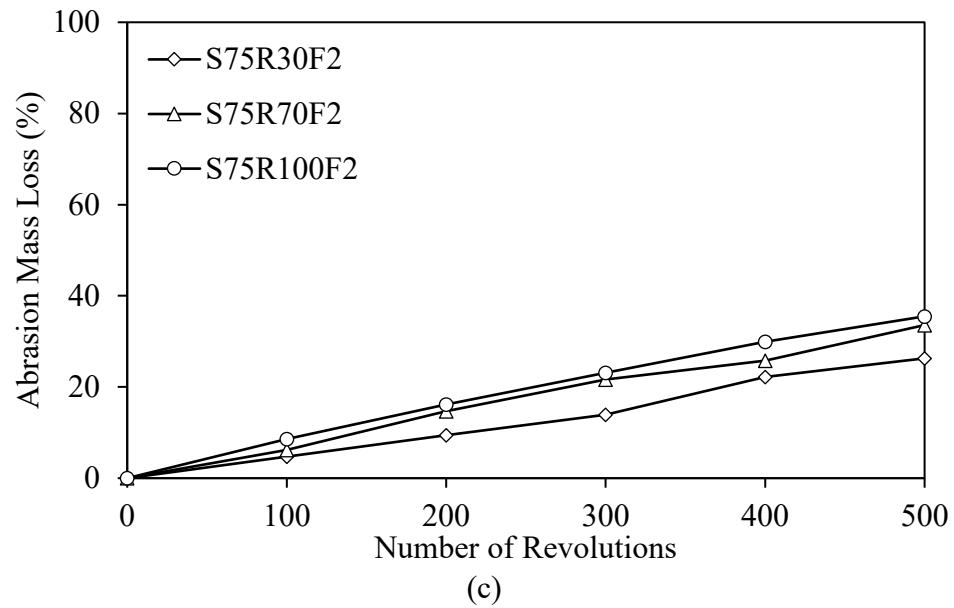
Figure 56: Abrasion resistance of slag-fly ash blended geopolymer concrete mixes over time: (a) SF 0%; (b) SF 1%; (c) SF 2% (Continued)

Chapter 5: Comparative Analysis

5.1 Introduction

This chapter offers a comparative analysis of the results of 100% slag and slag-fly ash blended geopolymer concrete. The comparison comprises the compressive strength, compressive stress-strain behavior, modulus of elasticity, splitting tensile strength, flexural properties, water absorption, bulk resistivity, UPV, and abrasion resistance. Each parameter is discussed in the following sections.

5.2 Compressive Strength

The cube compressive strength of 100% slag and slag-fly ash blended geopolymer concrete was determined at the ages of 1, 7, and 28 days to evaluate the strength development profile, as summarized in Table 15. At the age of 1 day, geopolymer concrete mixes made with 100% slag had superior f_{cu} than slag-fly ash blended counterparts. This is believed to be owed to the accelerated reaction of calcium compounds in slag to produce calcium silicate hydrate (C-S-H) and calcium aluminosilicate hydrate (C-A-S-H) gels [64, 140-142]. With lower slag content, such accelerated reaction was less intense in slag-fly ash blended geopolymer concrete.

Nevertheless, the difference between the f_{cu} of both geopolymer concretes decreased at the age of 7 days, owing to high increases in f_{cu} from 1 to 7 days for slag-fly ash blended geopolymers. While the 100% slag geopolymers increased by 20-63% (average = 35%), slag-fly ash blended counterparts increased by 40-91% (average = 59%).

A similar finding is noted between 7 and 28 days, where the average increase in f_{cu} was 11 and 28% for 100% slag and slag-fly ash geopolymer concrete, respectively. Such a continuous increase in the latter is primarily due to the delayed formation of sodium aluminosilicate hydrate gel (N-A-S-H) from the activation of fly ash at room temperature [93]. Accordingly, the 28-day f_{cu} of 100% slag geopolymer concrete was, on average, 7% lower than that of slag-fly ash blended equivalents. Yet, it should be noted that less binder was used in the latter geopolymer concrete mixes have similar design cylinder compressive strength (30 MPa) as the former.

Table 15: Compressive strength development of 100% slag and slag-fly ash blended geopolymer concrete

Mix Designation	100% Slag					Slag-Fly Ash Blend				
	f_{cu} (MPa)			Increase[a] (%)	Increase[b] (%)	f_{cu} (MPa)			Increase[a] (%)	Increase[b] (%)
	1	7	28			1	7	28		
R0F0	38.6	46.4	47.5	20.2	2.4	31.5	44.2	56.8	40.3	28.5
R30F0	36.9	45.6	47.8	23.6	4.8	26.3	41.8	52.6	58.8	25.8
R30F1	42.2	51.3	56.2	21.6	9.6	30.2	42.7	61.7	41.4	44.5
R30F2	43.2	51.8	59.1	19.9	14.1	33.8	45.5	63.8	34.6	40.2
R70F0	26.4	39.1	47.9	48.1	22.5	19.8	35.0	45.2	76.8	29.1
R70F1	32.5	45.3	51.4	39.4	13.5	24.0	40.1	49.1	67.1	22.4
R70F2	37.5	51.3	55.8	36.8	8.8	30.6	44.3	55.8	44.8	26.0
R100F0	21.8	35.6	37.8	63.3	6.2	18.4	35.1	42.5	90.8	21.1
R100F1	27.1	37.7	42.0	39.1	11.4	22.6	39.7	48.0	75.7	20.9
R100F2	28.6	39.1	46.4	36.7	18.7	25.8	41.7	51.4	61.6	23.3

[a] Increase in f_{cu} from 1 to 7 days.

[b] Increase in f_{cu} from 7 to 28 days.

The effect of RCA replacement and steel fiber incorporation was also different in each type of geopolymer. For 100% slag geopolymer concrete, every 10% RCA

replacement reduced 1-, 7-, and 28-day f_{cu} by, on average, 3.4, 1.7, and 0.6%, respectively. Conversely, slag-fly ash geopolymers experienced respective decreases of 5, 2.3, and 2.6%. Apparently, the replacement of NA by RCA was more impactful on mixes incorporating fly ash. Yet, the values of f_{cu} were still higher when slag was replaced by 25% fly ash. Moreover, this negative impact of RCA replacement could be countered by steel fiber inclusion. For the former mixes, the 1-, 7-, and 28-day f_{cu} increased by, on average, 17.9, 10.3, and 11.2%, respectively, for each 1% steel fiber added to the mix, by volume. Similarly, it increased by, on average, 20.1, 9.5, and 12.0% for the latter mixes. This shows that steel fibers have a similar effect on both types of geopolymers, but with higher increases at 1 day, they were more clearly impactful at a very early age.

Furthermore, the 28-day cylinder compressive strength of 100% slag (100S) and slag-fly ash blended (75S-25F) geopolymer concrete mixes were compared, as shown in Figure 57. With reference to f'_c of the control mix (31.8 MPa), that of 100% slag geopolymer concrete made with 30, 70, and 100% decreased by 5, 5, and 21%, respectively. While f'_c of the control mix of slag-fly ash blended geopolymer counterpart was similar (31.5 MPa), the respective strength reductions were 10, 42, and 50%. Such results show that the confinement effect of cubes under compression was more impactful on slag-fly ash blended geopolymers. Still, for both concretes, it was possible to reverse the impact of RCA by steel fiber addition to the extent that mixes made with 100% RCA and 2% steel fiber, by volume, had similar compressive strength as the NA-based controls.
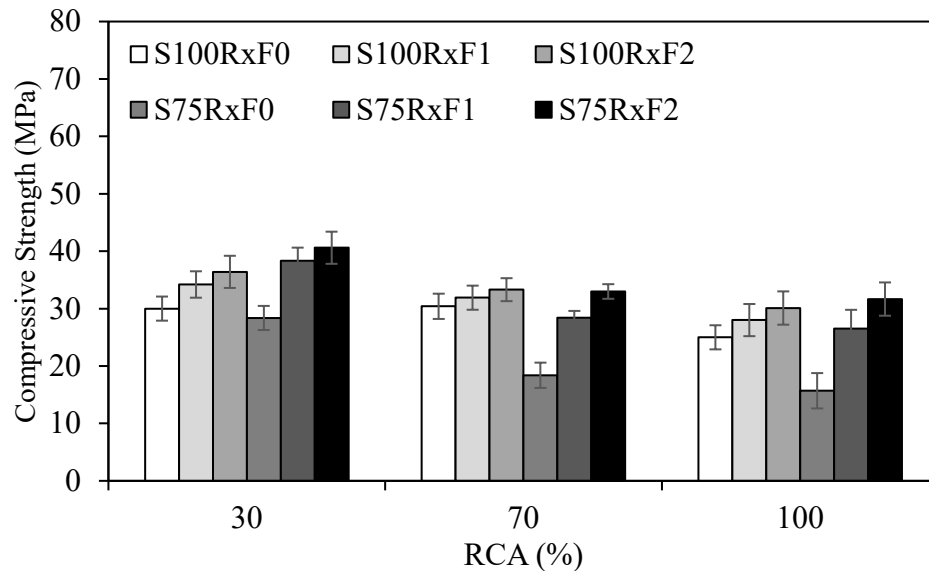
Figure 57: Cylinder compressive strength of 100% slag and slag-fly ash blended geopolymer concrete

5.3 Modulus of Elasticity

The modulus of elasticity (E_c) of 100% slag and slag-fly ash blended geopolymer concrete made with NA were 29.5 and 22.4 GPa, as shown in Figure 58. Despite having similar compressive stress, it seems that the slope of the stress-strain curves was higher for the former mixes, leading to higher E_c. The RCA replacement of 30, 70, and 100% in plain 100% slag geopolymer concrete reduced E_c by 42, 44, and 56%, respectively. Conversely, E_c of plain slag-fly ash blended geopolymer counterparts decreased by 28, 42, and 52%. This shows that the RCA replacement had a slightly more pronounced influence on the plain 100% slag geopolymer concrete mixes. Still, the E_c values of concrete made with 100% slag were higher than those incorporating fly ash.

The effect of steel fiber addition on E_c was also investigated in Figure 57. For mixes made with 100% slag, E_c increased by, on average, 18% for every 1% steel fiber

added, by volume, regardless of RCA replacement. As a result, the E_c of steel fiber-reinforced concrete were 56 to 83% that of the control mix. Conversely, slag-fly ash blended geopolymer concrete noted an average increase of 36% for every 1% steel fiber volume fraction. The resultant E_c for steel fiber-reinforced concrete were 73 to 118% that of the control mix. As such, steel fiber addition was more impactful on E_c of slag-fly ash blended geopolymer concrete than slag-based counterparts. This is possibly due to the better bond between the steel fibers and the binding matrix made with slag and fly ash.
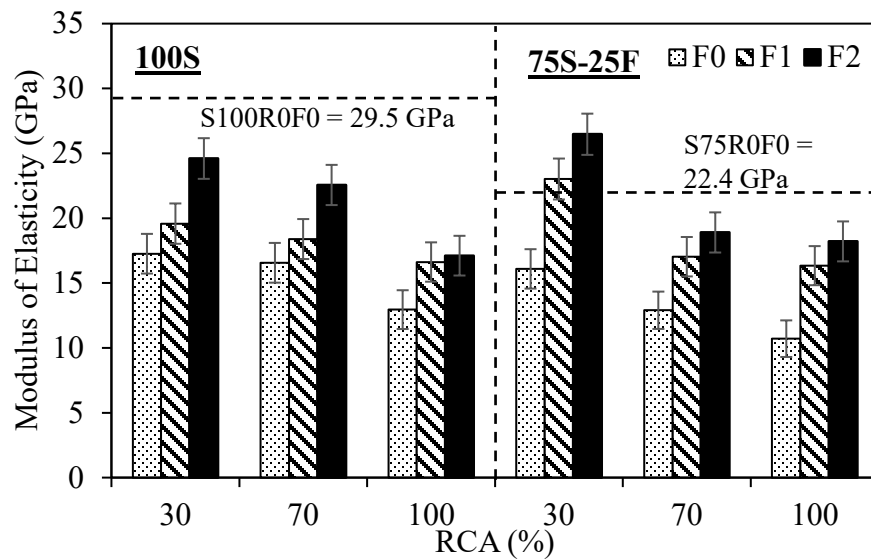
Figure 58: Modulus of elasticity of 100% slag and slag-fly ash blended geopolymer concrete

5.4 Splitting Tensile Strength

The splitting tensile strengths of the control mixes for concrete made with 100% slag and 75:25 slag:fly ash ratio were 3.0 and 2.9 MPa, respectively, based on the results of Figure 59. Upon replacing NA by 30, 70, and 100% RCA, the former was reduced by 23, 23, and 25%, respectively, while the latter experienced respective decreases of 13, 31,

and 35%. It thus seems that RCA replacement was more impactful on f_{sp} of mixes made with 25% fly ash. Moreover, replacing NA with RCA caused an increase in the f_{sp}-to-f'_c ratio of 100% slag geopolymer concrete, indicating that f'_c was more affected by RCA replacement than f_{sp}. An opposite finding was noted for slag-fly ash blended geopolymer, whereby the f_{sp}-to-f'_c ratio decreased due to a prominent influence of RCA replacement on f_{sp}.

The effect of steel fiber addition on each geopolymer mix was examined in Figure 58. For 100% slag and slag-fly ash geopolymer concrete, f_{sp} increased by, on average, 95 and 94%, respectively, for every 1% steel fiber added to the mixes. This shows that not only can the steel fiber incorporation reverse the adverse impact of RCA replacement, it can also lead to f_{sp} higher than that of the control mixes. Compared to the improvement noted for f'_c, the enhancement in f_{sp} is superior for both geopolymer concrete mixes. This shows that steel fiber addition was more influential on f_{sp} rather than f'_c.
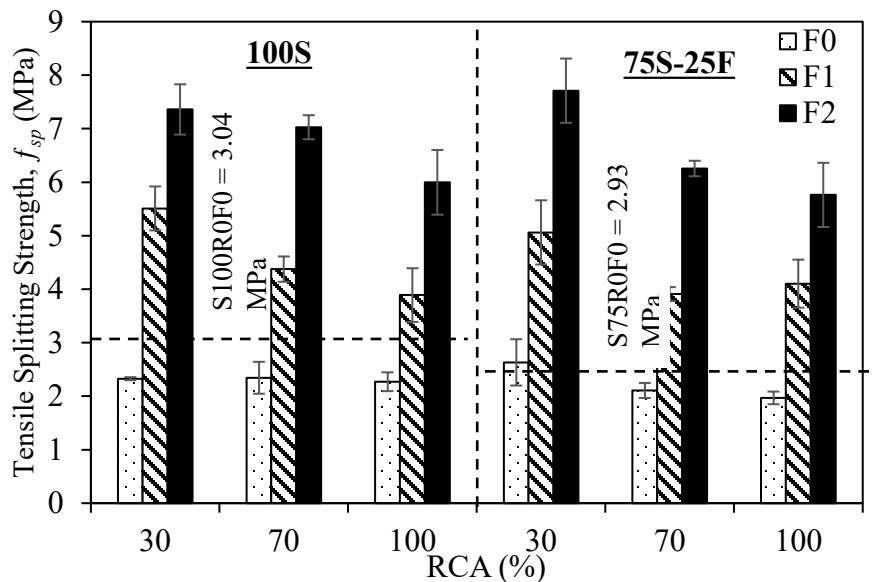
Figure 59: Splitting tensile strength of 100% slag and slag-fly ash blended geopolymer concrete

5.5 Flexural Properties

5.1.1 Load-Deflection Curves

The flexural load-deflection curves of 100% slag and slag-fly ash blended geopolymer were affected by RCA replacement and steel fiber addition. For both plain concrete mixes, every 10% RCA replacement decreased the slope of the load-deflection curve by an average of 25%, highlighting a similar negative impact regardless of the binder composition. Yet, this adverse effect of RCA replacement was not as significant in steel fiber-reinforced geopolymer concrete. Furthermore, every 1% steel fiber volume fraction increased the slope of 100% slag geopolymer concrete made with 30, 70, and 100% RCA by, on average, 1.7, 3.2, and 11.4 times, respectively. In contrast, the slope of the slag-fly ash geopolymer counterpart increased by, on average, 2.5, 3.0, and 3.5 times. While the former concrete showed higher slope values and increases than the latter in 70 and 100% RCA concrete, the latter was superior at 30% RCA replacement. Such findings are analogous to those of the modulus of elasticity.

5.1.2 Flexural Strength

The effect of RCA replacement and steel fiber inclusion on the flexural strength of 100% slag and slag-fly ash geopolymer concrete is presented in Figure 60. The control mixes had respective f_r of 6.3 and 6.1 MPa. For the 100% slag geopolymer concrete, replacement of NA by 30, 70, and 100% RCA reduced f_r by 11, 29, and 51%, respectively. This negative impact was more severe on f_r than f'_c, evidenced by a decrease in the f_r-to-f'_c ratio. Conversely, slag-fly ash counterparts showed respective reductions of 27, 40, and

53%. It is clear that RCA replacement has a more pronounced influence on mixes with 25% fly ash. Yet, such influence was analogous to that reported for f'_c, implied through the little to no change in the f_r-to-f'_c ratio.

The negative effect of RCA replacement could be reversed through the addition of steel fibers. For mixes made with 100% slag, 1 and 2% steel fiber volume fractions increased f_r by, on average, 30 and 105%, respectively. Counterparts made with slag and fly ash noted average respective increases of 56 and 110%. These increases are much higher than those reported for f'_c. As such, it can be stated that the effect of steel fibers was more pronounced on f_r rather than f'_c. Also, steel fiber addition was more impactful on slag-fly ash blended geopolymer concrete mixes. Still, in both concretes, it was possible to produce a geopolymer concrete made with 100% RCA and 2% steel fiber, by volume, with similar flexural strength as the control mixes.
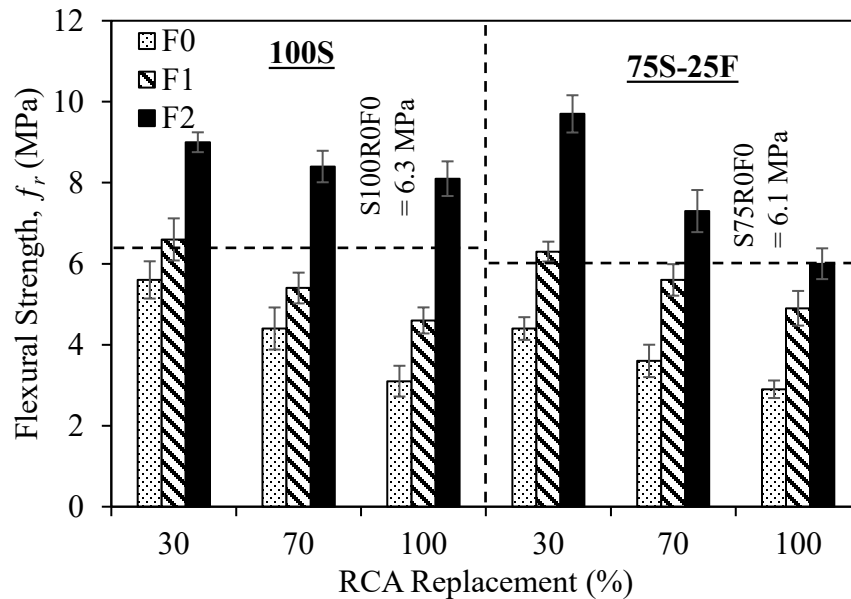
Figure 60: Flexural strength of 100% slag and slag-fly ash blended geopolymer concrete

5.1.3 Deflection

The peak deflection at mid-span of 100% slag and slag-fly ash blended geopolymer concrete prisms were investigated, as illustrated in Figure 61. For the former mixes, the replacement of NA by 30, 70, and 100% RCA increased the deflection by 75, 130, and 160%, respectively. In contrast, it increased by 43, 112, and 178% for the latter mixes. Furthermore, steel fiber addition of 1 and 2%, by volume, increased the deflection by, on average, 43 and 239%, respectively for 100% slag geopolymer concrete and, on average, 44 and 195%, for slag-fly ash counterparts. Despite the relatively similar changes to the deflection, it is worth noting that the values of δ_p were, on average, 15% higher in slag-fly ash blended geopolymer concrete, signifying a slight improvement in the deflection capacity upon the replacement of slag with 25% fly ash.
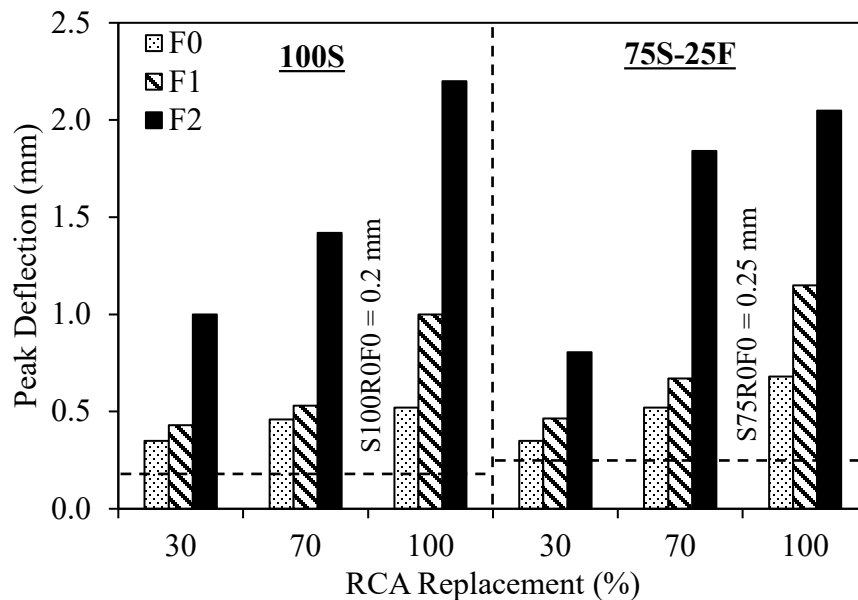
Figure 61: Peak deflection of 100% slag and slag-fly ash blended geopolymer concrete

5.1.4 Residual Strength

Figure 62 presents the residual strength of 100% slag and slag-fly ash blended geopolymer concrete. Results show that increasing the RCA replacement from 30 to 100% led to, on average, 19 and 51% respective decreases in f_{150}^{100} of 100% slag geopolymer concrete. In contrast, f_{150}^{100} of slag-fly ash geopolymer counterparts decreased by, on average, 21 and 44%, respectively. Yet, the f_{150}^{100} values of the former were higher, owing to generally higher flexural strength. So, to better understand the strength retention capacity of each type of geopolymer concrete, the ratio of f_{150}^{100}-to-f_r was determined. Based on the results shown herein, the ratios were, on average, 50.5 and 50.0%, for 100% slag and slag-fly ash geopolymer concrete, respectively. This highlights that RCA and steel fibers have a similar impact on the residual strength for both types of geopolymer concrete.
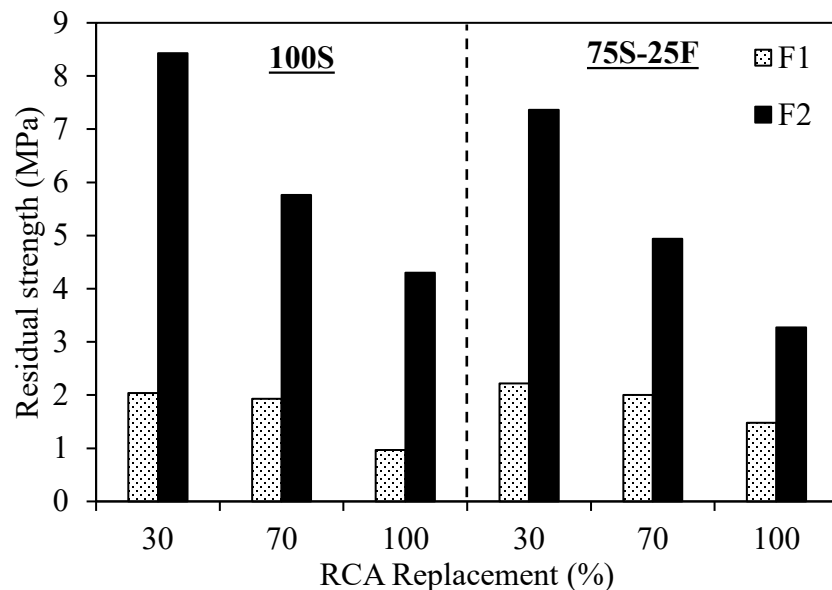
Figure 62: Residual strength of 100% slag and slag-fly ash blended geopolymer concrete

5.1.5 Flexural Toughness

The flexural toughness of plain 100% slag geopolymer concrete ranged between 2 and 4 J, while that of slag-fly ash blended geopolymer counterparts were in the range of 1.6-3.2 J, as shown in Figure 63. In comparison, former mixes incorporating steel fibers presented toughness values between 21 and 33 J, whereas the latter ones were between 22 and 49 J. In general, the inclusion of 25% fly ash as a binder in plain geopolymer concrete had a limited impact on the flexural toughness, while its incorporation in steel fiber-reinforced geopolymer concrete resulted in higher flexural toughness. Nonetheless, the adverse effect of RCA replacement was slightly more pronounced in slag-fly ash blended geopolymer concrete. Yet, this negative impact of RCA replacement was countered by steel fiber inclusion, whereby 1 and 2% steel fiber volume fractions increased the toughness of said concrete by 9.2 and 19.6 times, respectively. In turn, that of 100% slag geopolymer concrete increased by 8.3 and 14.5 times upon adding 1 and 2% steel fibers, by volume. Based on these findings, it can be concluded that geopolymer concrete made with a blend of slag and fly ash was more influenced by RCA replacement and steel fiber addition.
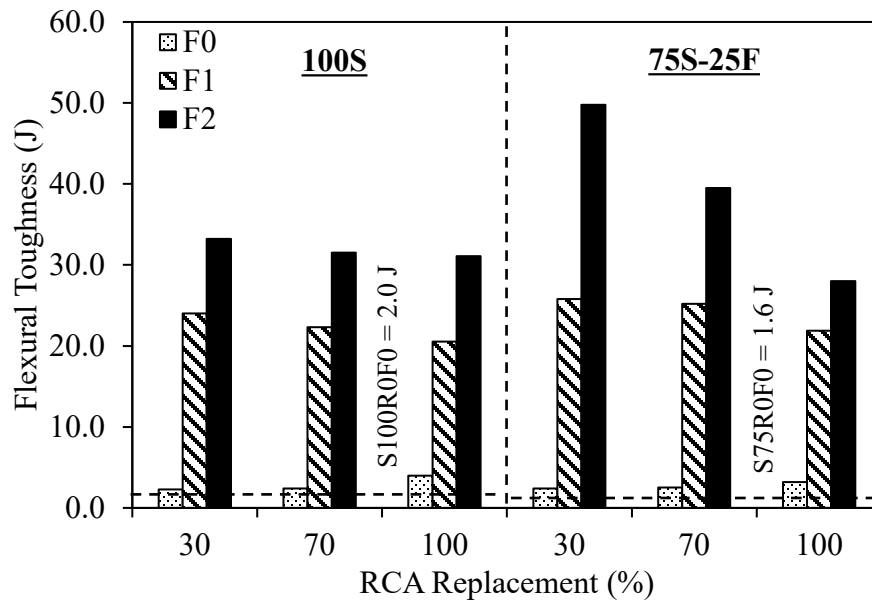
Figure 63: Flexural toughness of 100% slag and slag-fly ash blended geopolymer concrete

5.1.6 Equivalent Flexural Strength Ratio

Figure 64 shows the equivalent flexural strength ratio of geopolymer concrete. While the control mix of 100% slag geopolymer had a larger $R_{T,150}^{100}$ than slag-fly ash counterparts, the values tended to alternate in superiority with RCA replacement of plain mixes. Yet, the impact of RCA replacement was more apparent in the slag-fly ash blended plain geopolymer concrete mixes with 30, 70, and 100% RCA causing respective increases of 110, 167, and 326% compared to 32, 75, and 311% for the 100% slag concrete. Furthermore, the influence of steel fiber addition was also evaluated. Results showed that 1 and 2% steel fiber, by volume, enhanced $R_{T,150}^{100}$ of 100% slag concrete by, on average, 6.6 and 12.1 times, while the increase was 6.4 and 12.6 times for slag-fly ash blended equivalents. As such, it can be noted that steel fiber inclusion had a similar impact

on geopolymer concrete regardless of the binder composition. Still, a comparison between the values of both concretes shows that $R_{T,150}^{100}$ was 7.8% higher when slag was replaced with 25% fly ash.
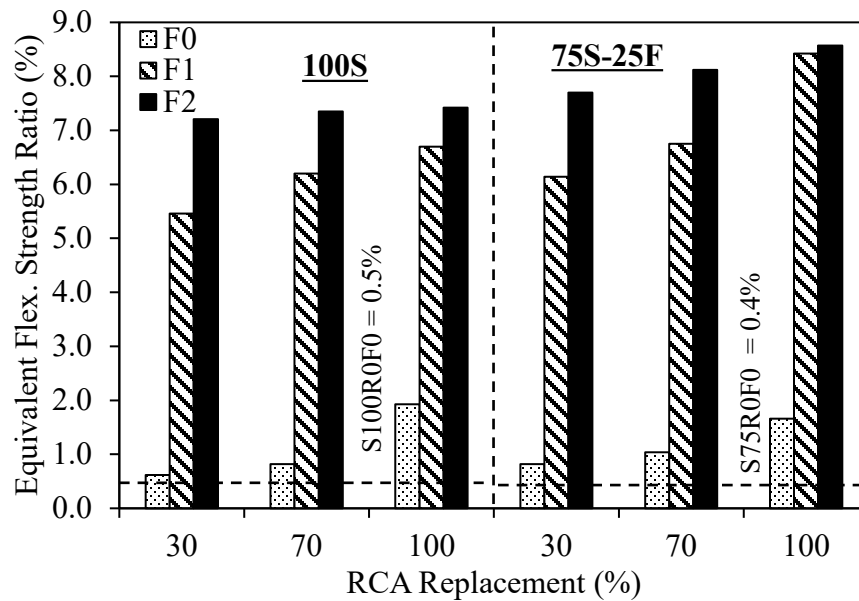
Figure 64: Equivalent flexural strength ratio of 100% slag and slag-fly ash blended geopolymer concrete

5.6 Water Absorption

The effect of RCA replacement on the water absorption of 100% slag and slag-fly blended geopolymer concrete is shown in Figure 65. An increase in water absorption is noted with RCA replacement. In fact, for both types of plain geopolymer concretes, every 10% RCA replacement led to, on average, a 23% increase in water absorption. Yet, the values of the 100% slag geopolymer concrete were lower than those of slag-fly ash blended counterparts by, on average, 21%. This is in line with the generally superior mechanical properties of the former compared to the latter. Nevertheless, the toughness

and equivalent flexural strength ratio of the latter were superior, owing to 15% higher deflection capacity and more pore space, i.e., higher water absorption. Furthermore, the addition of steel fiber seemed to have a more prominent impact on the water absorption of 100% slag geopolymer concrete, as it was reduced by, on average, 25 and 43% for 1 and 2% steel fiber inclusion, by volume, respectively, compared to respective average decreases of 11 and 34% for slag-fly ash geopolymer concrete. Similar findings were noted for the initial sorptivity.
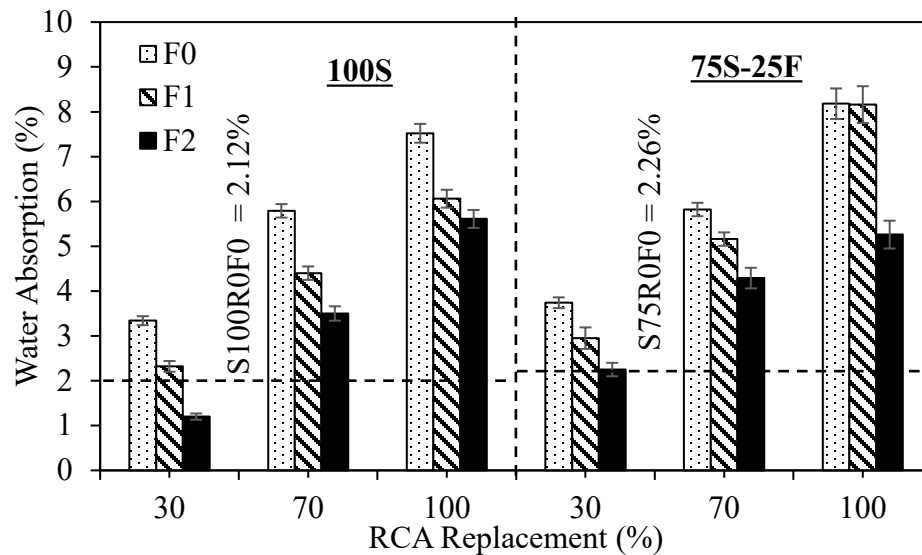
Figure 65: Water absorption of 100% slag and slag-fly ash blended geopolymer concrete

5.7 Bulk Resistivity and UPV

The bulk resistivity of 100% slag and slag-fly ash blended geopolymer concrete are shown in Figure 66(a). While values of the two types of concrete were relatively similar with 0 and 30% RCA replacement, the difference increased as more NA was replaced by RCA. In fact, the bulk resistivity of the former made with 0, 30, 70, and 100% RCA were 3.7, 3.3, 32.7, and 26.5% larger than those of the latter counterparts,

respectively. Similarly, the UPV of the former was, on average, 8.2% higher than the latter, as illustrated in Figure 66(b). This is well-aligned with the water absorption results. Furthermore, RCA replacement was more impactful on the bulk resistivity and UPV of geopolymer concrete made with 25% fly ash. For instance, every 10% RCA replacement decreased the bulk resistivity by, on average, 6.2 and 7.5% for 100% slag and slag-fly ash blended geopolymer concrete, respectively. Such a finding is analogous to that reported for most mechanical properties. Yet, it should be noted that while 100% slag geopolymer concrete was designed to attain the same cylinder compressive strength as slag-fly ash blended equivalents (30 MPa), the binder content of the latter was lower. If it were the same, it is believed that slag-fly ash blended geopolymer concrete would present superior overall performance. Such a hypothesis is based on the results of past work that investigated the addition of fly ash to slag-based geopolymer concrete (no RCA or steel fibers were included) [38, 49, 156].
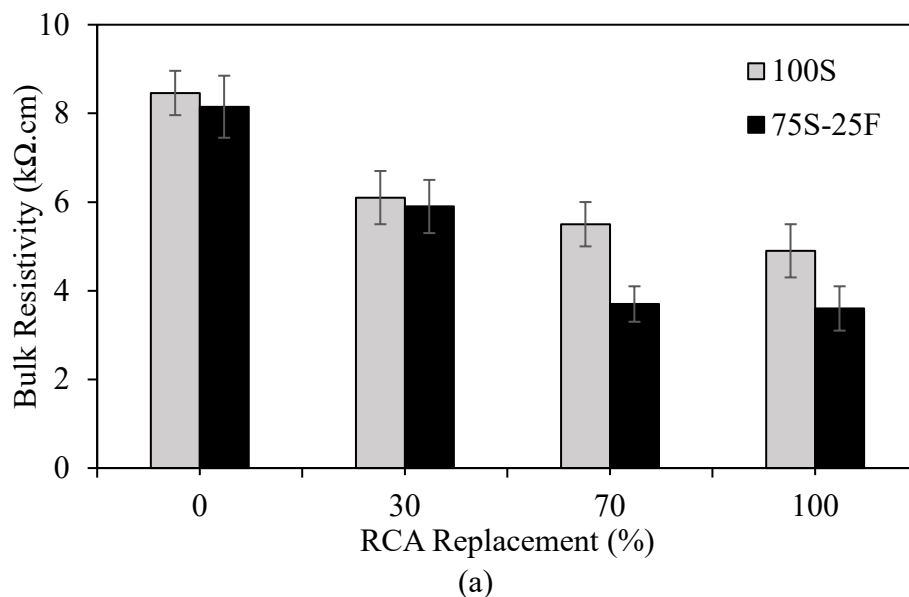
Figure 66: Bulk resistivity (a) and UPV (b) of 100% slag and slag-fly ash blended geopolymer concrete
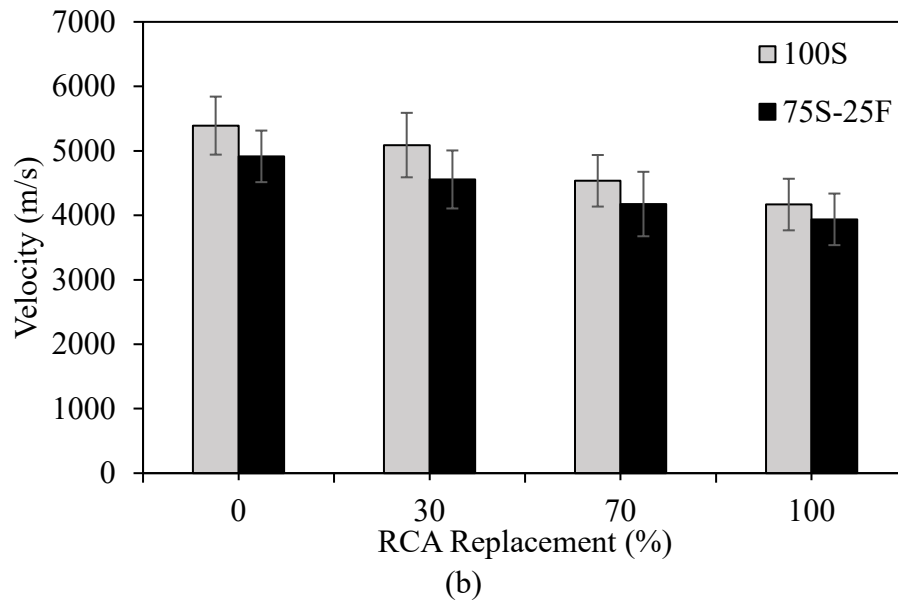
Figure 66: Bulk resistivity (a) and UPV (b) of 100% slag and slag-fly ash blended geopolymer concrete (Continued)

5.8 Abrasion Resistance

The abrasion resistance of 100% slag and slag-fly ash blended geopolymer concrete was characterized by mass loss. For plain mixes, the former had mass losses of 33, 92, 97, and 100% upon incorporating 0, 30, 70, and 100% RCA, respectively. Conversely, the corresponding mass losses for the latter mixes were 35, 43, 73, and 88%. This shows that plain geopolymer concrete made with 25% fly ash was more resistant to abrasive loading. For steel fiber-reinforced mixes, 100% slag geopolymer concrete had a slightly better abrasion resistance with mass losses, on average, 7% lower than those of slag-fly ash blended counterparts. This is associated with 44 and 26% respective average decreases in abrasion mass losses of former and latter mixes for every 1% steel fiber volume fractions.

Chapter 6: Conclusions and Recommendations

6.1 Introduction

The feasibility of recycling locally available industrial by-products and recycled concrete aggregates in producing geopolymer concrete for structural applications was evaluated in this study. The binding material was alternated between 100% slag and a blend of 75% slag and 25% fly ash. Steel fibers were added to the mixes made with RCA to promote their use as structural geopolymer concrete. Such steel fiber-reinforced RCA geopolymer concrete offers to be an innovative and sustainable alternative to conventional cement-based concrete that addresses multiple globally recognized challenges, including the emission of carbon dioxide, production of industrial by-products, and depletion of non-renewable natural resources.

The experimental testing program aimed to examine the effect of RCA replacement and steel fiber inclusion on the performance of 100% slag and slag-fly ash blended geopolymer concrete. It involved testing twenty concrete mixes made with RCA replacements of 0, 30, 70, and 100% and steel fiber volume fractions of 0, 1, and 2%. To investigate the mechanical properties, the compressive strength, splitting tensile strength, flexural performance, and modulus of elasticity were determined. In turn, the durability properties were evaluated by measuring the water absorption, sorptivity, bulk resistivity, UPV, and abrasion resistance. This chapter outlines the main findings and limitations of this research work and recommendations for future studies.

6.2 Limitations

The results and findings of this work are limited to the specific types of slag and fly ash utilized as binders. The fine aggregates were dune sand, while the coarse aggregates were dolomitic limestone. Also, the alkaline activator solution was a mixture of grade N sodium silicate solution and sodium hydroxide solution with a molar concentration of 14 M. The steel fiber reinforcement was double hooked end with a specific diameter and aspect ratio. Variations in these components could lead to different results and conclusions than those shown in this thesis. Additionally, the durability performance was limited to indirect tests related to transport properties and abrasion resistance. Other deterioration mechanisms were not considered.

6.3 Conclusions

Based on the experimental testing program carried out in this work, the following conclusions can be drawn:

- The compressive strength development profile of 100% slag geopolymer concrete showed that 81 and 98% of the 28-day cube compressive strength was attained within 1 and 7 days. Conversely, the 1- and 7-day strengths of slag-fly ash blended geopolymer concrete were 55 and 78% that after 28 days. Yet, the 28-day strengths of the latter were superior to those of the former despite having lower binder content. This signifies that the addition of 25% fly ash resulted in lower early-age (1 day) and higher late-age (28 days) cube compressive strength.

- The 1-, 7-, and 28-day cube compressive strengths of 100% slag geopolymer concrete were reduced by up to 44, 23, and 20%, respectively, upon RCA

replacement compared to the NA-based control mix. In comparison, those of slag-fly ash blended geopolymer concrete decreased by up to 42, 21, and 25%. However, this adverse effect of RCA replacement could be countered by steel fiber inclusion. Actually, the addition of up to 2% steel fiber volume fraction increased the 1-, 7-, and 28-day 100% slag geopolymer cube compressive strength by up to 42, 31, and 23%, respectively, while those of slag-fly ash blended counterpart experienced respective increases of up to 41, 18, and 22%. This indicates that steel fibers have a more significant impact at 1 day.

- The effect of RCA replacement and steel fiber addition on the 28-day cylinder compressive strength is similar to that of the cube strength. While this finding applied to both types of geopolymer concrete examined herein, mixes with 25% fly ash experienced slightly higher losses and gains in f'_c due to RCA replacement and steel fiber inclusion. As such, f'_c and f_{cu} of each of 100% slag and slag-fly ash blended geopolymer concrete were related using linear regression models to predict one property from the other with high accuracy ($R^2 > 0.90$).

- The replacement of NA by RCA decreased the peak stress and increased the peak strain of 100% slag and slag-fly ash blended geopolymer concrete. Yet, steel fiber addition increased the peak stress and further increased the peak strain, owing to the steel fibers' bridging effect. This is indicative of enhanced deformability and energy absorption capacity.

- The slope of the compression stress-strain curves characterized the modulus of elasticity. The values of E_c decreased by up to 56 and 52% with 100% RCA replacement in 100% slag and slag-fly ash geopolymer concrete, respectively. The

addition of steel fibers could enhance respective E_c by up to 43 and 70%. Still, E_c of the former mixes were superior to those of the latter, bearing in mind a higher binder content was used in the former. Also, for both types of geopolymers, mixes made with 100% RCA and 2% steel fiber, by volume, could not attain E_c of the respective NA-based control mixes.

- The splitting tensile strength of 100% slag geopolymer concrete decreased by up to 25% upon RCA replacement. Yet, every 1% steel fiber added led to, on average, a 97% increase in f_{sp} compared to plain counterparts, thus reversing the negative effect of RCA on f_{sp}. These results also show that RCA replacement and steel fiber addition had a more pronounced impact on f_{sp} than f'_c of 100% slag geopolymer concrete. Similar changes in f_{sp} were noted in slag-fly ash blended geopolymer concrete. Yet, the influence of RCA replacement was more prominent on f'_c than f_{sp}, while the steel fiber inclusion was vice versa.

- The peak flexural strength, peak deflection, residual flexural strength, flexural toughness, and equivalent flexural strength ratio were employed in evaluated the flexural performance of 100% slag and slag-fly ash blended geopolymer concrete. For both types of geopolymers, an increase in RCA replacement percentage resulted in a decrease in the slope of the flexural load-deflection curve, flexural strength, and residual flexural strength. In turn, it caused an increase in peak deflection and equivalent flexural strength ratio and a limited impact on the flexural toughness. Nevertheless, the inclusion of steel fibers enhanced all flexural performance indicators, exceeding those of the control mixes, with more pronounced impact on mixes incorporating 25% fly ash.

- For 100% slag and slag-fly ash blended geopolymer concrete, the 28-day cylinder compressive strength was correlated to the various mechanical and durability properties tested herein. These include E_c, f_{sp}, and f_r. The newly-developed regression models can be used to predict such properties from f'_c with good accuracy, as $R^2 > 0.90$. A comparison with codified equations shows that they provide less accurate predictions for 100% slag and slag-fly ash blended geopolymer concrete incorporating RCA and steel fibers.

- For 100% slag and slag-fly ash blended geopolymer concrete, the water absorption increased by up to 255 and 262% upon replacing NA by RCA, respectively. Yet, it could be decreased by up to 65 and 40% when steel fibers were added to respective mixes. Generally, the values of mixes without fly ash were lower than those with 25% fly ash. While the strength results of the two geopolymers were similar, it seems that reducing the binder content in the latter may have reduced the overall durability. The effect of RCA replacement and steel fiber incorporation on the initial sorptivity was similar to that noted for the water absorption.

- The bulk resistivity of 100% slag and slag-fly ash blended geopolymer concrete decreased by up to 42 and 56% when NA was replaced by 100% RCA, respectively. In turn, the UPV values experienced respective decreases of 23 and 20%. Yet, the plain mix with 30% RCA was reported to have "Excellent" quality, while those made with 70 and 100% RCA had "Good" quality.

- For both types of geopolymers, RCA replacement led to lower abrasion resistance, i.e. higher mass loss, than the control mixes. However, the addition of steel fibers

improved the resistance by up to 74 and 60% to be comparable to that of the control mixes.

6.4 Recommendations for Future Studies

Experimental results and findings of this thesis highlighted the feasibility of employing steel fiber-reinforced RCA geopolymer concrete for structural applications. Still, the following research works are recommended for future studies:

- Evaluate the influence of steel fibers with different geometric shapes, lengths, and aspect ratios.

- Study the effect of various types and quantities of water reducers on the rheological and fresh concrete properties of 100% slag and slag-fly ash blended steel fiber-reinforced RCA geopolymer concrete.

- Examine the resistance of slag-based and slag-fly ash blended geopolymer concrete to seawater exposure, acid attack, sulfate attack, and elevated temperatures.

- Investigate the mechanical and durability properties of slag-fly ash blended geopolymer concrete incorporating other by-products in ternary and quaternary mixtures.

- Develop numerical models to characterize the structural behavior of steel fiber-reinforced geopolymer concrete made with RCA and validate their accuracy with experimental testing of the large-scale concrete beam.

- Evaluate the feasibility of employing slag-based and slag-fly ash blended geopolymer concrete in structural applications through a lifecycle assessment and cost-impact analysis.

References

[1]   T. C. Hansen and E. Boegh, "Elasticity and drying shrinkage concrete of recycled-aggregate," *ACI Journal,* vol. 82, no. 56, pp. 648-652, 1985.

[2]   A. Akbarnezhad, K. C. G. Ong, M. H. Zhang, C. T. Tam, and T. W. J. Foo, "Microwaveassisted beneficiation of recycled concrete aggregates," *Construction and Building Materials,* vol. 25, no. 8, pp. 3469-3479, 2011.

[3]   M. Jiang, X. Chen, F. Rajabipour, and C. T. Hendrickson, "Comparative Life Cycle Assessment of Conventional, Glass Powder, and Alkali-Activated Slag Concrete and Mortar," *Journal of Infrastructure Systems,* vol. 20, no. 4, p. 04014020, 2014, doi: doi:10.1061/(ASCE)IS.1943-555X.0000211.

[4]   K. Parthiban and K. Saravana Raja Mohan, "Influence of recycled concrete aggregates on the engineering and durability properties of alkali activated slag concrete," *Construction and Building Materials,* vol. 133, no. Supplement C, pp. 65-72, 2017, doi: https://doi.org/10.1016/j.conbuildmat.2016.12.050.

[5]   P. Kathirvel and S. R. M. Kaliyaperumal, "Influence of recycled concrete aggregates on the flexural properties of reinforced alkali activated slag concrete," *Construction and Building Materials,* vol. 102, no. Part 1, pp. 51-58, 2016, doi: https://doi.org/10.1016/j.conbuildmat.2015.10.148.

[6]   Y. Hu, Z. Tang, W. Li, Y. Li, and V. W. Y. Tam, "Physical-mechanical properties of fly ash/GGBFS geopolymer composites with recycled aggregates," *Construction and Building Materials,* vol. 226, pp. 139-151, 2019, doi: https://doi.org/10.1016/j.conbuildmat.2019.07.211.

[7]   Z. Tang, Y. Hu, V. W. Y. Tam, and W. Li, "Uniaxial compressive behaviors of fly ash/slag-based geopolymeric concrete with recycled aggregates," *Cement and Concrete Composites,* vol. 104, p. 103375, 2019, doi: https://doi.org/10.1016/j.cemconcomp.2019.103375.

[8]   D. Gao, J. Jing, G. Chen, and L. Yang, "Experimental investigation on flexural behavior of hybrid fibers reinforced recycled brick aggregates concrete," *Construction and Building Materials,* vol. 227, p. 116652, 2019, doi: https://doi.org/10.1016/j.conbuildmat.2019.08.033.

[9]   D. Gao and L. Zhang, "Flexural performance and evaluation method of steel fiber reinforced recycled coarse aggregate concrete," *Construction and Building Materials,* vol. 159, pp. 126-136, 2018, doi: https://doi.org/10.1016/j.conbuildmat.2017.10.073.

[10]   D. Gao, L. Zhang, and M. Nokken, "Compressive behavior of steel fiber reinforced recycled coarse aggregate concrete designed with equivalent cubic compressive strength," *Construction and Building Materials,* vol. 141, pp. 235-244, 2017, doi: https://doi.org/10.1016/j.conbuildmat.2017.02.136.

[11]   D. Gao, L. Zhang, and M. Nokken, "Mechanical behavior of recycled coarse aggregate concrete reinforced with steel fibers under direct shear," *Cement and Concrete Composites,* vol. 79, pp. 1-8, 2017, doi: https://doi.org/10.1016/j.cemconcomp.2017.01.006.

[12]   J. Han, M. Zhao, J. Chen, and X. Lan, "Effects of steel fiber length and coarse aggregate maximum size on mechanical properties of steel fiber reinforced concrete," *Construction and Building Materials,* vol. 209, pp. 577-591, 2019, doi: https://doi.org/10.1016/j.conbuildmat.2019.03.086.

[13]   F. Hasan-Nattaj and M. Nematzadeh, "The effect of forta-ferro and steel fibers on mechanical properties of high-strength concrete with and without silica fume and nano-silica," *Construction and Building Materials,* vol. 137, pp. 557-572, 2017, doi: https://doi.org/10.1016/j.conbuildmat.2017.01.078.

[14]   H. Hiroshi and B. Nemkumar, "Correlating Flexural and Shear Toughness of Lightweight Fiber-Reinforced Concrete," *ACI Materials Journal,* vol. 105, no. 3, 2008, doi: 10.14359/19821.

[15]   A. Islam, U. J. Alengaram, M. Z. Jumaat, N. B. Ghazali, S. Yusoff, and I. I. Bashar, "Influence of steel fibers on the mechanical properties and impact resistance of lightweight geopolymer concrete," *Construction and Building Materials,* vol. 152, no. Supplement C, pp. 964-977, 2017, doi: https://doi.org/10.1016/j.conbuildmat.2017.06.092.

[16]   N. Kachouh, H. El-Hassan, and T. El Maaddawy, "The Use of Steel Fibers to Enhance the Performance of Concrete Made With Recycled Aggregate," in *Fifth International Conference on Sustainable Construction Materials and Technologies (SCMT5)*, London, UK, P. Claisse, Ed., 2019.

[17]   R. Perumal, "Correlation of Compressive Strength and Other Engineering Properties of High-Performance Steel Fiber-Reinforced Concrete," *Journal of Materials in Civil Engineering,* vol. 27, no. 1, p. 04014114, 2015, doi: doi:10.1061/(ASCE)MT.1943-5533.0001050.

[18]   N. Tamrakar, "The Effect of Steel Fibers Type and Content on the Development of Fresh and Hardened Properties and Durability of Self-consolidating Concrete," Master of Applied Science, Civil Engineering, Ryerson University, Toronto, ON, 794, 2012.

[19]   B. W. Xu and H. S. Shi, "Correlations among mechanical properties of steel fiber reinforced concrete," *Construction and Building Materials,* vol. 23, no. 12, pp. 3468-3474, 2009, doi: https://doi.org/10.1016/j.conbuildmat.2009.08.017.

[20]   N. Kachouh, T. El-Maaddawy, H. El-Hassan, and B. El-Ariss, "Shear Behavior of Steel-Fiber-Reinforced Recycled Aggregate Concrete Deep Beams," *Buildings,* vol. 11, no. 9, p. 423, 2021. [Online]. Available: https://www.mdpi.com/2075-5309/11/9/423.

[21]   US Geological Survey. "Minerals commodity summary - cement." USGS. (accessed October 6, 2021).

[22]   Statistica. "Major countries in worldwide cement production from 2015 to 2019." Statistica. (accessed October 6, 2021).

[23]   J. Kline and C. Kline, "Cement and CO2: What is Happening," *IEEE Transactions on Industry Applications,* vol. 51, no. 2, pp. 1289-1294, 2015, doi: 10.1109/TIA.2014.2339396.

[24]   A. Aleem and P. Arumairaj, "Geopolymer concrete - A review," *International Journal of Engineering Sciences & Emerging Technologies,* vol. 1, pp. 118-122, 02/01 2012, doi: 10.7323/ijeset/v1_i2_14.

[25]   B. Afkhami, B. Akbarian, N. Beheshti A, A. H. Kakaee, and B. Shabani, "Energy consumption assessment in a cement production plant," *Sustainable Energy Technologies and Assessments,* vol. 10, pp. 84-89, 2015, doi: http://dx.doi.org/10.1016/j.seta.2015.03.003.

[26]   R. N. Thakur and Z. Wu, "Development of High-Performance Blended Cements," PhD, College of Engineering and Applied Science, The University of Wisconsin, USA, 2000.

[27]   J. Davidovits, "High-Alkali Cements for 21st Century Concretes," *Special Publication,* vol. 144, 1994, doi: 10.14359/4523.

[28]   E. Benhelal, G. Zahedi, E. Shamsaei, and A. Bahadori, "Global strategies and potentials to curb CO2 emissions in cement industry," *Journal of Cleaner Production,* vol. 51, pp. 142-161, 2013, doi: http://dx.doi.org/10.1016/j.jclepro.2012.10.049.

[29]   P. K. Mehta, and Monteiro, J. P., *Concrete Microstructure, Properties and Material*. New York: McGraw Hill, 2006.

[30]   J. Zhang, C. Shi, Y. Li, X. Pan, C. S. Poon, and Z. Xie, "Performance Enhancement of Recycled Concrete Aggregates through Carbonation," *Journal of Materials in Civil Engineering,* vol. 27, no. 11, 2015.

[31]   D. Kong, T. Lei, C. Ma, and J. Jiang, "Effect and mechanism of surface-coating pozzolanic materials around aggregate on properties and ITZ microstructure of recycled aggregate concrete," *Construction and Building Materials,* vol. 24, no. 5, pp. 701-708, 2010.

[32]   C. Poon and D. Chan, "The use of recycled aggregate in concrete in Hong Kong," *Resources Conservation Recycling,* vol. 50, no. 3, pp. 293-305, 2007.

[33]   J. Stoner and C. Wankel, *Global Sustainability Initiatives: New Models and New Approaches*. USA: Information Age Publishing, 2008, p. 248.

[34]   T. Ikea, S. Yamane, and A. Sakamoto, "Strength of concrete containing recycled aggregate concrete," in *2nd RILEM Symp. on Demolition and Reuse of Waste*, Bagneux, France, 1988: RILEM Publications.

[35]   M. H. Alzard, H. El-Hassan, and T. El-Maaddawy, "Environmental and Economic Life Cycle Assessment of Recycled Aggregates Concrete in the United Arab Emirates," *Sustainability,* vol. 13, no. 18, p. 10348, 2021. [Online]. Available: https://www.mdpi.com/2071-1050/13/18/10348.

[36]   J. Davidovits, "Geopolymers: inorganic polymeric new materials," *Journal of Thermal Analysis,* vol. 37, pp. 1633-1656, 1991.

[37]   C. Li, H. Sun, and L. Li, "A review: The comparison between alkali-activated slag (Si+Ca) and metakaolin (Si+Al) cements," *Cement and Concrete Research,* vol. 40, no. 9, pp. 1341-1349, 2010, doi: https://doi.org/10.1016/j.cemconres.2010.03.020.

[38]   H. El-Hassan and S. Elkholy, "Performance Evaluation and Microstructure Characterization of Steel Fiber-Reinforced Alkali-Activated Slag Concrete Incorporating Fly Ash," *Journal of Materials in Civil Engineering,* vol. 31, no. 10, p. 04019223, 2019, doi: doi:10.1061/(ASCE)MT.1943-5533.0002872.

[39]   H. El-Hassan and N. Ismail, "Effect of process parameters on the performance of fly ash/GGBS blended geopolymer composites," *Journal of Sustainable Cement-Based Materials,* vol. 7, no. 2, pp. 122-140, 2018, doi: https://doi.org/10.1080/21650373.2017.1411296.

[40]   H. El-Hassan, E. Shehab, and A. Al-Sallamin, "Influence of Different Curing Regimes on the Performance and Microstructure of Alkali-Activated Slag Concrete," *Journal of Materials in Civil Engineering,* vol. 30, no. 9, p. 04018230, 2018, doi: doi:10.1061/(ASCE)MT.1943-5533.0002436.

[41]   S. Aydın and B. Baradan, "Effect of activator type and content on properties of alkali-activated slag mortars," *Composites Part B: Engineering,* vol. 57, pp. 166-172, 2014, doi: http://dx.doi.org/10.1016/j.compositesb.2013.10.001.

[42]   H. El-Hassan and S. Elkholy, "Enhancing the performance of Alkali-Activated Slag-Fly ash blended concrete through hybrid steel fiber reinforcement," *Construction and Building Materials,* vol. 311, p. 125313, 2021, doi: https://doi.org/10.1016/j.conbuildmat.2021.125313.

[43]   O. Najm, H. El-Hassan, and A. El-Dieb, "Ladle slag characteristics and use in mortar and concrete: A comprehensive review," *Journal of Cleaner Production,* vol. 288, p. 125584, 2021, doi: https://doi.org/10.1016/j.jclepro.2020.125584.

[44]   A. Fernández-Jiménez and F. Puertas, "Effect of activator mix on the hydration and strength behaviour of alkali-activated slag cements," *Advances in Cement Research,* vol. 15, no. 3, pp. 129-136, 2003, doi: 10.1680/adcr.2003.15.3.129.

[45]   S. Akçaözoğlu and C. D. Atiş, "Effect of Granulated Blast Furnace Slag and fly ash addition on the strength properties of lightweight mortars containing waste PET aggregates," *Construction and Building Materials,* vol. 25, no. 10, pp. 4052-4058, 2011, doi: http://dx.doi.org/10.1016/j.conbuildmat.2011.04.042.

[46]   R. R. Bellum, K. Muniraj, and S. R. C. Madduru, "Investigation on modulus of elasticity of fly ash-ground granulated blast furnace slag blended geopolymer concrete," *Materials Today: Proceedings,* vol. 27, pp. 718-723, 2020, doi: https://doi.org/10.1016/j.matpr.2019.11.299.

[47]   M. Chi and R. Huang, "Binding mechanism and properties of alkali-activated fly ash/slag mortars," *Construction and Building Materials,* vol. 40, pp. 291-298, 2013, doi: http://dx.doi.org/10.1016/j.conbuildmat.2012.11.003.

[48] P. S. Deb, P. Nath, and P. K. Sarker, "The effects of ground granulated blast-furnace slag blending with fly ash and activator content on the workability and strength properties of geopolymer concrete cured at ambient temperature," *Materials & Design (1980-2015),* vol. 62, pp. 32-39, 2014, doi: https://doi.org/10.1016/j.matdes.2014.05.001.

[49] H. El-Hassan, E. Shehab, and A. Al-Sallamin, "Effect of Curing Regime on the Performance and Microstructure Characteristics of Alkali-Activated Slag-Fly Ash Blended Concrete," *Journal of Sustainable Cement-Based Materials,* vol. 10, no. 5, pp. 289-317, 2021, doi: 10.1080/21650373.2021.1883145.

[50] L. Garanayak, "Behavior of alkali activated fly ash slag paste at room temperature," *Materials Today: Proceedings,* 2020, doi: https://doi.org/10.1016/j.matpr.2020.10.818.

[51] M. Guerrieri and J. G. Sanjayan, "Behavior of combined fly ash/slag-based geopolymers when exposed to high temperatures," *Fire and Materials,* vol. 34, no. 4, pp. 163-175, 2010, doi: 10.1002/fam.1014.

[52] I. Ismail, S. A. Bernal, J. L. Provis, S. Hamdan, and J. S. J. van Deventer, "Microstructural changes in alkali activated fly ash/slag geopolymers with sulfate exposure," *Materials and Structures,* journal article vol. 46, no. 3, pp. 361-373, 2013, doi: 10.1617/s11527-012-9906-2.

[53] N. Ismail and H. El-Hassan, "Development and Characterization of Fly Ash/Slag-Blended Geopolymer Mortar and Lightweight Concrete," *Journal of Materials in Civil Engineering,* vol. 30, no. 4, 2018, doi: 10.1061/(ASCE)MT.1943-5533.0002209.

[54] A. Karthik, K. Sudalaimani, and C. T. Vijaya Kumar, "Investigation on mechanical properties of fly ash-ground granulated blast furnace slag based self curing bio-geopolymer concrete," *Construction and Building Materials,* vol. 149, pp. 338-349, 2017, doi: https://doi.org/10.1016/j.conbuildmat.2017.05.139.

[55] W.-H. Lee, J.-H. Wang, Y.-C. Ding, and T.-W. Cheng, "A study on the characteristics and microstructures of GGBS/FA based geopolymer paste and concrete," *Construction and Building Materials,* vol. 211, pp. 807-813, 2019, doi: https://doi.org/10.1016/j.conbuildmat.2019.03.291.

[56] J. Li and S. Liu, "Influence of Slag as Additive on Compressive Strength of Fly Ash-Based Geopolymer," *Journal of Materials in Civil Engineering,* vol. 19, no. 6, 2007.

[57]   A. Mehta, R. Siddique, T. Ozbakkaloglu, F. Uddin Ahmed Shaikh, and R. Belarbi, "Fly ash and ground granulated blast furnace slag-based alkali-activated concrete: Mechanical, transport and microstructural properties," *Construction and Building Materials,* vol. 257, p. 119548, 2020, doi: https://doi.org/10.1016/j.conbuildmat.2020.119548.

[58]   H. El-Hassan, A. Hussein, J. Medljy, and T. El-Maaddawy, "Performance of Steel Fiber-Reinforced Alkali-Activated Slag-Fly Ash Blended Concrete Incorporating Recycled Concrete Aggregates and Dune Sand," *Buildings,* vol. 11, no. 8, p. 327, 2021. [Online]. Available: https://www.mdpi.com/2075-5309/11/8/327.

[59]   H. El-Hassan, J. Medljy, and T. El-Maaddawy, "Properties of Steel Fiber-Reinforced Alkali-Activated Slag Concrete Made with Recycled Concrete Aggregates and Dune Sand," *Sustainability,* vol. 13, no. 14, p. 8017, 2021. [Online]. Available: https://www.mdpi.com/2071-1050/13/14/8017.

[60]   F. Abu Obaida, T. El-Maaddawy, and H. El-Hassan, "Bond Behavior of Carbon Fabric-Reinforced Matrix Composites: Geopolymeric Matrix versus Cementitious Mortar," *Buildings,* vol. 11, no. 5, p. 207, 2021. [Online]. Available: https://www.mdpi.com/2075-5309/11/5/207.

[61]   C. K. Yip, G. C. Lukey, and J. S. J. van Deventer, "The coexistence of geopolymeric gel and calcium silicate hydrate at the early stage of alkaline activation," *Cement and Concrete Research,* vol. 35, no. 9, pp. 1688-1697, 2005, doi: http://dx.doi.org/10.1016/j.cemconres.2004.10.042.

[62]   C. Shi, D. Roy, and P. Krivenko, *Alkali-Activated Cements and Concretes*. Routledge, 2006.

[63]   Á. Palomo, A. Fernández Jiménez, C. López Hombrados, and J. L. Lleyda, "Railway sleepers made of alkali activated fly ash concrete," *Revista ingeniería de construcción,* vol. 22, pp. 75-80, 2007. [Online]. Available: https://scielo.conicyt.cl/scielo.php?script=sci_arttext&pid=S0718-50732007000200001&nrm=iso.

[64]   A. Palomo, M. W. Grutzeck, and M. T. Blanco, "Alkali-activated fly ashes: A cement for the future," *Cement and Concrete Research,* vol. 29, no. 8, pp. 1323-1329, 8// 1999, doi: http://dx.doi.org/10.1016/S0008-8846(98)00243-9.

[65] W. K. Part, M. Ramli, and C. B. Cheah, "Chapter 11 - An Overview on the Influence of Various Factors on the Properties of Geopolymer Concrete Derived From Industrial Byproducts," in *Handbook of Low Carbon Concrete*, A. Nazari and J. G. Sanjayan Eds.: Butterworth-Heinemann, 2017, pp. 263-334.

[66] F. Puertas *et al.*, "Alkali-activated slag concrete: Fresh and hardened behaviour," *Cement and Concrete Composites,* vol. 85, pp. 22-31, 2018, doi: https://doi.org/10.1016/j.cemconcomp.2017.10.003.

[67] T. Ray, N. Ranjan Mohanta, M. Hitesh Kumar, I. Saikrishna macharyulu, and S. Samantaray, "Study of effect of temperature on behavior of alkali activated slag concrete," *Materials Today: Proceedings,* 2020, doi: https://doi.org/10.1016/j.matpr.2020.09.169.

[68] S. A. Bernal, R. Mejía de Gutiérrez, A. L. Pedraza, J. L. Provis, E. D. Rodriguez, and S. Delvasto, "Effect of binder content on the performance of alkali-activated slag concretes," *Cement and Concrete Research,* vol. 41, no. 1, pp. 1-8, 2011, doi: https://doi.org/10.1016/j.cemconres.2010.08.017.

[69] F. Collins and J. G. Sanjayan, "Microcracking and strength development of alkali activated slag concrete," *Cement and Concrete Composites,* vol. 23, no. 4, pp. 345-352, 2001, doi: https://doi.org/10.1016/S0958-9465(01)00003-8.

[70] F. G. Collins and J. G. Sanjayan, "Workability and mechanical properties of alkali activated slag concrete," *Cement and Concrete Research,* vol. 29, no. 3, pp. 455-458, 1999, doi: https://doi.org/10.1016/S0008-8846(98)00236-1.

[71] T. Bakharev, J. G. Sanjayan, and Y. B. Cheng, "Effect of admixtures on properties of alkali-activated slag concrete," *Cement and Concrete Research,* vol. 30, no. 9, pp. 1367-1374, 2000, doi: https://doi.org/10.1016/S0008-8846(00)00349-5.

[72] D. Bondar, S. Nanukuttan, J. L. Provis, and M. Soutsos, "Efficient mix design of alkali activated slag concretes based on packing fraction of ingredients and paste thickness," *Journal of Cleaner Production,* vol. 218, pp. 438-449, 2019/05/01/ 2019, doi: https://doi.org/10.1016/j.jclepro.2019.01.332.

[73] T. Yang, Z. Zhang, F. Zhang, Y. Gao, and Q. Wu, "Chloride and heavy metal binding capacities of hydrotalcite-like phases formed in greener one-part sodium carbonate-activated slag cements," *Journal of Cleaner Production,* vol. 253, p. 120047, 2020, doi: https://doi.org/10.1016/j.jclepro.2020.120047.

[74] B. Bhardwaj and P. Kumar, "Comparative study of geopolymer and alkali activated slag concrete comprising waste foundry sand," *Construction and Building Materials,* vol. 209, pp. 555-565, 2019, doi: https://doi.org/10.1016/j.conbuildmat.2019.03.107.

[75] A. A. Aliabdo, A. E. M. Abd Elmoaty, and M. A. Emam, "Factors affecting the mechanical properties of alkali activated ground granulated blast furnace slag concrete," *Construction and Building Materials,* vol. 197, pp. 339-355, 2019, doi: https://doi.org/10.1016/j.conbuildmat.2018.11.086.

[76] C. S. Thunuguntla and T. D. Gunneswara Rao, "Effect of mix design parameters on mechanical and durability properties of alkali activated slag concrete," *Construction and Building Materials,* vol. 193, pp. 173-188, 2018, doi: https://doi.org/10.1016/j.conbuildmat.2018.10.189.

[77] N. Li *et al.*, "A mixture proportioning method for the development of performance-based alkali-activated slag-based concrete," *Cement and Concrete Composites,* vol. 93, pp. 163-174, 2018, doi: https://doi.org/10.1016/j.cemconcomp.2018.07.009.

[78] J. Shang, J.-G. Dai, T.-J. Zhao, S.-Y. Guo, P. Zhang, and B. Mu, "Alternation of traditional cement mortars using fly ash-based geopolymer mortars modified by slag," *Journal of Cleaner Production,* vol. 203, pp. 746-756, 2018, doi: https://doi.org/10.1016/j.jclepro.2018.08.255.

[79] F. Puertas, S. Martiez-Ramirez, S. Alonso, and T. Vazquez, "Alkali-activated fly ash/slag cement strength behaviour and hydration products," *Cement and Concrete Reserach,* vol. 30, pp. 1625-1632, 2000.

[80] A. Rafeet, R. Vinai, M. Soutsos, and W. Sha, "Effects of slag substitution on physical and mechanical properties of fly ash-based alkali activated binders (AABs)," *Cement and Concrete Research,* vol. 122, pp. 118-135, 2019, doi: https://doi.org/10.1016/j.cemconres.2019.05.003.

[81] P. Nath and P. K. Sarker, "Effect of GGBFS on setting, workability and early strength properties of fly ash geopolymer concrete cured in ambient condition," *Construction and Building Materials,* vol. 66, pp. 163-171, 2014.

[82] M. Sofi, J. S. J. van Deventer, P. A. Mendis, and G. C. Lukey, "Engineering properties of inorganic polymer concretes (IPCs)," *Cement and Concrete Research,* vol. 37, no. 2, pp. 251-257, 2007, doi: https://doi.org/10.1016/j.cemconres.2006.10.008.

[83] AS3600, "Concrete Structures," Standards Australia, Australia, 2009.

[84] ACI Committee 318, "Building Code Requirements for Structural Concrete and Commentary," American Concrete Institute, Farmington Hills, Michigan, 2014.

[85] J. K. Prusty and B. Pradhan, "Effect of GGBS and chloride on compressive strength and corrosion performance of steel in fly ash-GGBS based geopolymer concrete," *Materials Today: Proceedings,* vol. 32, pp. 850-855, 2020, doi: https://doi.org/10.1016/j.matpr.2020.04.210.

[86] J. K. Prusty and B. Pradhan, "Multi-response optimization using Taguchi-Grey relational analysis for composition of fly ash-ground granulated blast furnace slag based geopolymer concrete," *Construction and Building Materials,* vol. 241, p. 118049, 2020, doi: https://doi.org/10.1016/j.conbuildmat.2020.118049.

[87] M. A. Yazdi, M. Liebscher, S. Hempel, J. Yang, and V. Mechtcherine, "Correlation of microstructural and mechanical properties of geopolymers produced from fly ash and slag at room temperature," *Construction and Building Materials,* vol. 191, pp. 330-341, 2018, doi: https://doi.org/10.1016/j.conbuildmat.2018.10.037.

[88] M. S. Reddy, P. Dinakar, and B. H. Rao, "Mix design development of fly ash and ground granulated blast furnace slag based geopolymer concrete," *Journal of Building Engineering,* vol. 20, pp. 712-722, 2018, doi: https://doi.org/10.1016/j.jobe.2018.09.010.

[89] C. K. Lau, M. R. Rowles, G. N. Parnham, T. Htut, and T. S. Ng, "Investigation of geopolymers containing fly ash and ground-granulated blast-furnace slag blended by amorphous ratios," *Construction and Building Materials,* vol. 222, pp. 731-737, 2019, doi: https://doi.org/10.1016/j.conbuildmat.2019.06.198.

[90] S. Samantasinghar and S. Singh, "Effects of curing environment on strength and microstructure of alkali-activated fly ash-slag binder," *Construction and Building Materials,* vol. 235, p. 117481, 2020, doi: https://doi.org/10.1016/j.conbuildmat.2019.117481.

[91]   N. Ismail, M. Mansour, and H. El-Hassan, "Development of a low-cost cement free polymer concrete using industrial by-products and dune sand," *MATEC Web Conf.,* vol. 120, p. 03005, 2017. [Online]. Available: https://doi.org/10.1051/matecconf/201712003005.

[92]   H. El-Hassan, N. Ismail, S. Al Hinaii, A. Alshehhi, and N. Al Ashkar, "Effect of GGBS and curing temperature on microstructure characteristics of lightweight geopolymer concrete," *MATEC Web Conf.,* vol. 120, p. 03004, 2017. [Online]. Available: https://doi.org/10.1051/matecconf/201712003004.

[93]   I. Ismail, S. A. Bernal, J. L. Provis, R. San Nicolas, S. Hamdan, and J. S. J. van Deventer, "Modification of phase evolution in alkali-activated blast furnace slag by the incorporation of fly ash," *Cement and Concrete Composites,* vol. 45, pp. 125-135, 1// 2014, doi: http://dx.doi.org/10.1016/j.cemconcomp.2013.09.006.

[94]   J. Medljy, H. El-Hassan, and T. El-Maaddawy, "Effect of Recycled Aggregate and Steel Fibers on the Mechanical Properties of Alkali-Activated Slag/Fly Ash Blended Concrete," *ACI Symposium Publication,* vol. 349, pp. 210-223, 2021.

[95]   Á. Salesa *et al.*, "Physico – mechanical properties of multi – recycled concrete from precast concrete industry," *Journal of Cleaner Production,* vol. 141, pp. 248-255, 2017, doi: https://doi.org/10.1016/j.jclepro.2016.09.058.

[96]   V. S. Peem Nuaklong, Prinya Chindaprasirt, "Influence of recycled aggregate on fly ash geopolymer concrete properties," 2016.

[97]   X. S. Shi, Q. Y. Wang, X. L. Zhao, and F. Collins, "Discussion on Properties and Microstructure of Geopolymer Concrete Containing Fly Ash and Recycled Aggregate," *Advanced Materials Research,* vol. 450-451, pp. 1577-1583, 2012, doi: 10.4028/www.scientific.net/AMR.450-451.1577.

[98]   P. Nuaklong, V. Sata, and P. Chindaprasirt, "Influence of recycled aggregate on fly ash geopolymer concrete properties," *Journal of Cleaner Production,* vol. 112, no. Part 4, pp. 2300-2307, 2016, doi: https://doi.org/10.1016/j.jclepro.2015.10.109.

[99]   F. U. A. Shaikh, "Mechanical and durability properties of fly ash geopolymer concrete containing recycled coarse aggregates," *International Journal of Sustainable Built Environment,* vol. 5, no. 2, pp. 277-287, 2016, doi: https://doi.org/10.1016/j.ijsbe.2016.05.009.

[100] S. Mesgari, A. Akbarnezhad, and J. Z. Xiao, "Recycled geopolymer aggregates as coarse aggregates for Portland cement concrete and geopolymer concrete: Effects on mechanical properties," *Construction and Building Materials,* vol. 236, p. 117571, 2020, doi: https://doi.org/10.1016/j.conbuildmat.2019.117571.

[101] J. Xie, W. Chen, J. Wang, C. Fang, B. Zhang, and F. Liu, "Coupling effects of recycled aggregate and GGBS/metakaolin on physicochemical properties of geopolymer concrete," *Construction and Building Materials,* vol. 226, pp. 345-359, 2019, doi: https://doi.org/10.1016/j.conbuildmat.2019.07.311.

[102] J. Xie, J. Wang, R. Rao, C. Wang, and C. Fang, "Effects of combined usage of GGBS and fly ash on workability and mechanical properties of alkali activated geopolymer concrete with recycled aggregate," *Composites Part B: Engineering,* vol. 164, pp. 179-190, 2019, doi: https://doi.org/10.1016/j.compositesb.2018.11.067.

[103] J. Xie, J. Wang, B. Zhang, C. Fang, and L. Li, "Physicochemical properties of alkali activated GGBS and fly ash geopolymeric recycled concrete," *Construction and Building Materials,* vol. 204, pp. 384-398, 2019, doi: https://doi.org/10.1016/j.conbuildmat.2019.01.191.

[104] X. Guo and X. Pan, "Mechanical properties and mechanisms of fiber reinforced fly ash–steel slag based geopolymer mortar," *Construction and Building Materials,* vol. 179, pp. 633-641, 2018, doi: https://doi.org/10.1016/j.conbuildmat.2018.05.198.

[105] S. Bernal, R. De Gutierrez, S. Delvasto, and E. Rodriguez, "Performance of an alkali-activated slag concrete reinforced with steel fibers," *Construction and Building Materials,* vol. 24, no. 2, pp. 208-214, 2010, doi: https://doi.org/10.1016/j.conbuildmat.2007.10.027.

[106] C. P. Devika and D. R. Nath, "Study of Flexural Behavior of Hybrid Fibre Reinforced Geopolymer Concrete Beam," *International Journal of Science and Research,* vol. 4, no. 8, pp. 130-135, 2015.

[107] M. H. Al-Majidi, A. Lampropoulos, and A. B. Cundy, "Steel fibre reinforced geopolymer concrete (SFRGC) with improved microstructure and enhanced fibre-matrix interfacial properties," *Construction and Building Materials,* vol. 139, pp. 286-307, 2017, doi: https://doi.org/10.1016/j.conbuildmat.2017.02.045.

[108] S. Elkholy and H. El-Hassan, "Mechanical and micro-structure characterization of steel fiber-reinforced geopolymer concrete," in *Interdependence between Structural Engineering and Construction Management*, Chicago, IL, D. Ozevin, H. Ataei, M. Modares, A. Gurgun, S. Yazdani, and A. Singh, Eds., 2019, vol. 6, no. 1: ISEC Press.

[109] Y. Liu, C. Shi, Z. Zhang, N. Li, and D. Shi, "Mechanical and fracture properties of ultra-high performance geopolymer concrete: Effects of steel fiber and silica fume," *Cement and Concrete Composites,* vol. 112, p. 103665, 2020, doi: https://doi.org/10.1016/j.cemconcomp.2020.103665.

[110] X. Guo and G. Xiong, "Resistance of fiber-reinforced fly ash-steel slag based geopolymer mortar to sulfate attack and drying-wetting cycles," *Construction and Building Materials,* vol. 269, p. 121326, 2021, doi: https://doi.org/10.1016/j.conbuildmat.2020.121326.

[111] M. E. Gülşan, R. Alzeebaree, A. A. Rasheed, A. Niş, and A. E. Kurtoğlu, "Development of fly ash/slag based self-compacting geopolymer concrete using nano-silica and steel fiber," *Construction and Building Materials,* vol. 211, pp. 271-283, 2019, doi: https://doi.org/10.1016/j.conbuildmat.2019.03.228.

[112] J. M. Their and M. Özakça, "Developing geopolymer concrete by using cold-bonded fly ash aggregate, nano-silica, and steel fiber," *Construction and Building Materials,* vol. 180, pp. 12-22, 2018, doi: https://doi.org/10.1016/j.conbuildmat.2018.05.274.

[113] F. U. A. Shaikh and A. Hosan, "Mechanical properties of steel fibre reinforced geopolymer concretes at elevated temperatures," *Construction and Building Materials,* vol. 114, pp. 15-28, 2016, doi: https://doi.org/10.1016/j.conbuildmat.2016.03.158.

[114] M. Z. N. Khan, Y. Hao, H. Hao, and F. U. A. Shaikh, "Mechanical properties of ambient cured high strength hybrid steel and synthetic fibers reinforced geopolymer composites," *Cement and Concrete Composites,* vol. 85, pp. 133-152, 2018, doi: https://doi.org/10.1016/j.cemconcomp.2017.10.011.

[115] *Standard Specification for Concrete Aggregates*, ASTM, West Conshohocken, PA, 2016.

[116] *Standard Test Method for Relative Density (Specific Gravity) and Absorption of Coarse Aggregate*, ASTM, West Conshohocken, PA, 2015.

[117] *Standard Test Method for Sieve Analysis of Fine and Coarse Aggregates*, ASTM, USA, 2014.

[118] *Standard Test Method for Soundness of Aggregates by Use of Sodium Sulfate or Magnesium Sulfate*, ASTM, West Conshohocken, PA, 2013.

[119] *Standard Test Method for Resistance to Degradation of Small-Size Coarse Aggregate by Abrasion and Impact in the Los Angeles Machine*, ASTM, West Conshohocken, PA, 2014.

[120] *Standard Test Method for Bulk Density ("Unit Weight") and Voids in Aggregate*, ASTM, West Conshohocken, PA, 2017.

[121] D. Kanesan, S. Ridha, R. Suppiah, and T. Ravichandran, "Mechanical properties of different alkali activated slag content for oilwell cement under elevated conditions," *Contemporary Engineering Sciences,* vol. 10, no. 4, pp. 165-177, 2017.

[122] S. V. Patankar, Y. M. Ghugal, and S. S. Jamkar, "Effect of Concentration of Sodium Hydroxide and Degree of Heat Curing on Fly Ash-Based Geopolymer Mortar," *Indian Journal of Materials Science,* vol. 2014, p. 6, 2014, no. 938789, doi: 10.1155/2014/938789.

[123] N. A. M. Sani, Z. Man, R. M. Shamsuddin, K. A. Azizli, and K. Z. K. Shaari, "Determination of Excess Sodium Hydroxide in Geopolymer by Volumetric Analysis," *Procedia Engineering,* vol. 148, pp. 298-301, 2016, doi: https://doi.org/10.1016/j.proeng.2016.06.621.

[124] Bekaert, "Dramix 3D 65/35 Report," Bekaert, Belgium, 2012.

[125] C. Montes, D. Zang, and E. N. Allouche, "Rheological behavior of fly ash-based geopolymers with the addition of superplasticizers," *Journal of Sustainable Cement-Based Materials,* vol. 1, no. 4, pp. 179-185, 2012, doi: 10.1080/21650373.2012.754568.

[126] M. Palacios and F. Puertas, "Effect of superplasticizer and shrinkage-reducing admixtures on alkali-activated slag pastes and mortars," *Cement and Concrete Research,* vol. 35, no. 7, pp. 1358-1367, 2005, doi: https://doi.org/10.1016/j.cemconres.2004.10.014.

[127] *Standard Test Method for Compressive Strength of Cylindrical Concrete Specimens*, ASTM, West Conshohocken, PA, 2015.

[128] *Testing hardened concrete - Compressive strength of test specimens*, British Standard, London, UK, 2009.

[129] *Standard Test Method for Static Modulus of Elasticity and Poisson's Ratio of Concrete in Compression*, ASTM, West Conshohocken, PA, 2014.

[130] *Standard Test Method for Splitting Tensile Strength of Cylindrical Concrete Specimens*, ASTM, West Conshohocken, PA, 2011.

[131] *Standard Test Method for Flexural Performance of Fiber-Reinforced Concrete*, ASTM, West Conshohocken, PA, 2019.

[132] *Standard Test Method for Density, Absorption, and Voids in Hardened Concrete*, ASTM, West Conshohocken, PA, 2013.

[133] *Standard Test Method for Measurement of Rate of Absorption of Water by Hydraulic-Cement Concretes,*, ASTM, West Conshohocken, PA, 2013.

[134] *Standard Test Method for Electrical Indication of Concrete's Ability to Resist Chloride Ion Penetration*, ASTM, West Conshohocken, PA, 2012.

[135] *Standard Test Method for Bulk Electrical Resistivity or Bulk Conductivity of Concrete*, ASTM, West Conshohocken, PA, 2019.

[136] *Standard Test Method for Pulse Velocity Through Concrete*, ASTM, West Conshohocken, PA, 2016.

[137] M. Safiuddin and B. Scott, "Abrasion resistance of concrete - design, construction, and case study," *Concrete Research Letters,* vol. 6, no. 3, pp. 136-148, 2015.

[138] C. Yalcinkaya, J. Sznajder, A. Beglarigale, O. Sancakoglu, and H. Yazici, "Abrasion Resistance Of Reactive Powder Concrete: The Influence Of Water-To-Cement Ratio And Steel Micro-Fibers," *Advanced Materials Letters,* vol. 5, no. 6, pp. 345-351, 2014, doi: 10.5185/amlett.2014.amwc.1021.

[139] *Standard Test Method for Determining Potential Resistance to Degradation of Pervious Concrete by Impact and Abrasion*, ASTM, West Conshohocken, PA, 2013.

[140] M. H. Al-Majidi, A. Lampropoulos, A. Cundy, and S. Meikle, "Development of geopolymer mortar under ambient temperature for in situ applications," *Construction and Building Materials,* vol. 120, pp. 198-211, 9/1/ 2016, doi: http://dx.doi.org/10.1016/j.conbuildmat.2016.05.085.

[141] M. Chi, "Effects of dosage of alkali-activated solution and curing conditions on the properties and durability of alkali-activated slag concrete," *Construction and Building Materials,* vol. 35, no. Supplement C, pp. 240-245, 2012, doi: https://doi.org/10.1016/j.conbuildmat.2012.04.005.

[142] J. Davidovits, *Geopolymer Chemistry and Applications*. France: Institut Géopolymère, 2008.

[143] J. Temuujin, R. P. Williams, and A. van Riessen, "Effect of mechanical activation of fly ash on the properties of geopolymer cured at ambient temperature," *Journal of Materials Processing Technology,* vol. 209, no. 12, pp. 5276-5280, 2009, doi: http://dx.doi.org/10.1016/j.jmatprotec.2009.03.016.

[144] X. S. Shi, F. G. Collins, X. L. Zhao, and Q. Y. Wang, "Mechanical properties and microstructure analysis of fly ash geopolymeric recycled concrete," *Journal of Hazardous Materials,* vol. 237–238, pp. 20-29, 2012, doi: http://dx.doi.org/10.1016/j.jhazmat.2012.07.070.

[145] Comité euro-international du béton and Federation International de la Precontrainte, *CEB-FIP Model Code 1990: Design Code.* T. Telford, 1993.

[146] F. Bencardino, L. Rizzuti, G. Spadea, and R. N. Swamy, "Implications of test methodology on post-cracking and fracture behaviour of Steel Fibre Reinforced Concrete," *Composites Part B: Engineering,* vol. 46, pp. 31-38, 2013/03/01/ 2013, doi: https://doi.org/10.1016/j.compositesb.2012.10.016.

[147] D.-Y. Yoo, Y.-S. Yoon, and N. Banthia, "Flexural response of steel-fiber-reinforced concrete beams: Effects of strength, fiber content, and strain-rate," *Cement and Concrete Composites,* vol. 64, pp. 84-92, 2015, doi: https://doi.org/10.1016/j.cemconcomp.2015.10.001.

[148] N. Kachouh, H. El-Hassan, and T. El-Maaddawy, "Influence of steel fibers on the flexural performance of concrete incorporating recycled concrete aggregates and dune sand," *Journal of Sustainable Cement-Based Materials,* pp. 1-28, 2020, doi: 10.1080/21650373.2020.1809546.

[149] A. M. Neville, *Properties of Concrete.* New York: Wiley, 1996.

[150] N. S. Martys and C. F. Ferraris, "Capillary transport in mortars and concrete," *Cement and Concrete Research,* vol. 27, no. 5, pp. 747-760, 1997, doi: http://dx.doi.org/10.1016/S0008-8846(97)00052-5.

[151] İ. Şanal, "Performance of Macrosynthetic and Steel Fiber–Reinforced Concretes Emphasizing Mineral Admixture Addition," *Journal of Materials in Civil Engineering,* vol. 30, no. 6, p. 04018101, 2018, doi: doi:10.1061/(ASCE)MT.1943-5533.0002292.

[152] P. Ramadoss and K. Nagamani, "Tensile strength and durability characteristics of high-performance fiber reinforced concrete," *Arabian Journal for Science and Engineering,* vol. 41, no. 17, pp. 307-319, 2008.

[153] N. Kachouh, H. El-Hassan, and T. El-Maaddawy, "Effect of steel fibers on the performance of concrete made with recycled concrete aggregates and dune sand," *Construction and Building Materials,* vol. 213, pp. 348-359, 2019, doi: https://doi.org/10.1016/j.conbuildmat.2019.04.087.

[154] *Non-destructive testing of concrete - part 1: ultrasonic pulse velocity*, IS 13311-1, India, 1992.

[155] H. Wu, B. Huang, X. Shu, and Q. Dong, "Laboratory Evaluation of Abrasion Resistance of Portland Cement Pervious Concrete," *Journal of Materials in Civil Engineering,* vol. 23, no. 5, pp. 697-702, 2011, doi: doi:10.1061/(ASCE)MT.1943-5533.0000210.

[156] I. Ismail *et al.*, "Influence of fly ash on the water and chloride permeability of alkali-activated slag mortars and concretes," *Construction and Building Materials,* vol. 48, pp. 1187-1201, 2013, doi: https://doi.org/10.1016/j.conbuildmat.2013.07.106.

List of Publications

- Medljy, J., El-Hassan, H., and El Maaddawy, T. "Effect of Recycled Aggregate and Steel Fibers on the Mechanical Properties of Alkali-Activated Slag/Fly Ash Blended Concrete", 11th ACI/RILEM International Conference on Cementitious Materials and Alternative Binders for Sustainable Concrete (ICCM), June 2021, Toulouse, France.

Appendix

Table A1: Mixture proportions of trial mixes

Mix #	Component (kg/m³)									Total (kg/m³)
	GGBS	FA	SS	SH	RCA	NA	DS	SP	SF	
1	500	0	179	71	0	1000	650	12.5	0	2412.5
2	500	0	179	71	0	1000	650	12.5	156	2568.5
3	500	0	179	71	1000	0	650	12.5	0	2412.5
4	500	0	179	71	1000	0	650	12.5	156	2568.5
5	450	0	161	64	0	1100	600	11.25	0	2386.25
6	450	0	161	64	0	1100	600	11.25	156	2542.25
7	450	0	161	64	1100		600	11.25	0	2386.25
8	450	0	161	64	0	1100	600	11.25	156	2542.25
9	300	0	99	66	0	1210	725	7.5	0	2407.5
10	300	0	99	66	1210	0	725	7.5	0	2407.5
11	300	0	99	66	1210	0	725	7.5	156	2563.5
12	375	125	179	71	0	1000	650	12.5	0	2412.5
13	375	125	179	71	0	1000	650	12.5	156	2568.5
14	375	125	179	71	1000	0	650	12.5	0	2412.5
15	375	125	179	71	1000	0	650	12.5	156	2568.5
16	337.5	112.5	161	64	0	1100	600	11.25	0	2386.25
17	337.5	112.5	161	64	0	1100	600	11.25	156	2542.25
18	337.5	112.5	161	64	1100		600	11.25	0	2386.25
19	337.5	112.5	161	64	0	1100	600	11.25	156	2542.25
20	225	75	99	66	0	1210	725	7.5	0	2407.5
21	225	75	99	66	1210	0	725	7.5	0	2407.5
22	225	75	99	66	1210	0	725	7.5	156	2563.5
23	187.5	62.5	99	66	0	1220	765	6.25	0	2406.25
24	187.5	62.5	99	66	1220	0	765	6.25	0	2406.25
25	187.5	62.5	99	66	1220	0	765	6.25	156	2562.25

Table A2: Mixture ratios of trial mixes

Mix #	Ratios							SF (%)
	FA/GGBS	AAS/B	SS/SH	CA/DS	RCA/DS	Agg/B	SP/B (%)	
1	0.00	0.50	2.52	1.54	0.00	3.30	2.50	0.0%
2	0.00	0.50	2.52	1.54	0.00	3.30	2.50	2.0%
3	0.00	0.50	2.52	0.00	1.54	3.30	2.50	0.0%
4	0.00	0.50	2.52	0.00	1.54	3.30	2.50	2.0%
5	0.00	0.50	2.52	1.83	0.00	3.78	2.50	0.0%
6	0.00	0.50	2.52	1.83	0.00	3.78	2.50	2.0%
7	0.00	0.50	2.52	0.00	1.83	3.78	2.50	0.0%
8	0.00	0.50	2.52	1.83	0.00	3.78	2.50	2.0%
9	0.00	0.55	1.50	1.67	0.00	6.45	2.50	0.0%
10	0.00	0.55	1.50	0.00	1.67	6.45	2.50	0.0%
11	0.00	0.55	1.50	0.00	1.67	6.45	2.50	2.0%
12	0.33	0.50	2.52	1.54	0.00	3.30	2.50	0.0%
13	0.33	0.50	2.52	1.54	0.00	3.30	2.50	2.0%
14	0.33	0.50	2.52	0.00	1.54	3.30	2.50	0.0%
15	0.33	0.50	2.52	0.00	1.54	3.30	2.50	2.0%
16	0.33	0.50	2.52	1.83	0.00	3.78	2.50	0.0%
17	0.33	0.50	2.52	1.83	0.00	3.78	2.50	2.0%
18	0.33	0.50	2.52	0.00	1.83	3.78	2.50	0.0%
19	0.33	0.50	2.52	1.83	0.00	3.78	2.50	2.0%
20	0.33	0.55	1.50	1.67	0.00	6.45	2.50	0.0%
21	0.33	0.55	1.50	0.00	1.67	6.45	2.50	0.0%
22	0.33	0.55	1.50	0.00	1.67	6.45	2.50	2.0%
23	0.33	0.66	1.50	1.59	0.00	7.94	2.50	0.0%
24	0.33	0.66	1.50	0.00	1.59	7.94	2.50	0.0%
25	0.33	0.66	1.50	0.00	1.59	7.94	2.50	2.0%

Table A3: Compressive strength development of trial mixes

Mix #	Compressive Strength (MPa)			Development (%)	
	1-day	7-day	28-day	1 to 7	1 to 28
1	54.9	64.3	60.6	17.0	10.3
2	56.2	77.5	84.3	38.0	50.0
3	32.1	38.5	45.7	19.9	42.3
4	42.3	64.8	61.9	53.3	46.3
5	42.0	49.9	54.4	19.0	29.5
6	58.7	75.2	77.2	28.2	31.5
7	28.4	36.1	41.0	27.0	44.2
8	36.6	45.3	47.6	24.0	30.3
9	25.1	27.5	30.8	9.6	22.7
10	18.4	23.3	24.7	26.6	34.2
11	21.4	27.3	31.2	27.6	45.8
12	49.5	66.2	60.5	33.7	22.2
13	56.0	79.3	80.5	41.6	43.7
14	29.8	39.1	38.0	31.2	27.4
15	33.4	49.1	46.6	47.1	39.7
16	46.5	61.0	61.3	31.2	31.7
17	49.7	72.7	73.4	46.1	47.5
18	27.1	35.3	35.7	30.0	31.6
19	29.4	42.1	43.7	43.4	48.8
20	30.5	43.1	45.8	41.3	50.3
21	18.1	24.8	27.2	37.0	50.3
22	24.1	34.0	40.3	41.1	67.2
23	17.1	24.3	30.4	42.1	77.8
24	8.1	13.3	16.1	64.2	98.8
25	18.5	24.1	30.9	30.3	67.0